University of Alberta

Regulation of Ca^{2+} signals in rat carotid glomus cells

by

Lei Yan

A thesis submitted to the Faculty of Graduate Studies and Research in partial fulfillment of the requirements for the degree of

Doctor of Philosophy

Centre for Neuroscience

Dedication

This thesis is dedicated to my parents and my husband. Without their constant

love and support, the body of work would never have been completed.

Abstract

Glomus cells of the carotid body are peripheral chemoreceptors that detect changes in arterial oxygen levels. Hypoxia suppresses oxygen-sensitive K^+ channels in glomus cells, resulting in cytosolic $[Ca^{2+}]$ ($[Ca^{2+}]_i$) elevation in glomus cells via the activation of voltage-gated Ca^{2+} channels. The resultant transmitter release stimulates the carotid sinus nerve (CSN) and the triggering of respiratory and cardiovascular reflexes.

Hypoxia also causes mitochondrial depolarization and mitochondrial inhibitors have been shown to cause depolarization in glomus cells via the inhibition of oxygen-sensitive K^+ channels. In the first project, with the patch clamp technique in conjunction with $[Ca^{2+}]_i$ measurement (with indo-1), I found that mitochondrial Ca^{2+} uptake played a dominant role in cytosolic Ca^{2+} clearance in rat glomus cells. Importantly, mitochondrial inhibition increased the duration of the Ca^{2+} signal triggered by a voltage-clamped depolarization, which contributed to an enhancement of exocytotic response. Under hypoxic conditions, there was a slowing in cytosolic Ca^{2+} clearance, consistent with the scenario that hypoxia caused mitochondrial depolarization and thus reduced mitochondrial Ca^{2+} uptake.

It has been reported that the hypoxia-triggered CSN discharge is enhanced in the presence of extracellular bicarbonate ion (HCO_3^-). Therefore, in the second project, I investigated the role of HCO_3^- in the regulation of Ca^{2+} dynamics in glomus cells. Extracellular HCO_3^- slowed the rate of cytosolic Ca^{2+} clearance in a concentration-dependent manner. Measurement of the mitochondrial Ca^{2+} signal with rhod-2 shows that HCO_3^- reduced mitochondrial Ca^{2+} uptake and this

inhibition was abolished in cells treated with scavengers of reactive oxygen species (ROS). Thus, HCO_3^- reduced mitochondrial Ca^{2+} uptake via a mechanism that was dependent on ROS.

Overall, my results show that mitochondrial Ca^{2+} uptake in glomus cells could be reduced by hypoxia or by the presence of a physiological concentration of extracellular HCO_3^-. This effect resulted in a slowing in cytosolic Ca^{2+} clearance and more transmitter release. The multiplicity of the influences of mitochondria on glomus cell Ca^{2+} signaling and exocytosis underscores the importance of mitochondria in hypoxic chemotransduction in the carotid bodies.

Acknowledgement

It is my pleasure to thank the people who made this thesis possible.

First and foremost, I would like to thank my supervisor Dr. Amy Tse and my co-supervisor Dr. Fred Tse for giving me the chance to study in their laboratories. Without their great efforts, constant encouragement and generous support, I would not have been able to complete my study and thesis work.

I would especially like to thank the research associate in our laboratory, Dr. Andy Lee, who contributed to this thesis by collaborating with me on the first project. I thank him for giving me a lot of good advice on my thesis work and teaching me the experimental techniques.

I am grateful to my supervisory committee members, Dr. Klaus Ballanyi and Dr. Declan Ali, who gave me valuable advice and guidance for my thesis.

I would like to thank my external examiner Dr. Naweed I. Syed who provided me thoughtful and detailed comments on my thesis. I thank Dr. Glen Baker and Dr. Dave Collins for reading my thesis and attending my thesis defense.

I would also like to thank two former students in our laboratory, Dr. Fenglian Xu, for teaching me the dissociation of the carotid glomus cells, and Dr. Valerie Yeung-Yam-Wah, for teaching me the patch clamp techniques and giving me a lot of valuable advice for my presentations. I thank the current students in our laboratory, Mr. Michael Simpson, for providing me the adrenal chromaffin cells and Ms. Su Su Liang and Ms. Weixiao (Iris) Zhao for helping me practice my thesis seminar.

Table of Contents

Chapter 2

Chapter 3

Chapter 4

Influence of bicarbonate ion (HCO_3^-) on mitochondrial Ca^{2+} transport in rat

carotid glomus cells   102

Chapter 5

List of Figures

List of Tables

List of Abbreviations

5-HT	serotonin / 5-hydroxytryptamine
Ψ_m	mitochondrial membrane potential
8-CPT-cAMP	8-(4-chlorophenylthio)-adenosine 3',5'-cyclic monophosphate
9-AC	anthracene-9-carboxylic acid
$[Ca^{2+}]_i$	cytosolic Ca^{2+} concentration
$[HCO_3^-]_{ext}$	extracellular HCO_3^- concentration
ACE	angiotensin-converting enzyme
ACh	acetylcholine
ADP	adenosine diphosphate
AICAR	5-aminoimidazole-4-carboxamide-riboside
AMP	adenosine monophosphate
AMPK	adenosine monophosphate-activated protein kinase
Ang II	angiotensin II
ATP	adenosine 5'-triphosphate (ATP)
BHQ	2,5-di(tert-butyl)-1,4-benzohydroquinone
BK	large conductance Ca^{2+}-activated K^+
BSA	bovine serum albumin
cAMP	adenosine 3',5'-cyclic monophosphate
CA	carbonic anhydrase
CBS	cystathionine β-synthase
CCCP	carbonyl cyanide m-chlorophenylhydrazone
CCE	capacitative Ca^{2+} entry
CPA	cyclopiazonic acid
CSN	carotid sinus nerve
CSE	cystathionine γ-lyase
DA	dopamine
DIDS	4,4'-diisothiocyanostilbene-2,2'-disulphonic acid
DMEM	Dulbecco's modified Eagle's medium

DOF	dofetilide
DRG	dorsal root ganglion
DPI	diphenylene iodonium
EGTA	ethylene glycol tetraacetic acid
ER	endoplasmic reticulum
ETC	electron transport chain
GABA	γ-aminobutyric acid
GPN	glossopharyngeal nerve
GSH	reduced L-glutathione
GSSH	oxidized glutathione
H_2O_2	hydrogen peroxide
H_2S	hydrogen sulphide
H_2-DCFDA	2',7'-dichlorodihydrofluorescein diacetate
HERG	human ether-a-go-go-related gene
HO	hemoxygenase
IMAC	inner membrane anion channel
IP_3R	inositol 1,4,5-trisphosphate receptor
K_{2P}	two-pore domain K^+ channels
NAC	N-acetyl-L-cysteine
mAChR	mucarinic acetylcholine receptor
MCUR1	mitochondrial calcium uniporter regulator 1
MICU1	mitochondrial calcium uptake 1
nAChR	nicotinic acetylcholine receptor
NaCN	sodium cyanide
NAD^+	nicotinamide adenine dinucleotide
NADH	nicotinamide adenine dinucleotide (reduced)
NADPH	nicotinamide adenine dinucleotide phosphate
$Na_2S_2O_4$	sodium dithionite
NCX	Na^+/Ca^{2+} exchanger
NMG^+	N-methylglucamine
NOS	nitric oxide synthase

NOX	nicotinamide adenine dinucleotide phosphate oxidase
PACAP	pituitary adenylate cyclase-activating polypeptide
PAG	DL-propargylglycine
pCO_2	partial pressure of CO_2
PKA	protein kinase A
PKC	protein kinase C
PMCA	plasma membrane Ca^{2+}-ATPase
pO_2	partial pressure of O_2
PTP	permeability transition pore
RaM	rapid mode of Ca^{2+} uptake
ROS	reactive oxygen species
RyR	ryanodine receptor
SERCA	sarco/endoplasmic reticulum Ca^{2+}-ATPase
SR	sarcoplasmic reticulum
TASK	tandem-pore acid-sensing K^+ channel
TCA	tricarboxylic acid
TEA	tetraethylammonium
TMRE	tetramethylrhodamine ethyl ester
TRAAK	TWIK-related arachidonic acid activated-K^+ channel
TREK	TWIK-1-related K^+ channel
TWIK-1	tandem of pore domains in a weak inward rectifying K^+ channel
VGCC	voltage-gated Ca^{2+} channel
ZnPP9	Zinc-protoporphyrin-9

Chapter 1

General Introduction

1.1 Carotid body anatomy, physiology and pathophysiology

The ability to maintain an adequate supply of oxygen (O_2) is essential for survival. Even a few minutes of shortage of O_2 supply can cause severe damage to the brain and heart. An immediate response to a hypoxic stress is a reflex increase in the rate of respiration. This important reflex is mediated via peripheral chemoreceptors. In air breathing vertebrates, the major peripheral chemoreceptors are the carotid and aortic bodies (Gonzalez *et al.*, 1992). The carotid bodies are responsible for ~90% of the hyperventilation seen in hypoxic hypoxia and for 20-50% of that seen in respiratory and metabolic acidosis (Gonzalez *et al.*, 1992).

1.1.1 Carotid body anatomy

The carotid body is a reddish brown oval structure located at the bifurcation of the common carotid artery (Fig. 1-1). The size of a rat carotid body is ~0.3-0.6 mm in diameter (McDonald & Blewett, 1981). There are four major components in the carotid body: glomus (type I) cells, sustentacular (type II) cells, nerve endings and blood vessels (Fig. 1-2). The ovoid glomus cells are electrically excitable and contain dense core granules (Gonzalez *et al.*, 1994; Prabhakar, 2000). The spindle-shaped sustentacular cells resemble glial cells and envelope clusters of glomus cells (Gonzalez *et al.*, 1994; Prabhakar, 2000). Sustentacular cells do not contain any dense core granules and do not express voltage-gated Ca^{2+} channels (VGCCs) or Na^+ channels (Xu *et al.*, 2003). Two kinds of nerve endings in the carotid body are in close synaptic contact with the glomus cells: the afferent nerve endings of the carotid sinus nerve (CSN) whose somata are in the

2

petrosal ganglion (McDonald, 1983; Gonzalez *et al.*, 1994) and the efferent nerve endings from the glossopharyngeal nerve (GPN) (Campanucci *et al.*, 2003; Campanucci & Nurse, 2005). The carotid body is richly supplied with blood vessels (Gonzalez *et al.*, 1994). In comparison with the brain, the vascularization of the carotid body is 5-6 times denser (Kumar & Bin-Jaliah, 2007) and the blood flow rate of the carotid body is ~15 times higher (Kumar & Bin-Jaliah, 2007; Gonzalez *et al.*, 2010). Even under a normoxic condition, the rate of O_2 consumption in the carotid body is near maximum (Duchen & Biscoe, 1992a). The rich blood supply and high rate of O_2 consumption in the carotid body account in part for the sensitivity of the carotid body to changes in arterial blood O_2 tension. Gap junctions are present between some glomus cells within the cell clusters (McDonald, 1983; Prabhakar, 2000). Hypoxia was found to reduce, increase or have no effect on glomus cell coupling (Monti-Bloch *et al.*, 1993; Abudara & Eyzaguirre, 1998). For example, exogenous application of dopamine (DA) and acetylcholine (ACh), transmitters that are released from glomus cells during hypoxia, caused cell decoupling, but elevation of cellular adenosine 3',5'-cyclic monophosphate (cAMP) which occurs during hypoxia, enhanced coupling (Monti-Bloch *et al.*, 1993; Abudara & Eyzaguirre, 1998).

1.1.2 O_2-sensing element(s) in the carotid body

The notion that glomus cells are the primary chemosensors was first suggested by de Castro in 1928 (Gonzalez *et al.*, 1992; Gonzalez *et al.*, 1994). However, others suggested that the CSN was the site of O_2 sensing because

microinjection of the mitochondrial inhibitor cyanide into the petrosal ganglion could elevate arterial blood pressure (Sun & Reis, 1994). The role of CSN as the O_2 sensor was subsequently refuted because exposure of the petrosal ganglion to hypoxia did not result in an increase in CSN discharge (Alcayaga *et al.*, 1999).

It is now generally accepted that glomus cells are the initial sites of O_2 sensing (Peers & Buckler, 1995; Prabhakar, 2000). Glomus cells were found to be sensitive to the decreases in arterial partial pressure of O_2 (pO_2), and hypoxia evoked a rise in cytosolic $[Ca^{2+}]$ ($[Ca^{2+}]_i$) in glomus cells, resulting in transmitter release (Gonzalez *et al.*, 1994; Montoro *et al.*, 1996). When the glomus cells of rabbit carotid body were destroyed by local freezing, hypoxia failed to trigger an increase in CSN discharge and respiration (Verna *et al.*, 1975). Hypoxia was found to have no direct effect on petrosal neurons but increased the electrical activities of petrosal neurons that formed *de novo* synapses with glomus cells, suggesting that hypoxia evoked transmitter release from glomus cells which in turn stimulated the petrosal neurons (Zhong *et al.*, 1997; Nurse & Zhang, 1999). These findings suggest that glomus cells of the carotid body, not the CSN, are the primary peripheral O_2 sensors.

1.1.3 Physiological and pathophysiologcial roles of the carotid body

In 1928, De Castro raised the possibility that the carotid body acts as a chemosensor to detect changes in the blood chemical content and is involved in the triggering of cardiorespiratory reflexes. Later in 1930, Heymans *et al.* reported that the carotid body mediates the hyperventilation induced by hypoxia,

hypercapnia (an increase in the arterial partial pressure of CO_2 (pCO_2)) and acidosis (Gonzalez *et al.*, 1994). For example, at high altitude where the atmospheric O_2 pressure is low, the enhancement of respiratory responses is mediated by the carotid body (Joseph & Pequignot, 2009). In addition to sensing arterial blood pO_2, pCO_2 and pH, the carotid body also responds to changes in blood osmolarity, K^+ concentration, temperature, glucose levels as well as circulating hormones such as angiotensin II (Ang II) and pituitary adenylate cyclase-activating polypeptide (PACAP) (Pardal & Lopez-Barneo, 2002b; Kumar & Bin-Jaliah, 2007; Xu *et al.*, 2007). Therefore, the carotid body is considered as a polymodal sensor that regulates ventilatory responses (Kumar & Bin-Jaliah, 2007). It is well established that hypoxia or hypercapnia causes membrane depolarization in glomus cells, resulting in the activation of VGCCs. The rise in $[Ca^{2+}]_i$ triggers the release of multiple transmitters from glomus cells (Gonzalez *et al.*, 1994; Buckler & Vaughan-Jones, 1994a; Buckler & Vaughan-Jones, 1994b). Importantly, the amount of transmitter release from glomus cells and the increase in CSN activities have similar sensitivities to the reductions in pO_2 (Rigual *et al.*, 1986; Rigual *et al.*, 1991). As summarized in Fig.1-2, hypoxia or hypercapnia triggers the release of multiple transmitters from glomus cells, including DA (Urena *et al.*, 1994), ACh (Fitzgerald *et al.*, 1999), adenosine 5'-triphosphate (ATP) (Buttigieg & Nurse, 2004), histamine (Koerner *et al.*, 2004) and substance P (Kumar *et al.*, 2000; Kim *et al.*, 2001). Some of the transmitters (e.g. ACh and ATP) released by glomus cells can excite the nerve terminals of the CSN in the carotid body (Nurse & Piskuric, 2012). The stimulation of the CSN in turn

triggers respiratory and cardiovascular reflexes via the cardiorespiratory center in the brain stem (Gonzalez *et al.*, 1994; Peers & Buckler, 1995; Prabhakar, 2000). The afferent discharge induced by the carotid body is graded by the intensity of the stimulus (Kumar & Bin-Jaliah, 2007; Kumar, 2009). The threshold of arterial pO_2 for the activation of the CSN is 70-75 mmHg. When pO_2 is lowered to ~40 mmHg, the CSN activity reaches 50% of the maximum, and the maximal CSN activity occurs when pO_2 is lowered to ~10 mmHg (Gonzalez *et al.*, 1994; Gonzalez *et al.*, 2010).

There is growing evidence that repetitive episodes of hypoxia (e.g. during sleep apnea) lead to the stimulation of peripheral chemoreceptors, which in turn increases the sympathetic drive and contributes to an increased risk of stroke, coronary heart diseases, heart failure and hypertension (Narkiewicz & Somers, 2003; Prabhakar & Kumar, 2010). For example, patients with sleep apnea were found to have enhanced peripheral chemoreceptor sensitivity (Narkiewicz *et al.*, 1998; Narkiewicz *et al.*, 1999). Rats that were exposed to chronic intermittent hypoxia to mimic sleep apnea developed hypertension and an increase in sympathetic nerve activity (Fletcher *et al.*, 1992). Denervation of the carotid bodies in these rats blocked the increase in blood pressure and sympathetic activity induced by chronic intermittent hypoxia (Fletcher *et al.*, 1992; Fletcher, 2001). Chronic intermittent hypoxia has also been shown to increase the hypoxic sensory response of the carotid body (Peng *et al.*, 2003; Peng & Prabhakar, 2004). These findings suggest that an enhancement in the sensitivity of the carotid bodies

to hypoxia contributes to an increase in sympathetic activity and blood pressure associated with sleep apnea.

1.2 Ion channels in glomus cells

Glomus cells express a variety of ion channels and the type of ion channels expressed on glomus cells is species-dependent. Since the glomus cells of rabbit and rat have been investigated extensively, I shall focus on these two species in the following review (summarized in Table 1-1).

Na^+ channels are expressed in both rabbit and rat glomus cells. In rabbit glomus cells, voltage-gated Na^+ channels contribute to the generation of action potentials (Lopez-Barneo *et al.*, 1988; Lopez-Lopez *et al.*, 1989). In rat glomus cells, however, the expression of voltage-gated Na^+ channels is low or absent (Stea & Nurse, 1991b; Fieber & McCleskey, 1993). Interestingly, in rat glomus cells, a voltage-independent, background Na^+ current was found to have an important role in the maintenance of the resting membrane potential (Carpenter & Peers, 2001).

In rabbit glomus cells, several types of VGCCs including the L-, N-, P/Q-, and R-type are present, but the T-type is absent (Overholt & Prabhakar, 1997). However, only the L- and P/Q-types were thought to be associated with transmitter (catecholamine) release from glomus cells (Rocher *et al.*, 2005). In rat glomus cells, the dominant type of VGCCs is the L-type (Fieber & McCleskey, 1993; Silva & Lewis, 1995). Whether rat glomus cells express N-type VGCCs is

7

controversial. Silva & Lewis reported that ~40% of Ca^{2+} current in rat glomus cells could be inhibited by ω-conotoxin GIVA, a selective N-type VGCC inhibitor (Silva & Lewis, 1995). However, other studies using ω-conotoxin GIVA found that the N-type VGCCs were present in only a fraction of rat glomus cells (Fieber & McCleskey, 1993; Peers *et al.*, 1996). In contrast with rabbit glomus cells, the T-, P/Q- and R-type VGCCs are absent in rat glomus cells (Silva & Lewis, 1995). Since rat glomus cells express fewer voltage-gated Na^+ channels, VGCCs play a major role in the generation of action potentials in these cells (Buckler, 2007).

In rabbit glomus cells, several types of K^+ channels have been reported, including the 4-AP-sensitive, A-type K^+ channels (Lopez-Lopez *et al.*, 1993; Perez-Garcia *et al.*, 2000; Sanchez *et al.*, 2002), the delayed rectifier K^+ channels (Lopez-Lopez *et al.*, 1993), the large conductance Ca^{2+}-activated K^+ (BK) channels (Ganfornina & Lopez-Barneo, 1992) and the human ether-a-go-go-related gene (HERG)-like K^+ channels (Overholt *et al.*, 2000a; Overholt *et al.*, 2000b). Rat glomus cells express the A-type K^+ channels (Vandier *et al.*, 1999), the delayed rectifier K^+ channels (Lopez-Lopez *et al.*, 1997), the BK channels (Peers, 1990; Wyatt & Peers, 1995), the background tandem-pore acid-sensing K^+ channel (TASK)-like K^+ channels (Buckler, 1997; Buckler, 1999; Buckler *et al.*, 2000) and some tandem of pore domains in a weak inward rectifying K^+ channel (TWIK-1)-related K^+ channel (TREK) channels (Yamamoto *et al.*, 2002; Yamamoto & Taniguchi, 2006). In addition, HERG-like K^+ channels are reported in newborn rat glomus cells. The HERG-like K^+ current contributes to the control of resting membrane potential, which inhibits the hypoxia-evoked membrane

8

depolarization in these cells (Kim *et al.*, 2005). Interestingly, these HERG-like K^+ channels decline with the maturation of the rats: the current density was reduced by ~45% in ~2 weeks, leading to an enhancement of the sensitivity of the rat glomus cells to hypoxia (Kim *et al.*, 2005).

TASK and TREK channels belong to tandem P-domain K^+ channels or two-pore domain K^+ channels (K_{2P}) family (Buckler, 2010). Each K_{2P} channel consists of two subunits and each subunit contains four transmembrane domains and two pore-forming domains (Lesage *et al.*, 1996a; Lesage *et al.*, 1996b). Most of the channels in the K_{2P} family are not strongly affected by membrane potential and they play a role in the setting of the cell resting membrane potential (Buckler, 2010). The presence of TASK-like K^+ channels in rat glomus cells was first reported by Buckler (Buckler, 1997). The pharmacological and biophysical properties of the TASK-like K^+ channels are similar to the TASK-1 and -3 in the K_{2P} family (Buckler *et al.*, 2000; Williams & Buckler, 2004). The TASK-like K^+ channels are insensitive to classical K^+ channel inhibitors such as tetraethylammonium (TEA), 4-AP or charybdotoxin but can be inhibited by Ba^{2+}, Zn^{2+}, bupivacaine, quinidine or extracellular Mg^{2+}. In addition, these channels are pH-sensitive and are inhibited by low pH (acidosis). They show only weak outward rectification and play a main role in setting resting membrane potential of glomus cells. Immunohistochemistry showed that TASK-1, TASK-3 and TASK-1/TASK-3 heterodimers were expressed in rat glomus cells, and that the TASK-1/TASK-3 heterodimer was the dominant form (Kim *et al.*, 2009). TREK channels can be activated by membrane stretch, heat, acidosis, voltage, lipids and

inhalational anaesthetics (such as halothane) (Patel & Honore, 2001; Maingret *et al.*, 2002; Buckler & Honore, 2005; Kreneisz *et al.*, 2009). TREK-1, TREK-2, and TWIK-related arachidonic acid-activated K^+ channel (TRAAK) subfamilies were found to be expressed in rat glomus cells (Yamamoto *et al.*, 2002; Yamamoto & Taniguchi, 2006).

Three types of Cl^- channels have been reported in rat glomus cells, including a large conductance voltage-independent Cl^- channel which is sensitive to Cl^- channel inhibitor anthracene-9-carboxylic acid (9-AC) (Stea & Nurse, 1989; Stea & Nurse, 1991a), a pH- and 9-AC-sensitive hyperpolarization-activated Cl^- channel which exhibits inward rectification (Petheo *et al.*, 2001) and a swelling- and cAMP-activated weakly outward rectifying Cl^- channel which is sensitive to Cl^- channel inhibitors including niflumic acid and 4,4'-diisothiocyanostilbene-2,2'-disulphonic acid (DIDS) (Carpenter & Peers, 1997).

The above review indicates that carotid glomus cells express a variety of ion channels. In rat glomus cells, the resting membrane potential is mainly determined by the TASK-like K^+ current (Buckler, 2010), the background Na^+ current (Carpenter & Peers, 2001) and possibly the voltage-independent Cl^- current (Stea & Nurse, 1989; Stea & Nurse, 1991a). Since rat glomus cells express fewer voltage-gated Na^+ channels, the generation of action potentials is mainly caused by the activation of VGCCs in these cells (Buckler, 2007).

1.3 O$_2$ sensors in glomus cells

It is generally accepted that glomus cells are the initial site of O_2 sensing in the carotid body. However, the molecular identity of the O_2 sensor in glomus cells remains controversial. At present, there are four main hypotheses regarding the molecular identity of the O_2 sensor in glomus cells (summarized in Table 1-2). The first hypothesis proposes that some K^+ channels are O_2 sensors and they are named as O_2-sensitive K^+ channels. These channels can be inhibited by hypoxia, leading to membrane depolarization and the subsequent activation of VGCCs (Gonzalez *et al.*, 1994; Prabhakar, 2000). The second hypothesis proposes that some heme-containing proteins are the initial O_2 sensing site in glomus cells (Gonzalez *et al.*, 2010; Evans *et al.*, 2012; Prabhakar & Semenza, 2012; Prabhakar, 2012a). The third hypothesis proposes that adenosine monophosphate-activated protein kinase (AMPK) is the primary O_2 sensor in glomus cells (Gonzalez *et al.*, 2010; Peers *et al.*, 2010). The fourth hypothesis proposes that hydrogen sulphide (H_2S) is the O_2 sensor in glomus cells (Peng *et al.*, 2010; Prabhakar, 2012b). Note that there is a possibility that glomus cells possess more than one type of O_2 sensor. It has been postulated that glomus cells may utilize multiple O_2 sensors in order to detect pO_2 changes in a wide range and a rapid manner (Prabhakar, 2006).

1.3.1 *K^+ channels as O_2 sensors in glomus cells*

It is well established that certain types of K^+ channels in glomus cells can be inhibited by hypoxia, leading to membrane depolarization and activation of

VGCCs (Prabhakar, 2000). The type of the O_2-sensitive K^+ channels in glomus cells is species-dependent.

In rabbit glomus cells, HERG-like K^+ channels were active at the resting membrane potential and the blockade of these channels by dofetilide (DOF) resulted in membrane depolarization, a rise in $[Ca^{2+}]_i$, and an increase in CSN discharge (Overholt *et al.*, 2000a; Overholt *et al.*, 2000b). However, there is no direct evidence that hypoxia can inhibit HERG-like K^+ channels in rabbit glomus cells. In addition, studies have shown that BK channels do not play a role in the initiation of hypoxic response in rabbit glomus cells (Lopez-Lopez *et al.*, 1989; Ganfornina & Lopez-Barneo, 1992). For example, the opening probability of BK channels was reported to be unaffected by hypoxia (Ganfornina & Lopez-Barneo, 1992). In contrast, the O_2-sensitive K^+ channels are the delayed rectifier K^+ channels (Lopez-Lopez *et al.*, 1989; Lopez-Lopez *et al.*, 1993) and the A-type K^+ channels (Ganfornina & Lopez-Barneo, 1992; Lopez-Lopez *et al.*, 1993; Perez-Garcia *et al.*, 2000; Sanchez *et al.*, 2002).

In rat glomus cells, the involvement of the HERG-like K^+ channels (Kim *et al.*, 2005), TREK-1 channels (Buckler & Honore, 2005; Caley *et al.*, 2005) and the A-type K^+ channels (Doyle & Donnelly, 1994; Cheng & Donnelly, 1995; Buckler, 1997; Buckler, 1999; Xu *et al.*, 2006) in the initiation of the hypoxic response has been ruled out. In contrast, the BK and TASK-like K^+ channels are the main O_2-sensitive K^+ channels in rat glomus cells (Wyatt & Peers, 1995; Buckler, 1997). The role of BK channels in the hypoxic response has however been controversial. Since the activation of BK channels is dependent on

12

depolarization (membrane potential more positive than -30 mV) and a relatively large elevation in $[Ca^{2+}]_i$ (>1 μM), it is unclear whether BK channels are open at the resting membrane potential of glomus cells. Moreover, it has been reported that the inhibition of the BK channel (with charybdotoxin) failed to enhance transmitter release from intact rat carotid bodies or increase CSN discharge under normoxic conditions (Doyle & Donnelly, 1994; Cheng & Donnelly, 1995). In neonatal rat glomus cells, inhibition of BK channels (with TEA) did not affect membrane potential or $[Ca^{2+}]_i$ (Buckler, 1997; Buckler, 1999). However, a previous study in our laboratory (Xu *et al.*, 2006) showed that application of TEA evoked membrane depolarization and an elevation in $[Ca^{2+}]_i$ in ~60% of the glomus cells isolated from adult rats. Hypoxia was found to inhibit BK currents and the application of charybdotoxin caused membrane depolarization of single rat gomus cells (Peers, 1990; Wyatt & Peers, 1995). Iberiotoxin, a BK channel blocker, was found to evoke catecholamine release in rat carotid body slices (Pardal & Lopez-Barneo, 2002a). These findings suggest that some BK channels are open at the resting membrane potential of glomus cells and the closure of BK channels during hypoxia results in depolarization (Peers & Wyatt, 2007). On the other hand, there is growing evidence that the TASK-like K^+ channels are the main O_2-sensitive K^+ channels in rat glomus cells. The TASK-like K^+ channels are background channels that are open at the resting membrane potential of rat glomus cells. It is well established that hypoxia leads to the stabilization of the closed state of TASK-like K^+ channels, resulting in membrane depolarization and subsequent activation of VGCCs in rat glomus cells (Buckler, 1997; Buckler *et al.*,

2000; Williams & Buckler, 2004). In transgenic mice with TASK-1 knockout or TASK-1/TASK-3 double knockout, there was ~50% reduction in the hypoxia-evoked increase in CSN discharge (Trapp *et al.*, 2008).

The activity of O_2-sensitive K^+ channels was thought to be regulated directly by pO_2 (Lopez-Barneo *et al.*, 2001). However, there is growing evidence that O_2-sensitive K^+ channels themselves are not the initial O_2 sensors and that the activities of these channels are regulated by some O_2-sensitive factors in the glomus cells. For example, it has been shown that the inhibition of BK or TASK-like K^+ channels by hypoxia could be observed in cell-attached patch recordings but lost in excised patches, indicating that the activities of BK or TASK-like K^+ channels could not be directly modulated by hypoxia (Wyatt & Peers, 1995; Buckler *et al.*, 2000).

The literature suggests that voltage-gated Na^+ channels and VGCCs are not directly involved in the O_2 sensing in glomus cells. In both rat and rabbit glomus cells, the voltage-gated Ca^{2+} and Na^+ currents were unaffected by hypoxia (Lopez-Barneo *et al.*, 1988; Lopez-Lopez *et al.*, 1989; Lopez-Lopez *et al.*, 1997). In rabbit glomus cells, however, hypoxia-induced inhibition (Montoro *et al.*, 1996) as well as enhancement (Summers *et al.*, 2000) of voltage-gated Ca^{2+} currents have also been reported.

1.3.2 Heme-containing proteins as primary O_2 sensors in glomus cells

The literature suggests that some heme-containing proteins, including mitochondrial cytochromes and some non-mitochondrial enzymes, may be the O_2 sensors in the carotid glomus cells.

1.3.2.1 Mitochondrial cytochromes

Early studies suggested that some mitochondrial cytochromes were the O_2 sensors in glomus cells. In rabbit glomus cells, there are two types of cytochrome a3 in the mitochondria; one type that has low affinity to O_2 (50% of this type is reduced when pO_2 is ~90 mm Hg) and another type has high affinity to O_2 (this type is not reduced until pO_2 is near 0 mmHg) (Mills & Jobsis, 1972). In glomus cells, when pO_2 is lower than 60 mmHg, the ratio of mitochondrial $NAD(P)H/NAD(P)^+$ is increased and this ratio increases with the severity of hypoxia (Duchen & Biscoe, 1992a). In contrast, in other cell types such as chromaffin cells and dorsal root ganglion neurons, an increase in the ratio of mitochondrial $NAD(P)H/NAD(P)^+$ can be detected only with pO_2 <5 mm Hg (Duchen & Biscoe, 1992a). A higher sensitivity of the mitochondria in glomus cells to hypoxia was further supported by the finding that glomus cells, but not the neurons from cervical and nodose ganglia, expressed cytochrome a592 which has low affinity to O_2 (Streller *et al.*, 2002). Moreover, inhibition of mitochondrial oxidative phosphorylation (with mitochondrial uncouplers or blockers of specific complexes in the respiratory chain) was reported to cause membrane depolarization and $[Ca^{2+}]_i$ elevation in glomus cells (Duchen & Biscoe, 1992b; Wyatt & Buckler, 2004), transmitter release from the carotid body (Ortega-Saenz

et al., 2003) and stimulation of the CSN (Mulligan *et al.*, 1981). These findings suggest that mitochondria are the primary O_2 sensors which couple hypoxia to the electrical excitability of glomus cells.

The link between mitochondria and the oxygen-sensitive K^+ channels in glomus cells is not well understood. Reactive oxygen species (ROS) as well as ATP have been suggested to be possible candidates. Hypoxia was reported to increase mitochondrial ROS production (mainly from complex III of the electron transport chain) in Hep 3B cell line (Chandel & Schumacker, 2000), but the role of ROS as the O_2 sensor in glomus cells has been disputed (Gonzalez *et al.*, 2010; Peers *et al.*, 2010). For instance, both mitochondrial inhibitors (e.g. cyanide and antimycin A) that increase mitochondrial ROS production and mitochondrial uncouplers (e.g. FCCP) that reduce mitochondrial ROS production can cause membrane depolarization and $[Ca^{2+}]_i$ elevation in glomus cells (Wyatt & Buckler, 2004). Pretreatment of the rabbit carotid bodies with the ROS scavengers N-acetyl-L-cysteine (NAC) or reduced glutathione (GSH) did not change the amount of the hypoxia-evoked catecholamine release from the carotid bodies (Sanz-Alfayate *et al.*, 2001; Gonzalez *et al.*, 2004). Moreover, Agapito *et al.* found discrepant results about the effect of the oxidizing agents on the hypoxia-evoked catecholamine release from rabbit carotid bodies: the release was enhanced by 2,2′-dithiodipyridine (DTDP) and unaffected by oxidized gluthtathione (GSSG) (Agapito *et al.*, 2009), suggesting that the redox state of glomus cells is not correlated with the hypoxic response of the carotid body. On the other hand, inhibitors of mitochondrial oxidative phosphorylation were found to inhibit

TASK-like K^+ channels in rat glomus cells (Wyatt & Buckler, 2004; Buckler, 2007). In patches of membrane obtained with the inside-out configuration, TASK-like K^+ channels could be activated by adding MgATP (EC_{50} = 2.3 mM) to the cytosolic side of the patch (Williams & Buckler, 2004; Varas *et al.*, 2007). These findings raise the possibility that a decrease in the level of cytosolic ATP during hypoxia leads to the inhibition of TASK-like K^+ channels and thus depolarization of glomus cell (Varas *et al.*, 2007). However, the precise mechanism remains unclear.

1.3.2.2 Non-mitochondrial heme-containing enzymes as O_2 sensors

Several non-mitochondrial heme-containing enzymes have been suggested to be the primary O_2 sensors in glomus cells of the carotid body, including nicotinamide adenine dinucleotide phosphate (NADPH) oxidase (NOX) (Weir & Archer, 1995; Gonzalez *et al.*, 2010), hemoxygenase (HO) (Prabhakar & Semenza, 2012; Prabhakar, 2012a) and nitric oxide synthase (NOS) (Prabhakar & Semenza, 2012).

NOX is a heme-containing enzyme that transfers electrons to O_2 to form superoxide anion which is then converted to other members of ROS such as hydrogen peroxide (H_2O_2) (Bedard & Krause, 2007). There are seven types of NOX including NOX1-5 and DUOX1-2 (Bedard & Krause, 2007). The mRNAs for NOX1, 2, 3 and 4 have been found in the rat carotid body (Peng *et al.*, 2009). The activity of some K^+ channels such as BK and delayed rectifier K^+ channels can be regulated by the redox state: the channel is open when oxidized and closed

17

when reduced (Weir & Archer, 1995). In rat pulmonary smooth muscle cells (which are sensitive to hypoxia), the whole-cell K^+ current was attenuated by GSH and enhanced by GSSG (Weir & Archer, 1995). In lung neuroepithelial bodies, hypoxia reduced the level of NOX-derived ROS which in turn led to the inhibition of K^+ current (Fu *et al.*, 2000; O'Kelly *et al.*, 2000). These findings raised the possibility that during hypoxia, the reduction of NOX-derived ROS led to the inhibition of O_2-sensitive K^+ channels in glomus cells. Consistent with this, diphenylene iodonium (DPI; an inhibitor of NOX) was reported to inhibit whole-cell K^+ current in isolated rat glomus cells (Wyatt *et al.*, 1994). However, recent findings have disputed the notion of NOX as the O_2 sensor in glomus cells. For example, in rat or rabbit carotid bodies, NOX inhibitors did not affect hypoxia-evoked catecholamine release (Obeso *et al.*, 1999; Obeso *et al.*, 2000). Exogenous application of H_2O_2 also failed to affect hypoxia-evoked Ca^{2+} signals in single rat glomus cells (Wyatt & Buckler, 2004). Nevertheless, studies on NOX deficient mice suggest that NOX-derived ROS may have a regulatory role in the hypoxic signaling of glomus cells (Sanders *et al.*, 2002; He *et al.*, 2005; He *et al.*, 2006). Hypoxia caused a rise in the cellular level of ROS in the glomus cells of wild type mice, but not in the glomus cells isolated from $p47^{phox}$ knockout mice ($p47^{phox}$ protein is one of regulatory subunits of NOX). In addition, the hypoxic response in glomus cells (e.g. inhibition of K^+ current, $[Ca^{2+}]_i$ rise) and the hypoxia-evoked CSN discharge and ventilation were significantly enhanced in $p47^{phox}$ knockout mice. These findings suggest that an elevation in the cellular level of NOX-derived ROS increases the opening of the O_2-sensitive K^+ channels. Thus, an

18

increase in NOX-derived ROS during hypoxia may limit the depolarization evoked by hypoxia.

Hemoxygenase-2 (HO-2) was found in the cytoplasm of rat glomus cells, but not in the sustentacular (type II) cells or the CSN endings (Prabhakar *et al.*, 1995). With NADPH, cytochrome P-450 and O_2 as co-factors, HO catalyzes the degeneration of heme into biliverdin, iron and carbon monoxide (CO) (Shibahara *et al.*, 1985). It has been suggested that HO-2 is the O_2 sensor in glomus cells (Prabhakar *et al.*, 1995; Prabhakar, 2012a). For instance, moderate hypoxia was reported to reduce CO production in rat carotid bodies (Prabhakar, 2012a). Application of a HO inhibitor, zinc-protoporphyrin-9 (ZnPP9), caused an increase in $[Ca^{2+}]_i$ in rat glomus cells and an enhancement of CSN discharge, and these effects could be reversed by exogenous CO (Prabhakar *et al.*, 1995; Overholt *et al.*, 1996). In HO-2 knockout mice, both the basal and the hypoxia-stimulated CSN discharge were enhanced (Prabhakar, 2012a). HO-2 was found to be closely associated with the BK channels and the activity of BK channels was enhanced by CO (Riesco-Fagundo *et al.*, 2001; Williams *et al.*, 2004). These findings suggest that during hypoxia, a reduction in the generation of CO by HO-2 leads to the suppression of BK channels (Prabhakar & Semenza, 2012; Prabhakar, 2012a). However, a role of HO-2 as the O_2 sensor in the carotid body is disputed by the finding that HO-2 knockout did not affect the hypoxia-triggered catecholamine release from carotid body (Ortega-Saenz *et al.*, 2006).

NOS catalyzes the generation of NO from arginine (arginine + O_2 $\leftrightarrow$ citrulline + NO) (Adhikari *et al.*, 2000). There are three isoforms of NOS:

neuronal NOS (nNOS/NOS1), endothenial NOS (eNOS/NOS3) and inducible NOS (iNOS/NOS2) (Prabhakar & Semenza, 2012). Glomus cells express iNOS (Del et $al.$, 2011). In contrast, glomus cells do not express nNOS and eNOS, but nNOS is expressed on the CSN endings and GPN endings (Prabhakar & Overholt, 2000; Campanucci & Nurse, 2005) and eNOS is expressed in the blood vessels of the carotid body (Wang et $al.$, 1994). In nNOS deficient mice, hypoxia-induced increase in respiration was enhanced (Kline et $al.$, 1998). In cats, L-arginine (the NOS substrate) and nitroglycerine (NO donor) inhibited, while a NOS inhibitor (L-NG-nitroarginine methylester) enhanced hypoxia-evoked CSN discharge (Wang et $al.$, 1994; Wang et $al.$, 1995). In addition, it was reported that NO donors could inhibit L-type voltage-gated Ca^{2+} current (Summers et $al.$, 1999) and cause membrane hyperpolarization in the glomus cells (Campanucci et $al.$, 2006). Based on these findings, it was postulated that under normoxia, NO is released from GPN which in turn activates K^{+} channels and inhibits L-type VGCCs in glomus cells (Prabhakar & Semenza, 2012). During hypoxia, NOS activity (which is O_2-dependent) is inhibited, and the decrease in NO production in GPN relieves the suppressive action on glomus cells, thus enhancing the hypoxic response (Prabhakar & Semenza, 2012). Therefore, NOS appears to be involved in the modulation of the hypoxic response of glomus cells, but is not a direct O_2 sensor that initiates the response of glomus cells to hypoxia (Lopez-Barneo, 2003).

1.3.3 AMPK as a primary O_2 sensor in glomus cells

There is growing evidence that AMPK is involved in the coupling of hypoxia to the inhibition of O_2-sensitive K^+ channels in glomus cells (Gonzalez *et al.*, 2010; Peers *et al.*, 2010). AMPK is a serine/threonine kinase with one catalytic α-subunit and two regulatory β- and γ-subunits. When a cell is in metabolic stress (e.g. hypoxia), the rise in the ADP/ATP ratio is converted into an increase in the AMP/ATP ratio by the action of adenylate kinase ($2ADP \leftrightarrow ATP + AMP$) (Hardie *et al.*, 2003; Hawley *et al.*, 2003). AMP binds to the γ-subunit of AMPK which is in turn phosphorylated by an upstream kinase (LKB1). The activated AMPK subsequently activates the downstream signaling pathways which facilitates ATP production and inhibits non-essential ATP consumption in the cell (Kahn *et al.*, 2005; Hardie *et al.*, 2006). Evans *et al.* found that during hypoxia the AMP/ATP ratio was increased and AMPK was activated in pulmonary arterial myocytes, which are also O_2-sensing cells (Evans *et al.*, 2005). They also found that the AMPKα1 subunit was present on the cell membrane of rat glomus cells and 5-aminoimidazole-4-carboxamide-riboside (AICAR), an AMPK activator, stimulated VGCC-dependent rise in $[Ca^{2+}]_i$ in glomus cells and the activation of CSN, mimicking the effects of hypoxia (Evans *et al.*, 2005; Evans *et al.*, 2006). Furthermore, the catalytic AMPKα1 subunit and BK channels were found to be co-localized on the cell membrane of glomus cells (Wyatt *et al.*, 2007). Activation of AMPK (with AICAR) reduced the BK and TASK-like K^+ currents, and inhibition of AMPK (with Compound C) reduced the hypoxia-evoked rise in $[Ca^{2+}]_i$ in rat glomus cells and the hypoxia-evoked increase in CSN discharge (Wyatt *et al.*, 2007; Peers *et al.*, 2010). The inhibition of BK and TASK-like K^+

21

channels by AMPK probably involves direct phosphorylation of the channels (Ross *et al.*, 2011; Evans *et al.*, 2012). Therefore, it has been suggested that during hypoxia, the AMP/ATP ratio is increased due to an impairment of mitochondrial oxidative phosphorylation (Evans *et al.*, 2005). The subsequent activation of AMPK inhibits the O_2-sensitive BK and TASK-like K^+ channels through direct phosphorylation, leading to membrane depolarization and the activation of VGCCs (Peers *et al.*, 2010; Evans *et al.*, 2012).

1.3.4 *H_2S as the O_2 sensor in glomus cells*

H_2S was recently reported to be involved in the mediation of the hypoxic signaling in glomus cells (Peng *et al.*, 2010; Prabhakar, 2012b). Two major enzymes, cystathionine γ-lyase (CSE) and cystathionine β-synthase (CBS), are responsible for the production of endogenous H_2S. CSE has been found in both rat and mouse glomus cells (Li *et al.*, 2010; Peng *et al.*, 2010) and CBS has been found in mouse and cat glomus cells (Li *et al.*, 2010; Fitzgerald *et al.*, 2011). H_2S is degraded into thiosulphate in the mitochondria through several reactions, some of which are O_2-dependent (Buckler, 2012). Therefore, during hypoxia, the degradation of H_2S is expected to be reduced, leading to an increase in H_2S content in the cell. In rats and mice, H_2S production in glomus cells was reported to be significantly increased during hypoxia, and the hypoxic response of the carotid body was attenuated by application of the CSE inhibitor DL-propargylglycine (PAG) and in CSE knockout mice (Peng *et al.*, 2010). In another study, however, application of the CBS inhibitors, but not the CSE inhibitors,

22

prevented the hypoxia-induced excitation of CSN in mice (Li *et al.*, 2010). Thus, the relative contribution of the two enzymes, CBS and CSE, to the hypoxic response remains unclear. Nevertheless, application of NaHS (an H_2S donor) to the rat or mouse carotid bodies enhanced the CSN discharge in a concentration-dependent manner (Li *et al.*, 2010; Peng *et al.*, 2010). It was postulated that H_2S inhibits BK and TASK-like K^+ channels, leading to membrane depolarization and activation of VGCCs (Telezhkin *et al.*, 2009; Li *et al.*, 2010; Telezhkin *et al.*, 2010; Buckler, 2012). However, it is still unclear how H_2S inhibits BK and TASK-like K^+ channels. One possibility is that H_2S inhibits mitochondrial oxidative phosphorylation, leading to the activation of AMPK or reduction of ATP production which in turn reduces the activities of TASK-like K^+ channels (Buckler, 2012). On the other hand, the inhibitory effect of H_2S on BK channels may not be related to mitochondrial function, because application of cyanide was reported to block the inhibitory effect of H_2S on TASK-like K^+ channels in rat glomus cells but not on recombinant BK channels expressed in HEK 293 cells (Telezhkin *et al.*, 2009; Buckler, 2012). Importantly, in some species, H_2S may exert an inhibitory action on hypoxic signaling. In cat carotid body, the application of Na_2S, a H_2S donor, caused the opening of K_{ATP} channels and reduction in transmitter (ACh and ATP) release, suggesting that H_2S generated during hypoxia attenuates the hypoxic response (Fitzgerald *et al.*, 2011).

Interestingly, recent studies suggest that HO-2/CO and CSE/H_2S may be coupled to control the sensory activity of the carotid body (Prabhakar & Semenza, 2012; Prabhakar, 2012a). Application of an HO-2 inhibitor enhanced H_2S

23

generation in the carotid body and increased the basal and hypoxia-evoked CSN discharge in wild type ($CSE^{+\backslash +}$) mice, but not in the CSE knockout ($CSE^{-/-}$) mice (Peng *et al.*, 2010). In addition, an HO-2 inhibitor increased H_2S production in rat carotid bodies under normoxic conditions while a CO donor abolished the hypoxia-induced increase in H_2S production (Peng *et al.*, 2010). These findings suggest that during hypoxia, the inhibition of CO generation causes an enhancement of H_2S production in glomus cells, which in turn stimulates the hypoxic chemotransduction of the carotid body (Peng *et al.*, 2010; Prabhakar, 2012a).

However, the hypothesis that H_2S is directly involved in the hypoxic sensing in glomus cells is challenged. Buckler reported that in isolated rat glomus cells, to evoke a comparable rise in $[Ca^{2+}]_i$ to that seen under hypoxia, ~8 μM exogenous H_2S is needed (Buckler, 2012). Although the endogenous cellular level of H_2S is not clear, it is very unlikely that the $[H_2S]_i$ can rise to ~8 μM under the physiological conditions. This suggests that H_2S may involve in the regulation, not the initiation of the response of the glomus cells to hypoxia (Buckler, 2012).

1.4 The mechanisms of CO_2/pH and glucose sensing in glomus cells

It is generally accepted that the excitation of glomus cells in response to hypercapnia is evoked by cytosolic acidification which is secondary to the hydration of CO_2 (Peers & Buckler, 1995; Kumar & Bin-Jaliah, 2007). In rat glomus cells, cytosolic pH changed rapidly (in seconds) with the changes of pCO_2 in the bath solution (with constant $[HCO_3^-]$): a rise in pCO_2 caused a decrease in

cytosolic pH and a decrease in pCO_2 evoked a rise in cytosolic pH (Buckler *et al.*, 1991a). Similar to hypoxia, hypercapnia evoked an increase in $[Ca^{2+}]_i$ in rat glomus cells via the triggering of membrane depolarization and the activation of VGCCs (Buckler & Vaughan-Jones, 1994a). The hypercapnia-mediated depolarization was due to a reduction in K^+ currents (Buckler & Vaughan-Jones, 1994a; Peers & Buckler, 1995). Two types of K^+ channels were found to be inhibited by hypercapnic acidosis, including the background TASK-like K^+ channels (Buckler *et al.*, 2000) and BK channels (Peers & Green, 1991). In rabbit glomus cells, hypercapnia was found to augment the L-type voltage-gated Ca^{2+} currents via a PKA-dependent mechanism, and interestingly, this effect was not caused by cytosolic acidification (Summers *et al.*, 2002). In addition, extracellular acidosis was reported to activate the Na^+-permeable acid-sensitive ion channels (ASICs) (Tan *et al.*, 2007; Lu *et al.*, 2012) and the pH-sensitive Cl^- channels (Petheo *et al.*, 2001) in rat glomus cells, suggesting that these channels may contribute to the acidosis-induced membrane depolarization and elevation in $[Ca^{2+}]_i$.

In addition to sensing changes in blood pO_2, pCO_2 and pH, glomus cells can also detect low levels of glucose (hypoglycemia). A decrease in extracellular glucose from 5 to 0 mM evoked membrane depolarization, activation of VGCCs (Garcia-Fernandez *et al.*, 2007) and catecholamine release from rat glomus cells (Pardal & Lopez-Barneo, 2002b). However, the link between low extracellular glucose and membrane depolarization in glomus cells is still controversial. Low glucose was found to cause a reduction in the voltage-gated K^+ current in rat

glomus cells and the inhibitory effect was not prevented by the BK channel blocker iberiotoxin (Pardal & Lopez-Barneo, 2002b). However, a subsequent study by the same group found that the inhibition of K^+ current did not contribute to the low glucose-evoked catecholamine release (Garcia-Fernandez *et al.*, 2007). Instead, the activation of a background Na^+ current [possibly involving the transient receptor potential C subtype (TRPC) channels] was found to be the major mechanism contributing to membrane depolarization and catecholamine release evoked by low glucose (Garcia-Fernandez *et al.*, 2007). Moreover, the role of the carotid body as a glucose sensor is not firmly established; low glucose was reported to stimulate sensory discharge in a co-culture of glomus cells and petrosal neurons (Zhang *et al.*, 2007) but failed to increase CSN discharge in intact rat carotid body (Conde *et al.*, 2007).

1.5 Transmitters and their functional role in the chemotransduction of the carotid body

Multiple neurotransmitters, including DA (Urena *et al.*, 1994), ACh (Fitzgerald *et al.*, 1999; Nurse & Zhang, 1999), ATP (Buttigieg & Nurse, 2004), histamine (Koerner *et al.*, 2004) and substance P (Kumar *et al.*, 2000; Kim *et al.*, 2001) are released from glomus cells in response to hypoxia. In addition, some neurotransmitters in glomus cells, including γ-aminobutyric acid (GABA) (Fearon *et al.*, 2003), serotonin (5-hydroxytryptamine, 5-HT) (Oomori *et al.*, 1994; Ramirez *et al.*, 2012) and Ang II (Lam & Leung, 2002) have been shown to modulate the hypoxic chemotransduction of the carotid body.

1.5.1 Biogenic amines and ACh

DA is the predominant form of catecholamines which are synthesized and stored in the dense core granules of glomus cells (Gonzalez *et al.*, 1994). DA was first suggested to be the main excitatory transmitter that mediates hypoxic chemotransduction of the carotid body. This speculation was based on the findings that hypoxia triggered DA release in a Ca^{2+}-dependent manner from intact carotid bodies or single glomus cells in different species (Gonzalez *et al.*, 1994; Urena *et al.*, 1994; Vicario *et al.*, 2000). Moreover, in rabbit or cat carotid bodies, DA synthesis and the CSN discharge increased with hypoxia (Fidone *et al.*, 1982; Rigual *et al.*, 1986). However, later studies found that the hypoxia-induced DA release was not proportional to the changes in CSN discharge (Iturriaga *et al.*, 1996; Donnelly, 1996; Iturriaga & Alcayaga, 1998). Importantly, DA was found to have an inhibitory action on both glomus cells and CSN terminals. In cats, the basal and hypoxia-induced CSN discharge was attenuated by intravenous or intracarotid injection of DA or DA analogues (Llados & Zapata, 1978; Lahiri *et al.*, 1980) but enhanced by the injection of DA antagonists (Lahiri *et al.*, 1980; Iturriaga *et al.*, 1994). In isolated cat petrosal ganglia, DA reduced the ATP-activated CSN discharge (Alcayaga *et al.*, 2003). In glomus cells, the stimulation of D_2 receptors by DA caused a reduction in VGCCs and a decrease in transmitter release, suggesting that DA released from glomus cells may act as a negative feedback regulator (Benot & Lopez-Barneo, 1990; Bairam *et al.*, 2000). DA was also found to cause vasodilation in the carotid body, suggesting that DA

may be involved in the regulation of blood flow in the carotid body (Gonzalez *et al.*, 2010).

ACh was one of the first candidates of excitatory transmitters in the carotid body (Fitzgerald *et al.*, 1999; Nurse & Zhang, 1999). Exogenous ACh or nicotinic agonists were reported to enhance the CSN discharge in different species, including rats, rabbits, cats and mice (Shirahata *et al.*, 2007). Nicotinic ACh receptors (nAChRs) and muscarinic ACh receptors (mAChRs) were found on glomus cells as well as CSN terminals (Wyatt & Peers, 1993; Shirahata *et al.*, 1998; Shirahata *et al.*, 2004; Shirahata *et al.*, 2007). Application of nAChR agonists evoked membrane depolarization and a rise in $[Ca^{2+}]_i$ in rat glomus cells, while application of mAChR agonists triggered intracellular Ca^{2+} release (Wyatt & Peers, 1993; Dasso *et al.*, 1997). In cat glomus cells, application of nAChR agonists, but not mAChR agonists, triggered an elevation in $[Ca^{2+}]_i$ (Shirahata *et al.*, 1997). In rabbit or cat glomus cells, the inhibition of the M1 form of mAChRs reduced both basal and hypoxia-triggered catecholamine release (Bairam *et al.*, 2000; Wang & Fitzgerald, 2002). These findings suggest that ACh may act as a positive feedback regulator for glomus cells. Importantly, in both carotid body and the co-culture model of glomus cell clusters and petrosal neurons, the hypoxia-induced CSN discharge could be partially inhibited by nAChR blockers (Nurse, 2010; Nurse & Piskuric, 2012), suggesting that ACh is an excitatory transmitter, but not the only transmitter released during hypoxia, that triggers CSN discharge.

The role of 5-HT in the chemotransduction of the carotid body is controversial. It was reported that 5-HT exerted its autocrine and paracrine effects on glomus cells via a positive feedback mechanism; application of the 5-HT receptor blocker ketanserin was found to reduce the spontaneous firing activity of rat glomus cells (Zhang & Nurse, 2000). Subsequently, exogenous 5-HT was found to inhibit BK channels in rat glomus cells via the activation of 5-HT$_{2a}$ receptor-protein kinase C (PKC) pathway, resulting in depolarization (Zhang *et al.*, 2003). However, the role of 5-HT is questioned by the finding that acute repetitive hypoxia failed to trigger 5-HT release from isolated rat carotid bodies (Peng *et al.*, 2009). Interestingly, the same study showed that acute repetitive hypoxia stimulated robust 5-HT release from isolated carotid bodies in rats that had been subjected to chronic intermittent hypoxia (Peng *et al.*, 2009), suggesting that 5-HT might be involved in the regulation of the sensitivity of the carotid body exposed to chronic intermittent hypoxia.

The H1-H4 forms of histamine receptors were found in glomus cells and the H1 and H3 forms were found in the CSN terminals (Koerner *et al.*, 2004; Lazarov *et al.*, 2006; Nurse & Piskuric, 2012). It is still controversial whether histamine is an excitatory or inhibitory transmitter in the carotid body. In cat carotid body, histamine increased CSN activity in a dose-dependent manner (Del *et al.*, 2008). However, in rat glomus cells, histamine reduced the mAChR agonist-evoked rise in $[Ca^{2+}]_i$ via H3 receptors, suggesting an inhibitory role of histamine (Thompson *et al.*, 2010).

1.5.2 ATP

At present, ATP is generally accepted to be the major excitatory transmitter (Nurse & Piskuric, 2012). ATP is co-released with ACh from glomus cells (Zhang *et al.*, 2000) and purinergic $P2X_2$ and $P2X_2/P2X_3$ receptors are present on CSN terminals (Zhang *et al.*, 2000; Prasad *et al.*, 2001). In co-cultures of glomus cells and petrosal neurons as well as in intact carotid body, P2X receptor blockers suppressed the increase in CSN discharge induced by hypoxia, hypercapnia or low glucose (Zhang *et al.*, 2000; Zhang & Nurse, 2004; Zhang *et al.*, 2007). Moreover, in $P2X_2$ or $P2X_2/P2X_3$ knockout mice, hypoxia failed to trigger respiratory responses (Rong *et al.*, 2003). Other than the excitatory effect of ATP on the CSN, previous studies in our laboratory suggest that ATP influences glomus cells and sustentacular cells via autocrine and paracrine actions. ATP, acting via $P2Y_1$ receptors, inhibited the hypoxia-evoked rise in $[Ca^{2+}]_i$ in rat glomus cells by reversing the hypoxia-induced membrane depolarization (Xu *et al.*, 2005). ATP also triggered intracellular Ca^{2+} release in single rat sustentacular cells via $P2Y_2$ receptors (Xu *et al.*, 2003). Moreover, adenosine, an ATP metabolite, acting via the A_{2A} receptor-PKA pathway caused membrane depolarization and activation of voltage-gated Ca^{2+} entry in rat glomus cells (Xu *et al.*, 2006). We speculated that during hypoxia, the autocrine/paracrine actions of ATP and adenosine may lead to an oscillatory Ca^{2+} signal in glomus cells which involves the following sequence of events (Tse *et al.*, 2012). Hypoxia triggers VGCC-mediated $[Ca^{2+}]_i$ rise and subsequent ATP release. ATP in turn acts on glomus cells, leading to membrane hyperpolarization and the inhibition of

hypoxia-triggered rise in $[Ca^{2+}]_i$. As a result, ATP release is terminated and the extracellular [ATP] decreases. The conversion of the released ATP into adenosine leads to a subsequent rise in the extracellular [adenosine], which in turn activates VGCCs and aids in the recovery of the hypoxia-triggered rise in $[Ca^{2+}]_i$. The rise in $[Ca^{2+}]_i$ triggers ATP release and evokes another cycle of Ca^{2+} signal oscillation. This mechanism ensures that glomus cells can continue to release transmitters while avoiding the cellular damage arising from a sustained $[Ca^{2+}]_i$ rise (Tse *et al.*, 2012).

1.5.3 GABA

GABA inhibits chemotransduction of the carotid body by affecting both glomus cells and postsynaptic CSN terminals (Nurse & Piskuric, 2012). In rat glomus cells, GABA, acting via $GABA_B$ receptors and G_i-proteins, reduced the hypoxia-triggered membrane depolarization by increasing the activities of TASK-like K^+ channels, suggesting that GABA is involved in autocrine and paracrine negative feedback regulation on glomus cells (Fearon *et al.*, 2003). On the other hand, inhibition of CSN by GABA was found to be mediated via $GABA_A$ receptors (Zhang *et al.*, 2009). Application of a GABA agonist (midazolam) reduced the basal and hypoxia-induced CSN discharge in rabbit carotid body (Kim *et al.*, 2006) and exogenous GABA reversed the ATP-induced membrane depolarization in isolated rat petrosal neurons (Zhang *et al.*, 2009).

1.5.4 Peptides

The glomus cells were found to have an intrinsic angiotensin (Ang)-generating system and Ang II can be synthesized locally via a renin-independent biosynthetic pathway (Lam & Leung, 2002). The production of endogenous Ang II was implicated in the increase in the hypoxic sensitivity of glomus cells upon chronic hypoxia (Leung *et al.*, 2003; Li *et al.*, 2006; Peng *et al.*, 2011). Application of Ang II evoked an increase in $[Ca^{2+}]_i$ in glomus cells (Fung *et al.*, 2001) and increased CSN discharge via AT1 receptors (Allen, 1998).

Substance P is another peptide released from glomus cells during hypoxia and is also present in the nerve fibers (Kumar *et al.*, 2000; Kim *et al.*, 2001). The literature has shown that substance P can stimulate the carotid bodies in several species such as rats and cats but intracarotid application of substance P inhibited ventilation in goats (Cragg *et al.*, 1994; Pizarro *et al.*, 1995; Kumar *et al.*, 2000).

The above findings suggest that under hypoxic conditions the peptides including Ang II and substance P released from glomus cells mainly play a positive feedback role on the activity to the glomus cells in several species except goats.

1.5.5 Interaction of multiple transmitters in the carotid body

In summary, during hypoxia, glomus cells of the carotid body not only release excitatory transmitters such as ATP and ACh, but also release some inhibitory transmitters such as GABA and DA, that act on the "sensory" nerve

32

terminals of the CSN. Importantly, many transmitters, including ATP and ACh also modulate the activity of glomus cells via autocrine and paracrine signaling pathways. Prabhakar (2006) suggested that a 'push-pull' mechanism may account for the slow adaptation of the carotid body to hypoxia (the increase in CSN activity can be sustained through the entire duration of hypoxia). It is postulated that the negative feedback mechanisms can prevent the overexcitation of the carotid body, thus ensuring a longer response to hypoxia or other stimuli (Prabhakar, 2006).

1.6 Objectives of my thesis

It is well known that the activation of the CSN is initiated by the Ca^{2+}-dependent release of transmitters from glomus cells. Changes in the amplitude or the duration of the Ca^{2+} signal can have a dramatic impact on transmitter release from glomus cells. However, the mechanisms underlying the regulation of Ca^{2+} dynamics in glomus cells are not well understood. This thesis focuses on the regulation of Ca^{2+} homeostasis in glomus cells of rat carotid body.

In the first project (chapter 3), I investigated the relative contribution of several major cytosolic Ca^{2+} clearance mechanisms in the regulation of Ca^{2+} homeostasis in rat glomus cells. These mechanisms include the sarco/endoplasmic reticulum Ca^{2+}-ATPase (SERCA) pump, mitochondria, Na^+/Ca^{2+} exchanger (NCX) and plasma membrane Ca^{2+}-ATPase (PMCA) pump. My findings indicate that mitochondrial Ca^{2+} uptake is the dominant mechanism of cytosolic Ca^{2+} clearance in glomus cells.

In the second project (chapter 4), I investigated the role of extracellular HCO_3^- in the regulation of Ca^{2+} signals. Glomus cells express several HCO_3^- transporters, including the Na^+/HCO_3^- cotransporter, HCO_3^-/Cl^- exchanger (Buckler *et al.*, 1991b) as well as an anion channel (Stea & Nurse, 1989) which is permeable to both Cl^- and HCO_3^-. The Na^+/HCO_3^- cotransporter and the HCO_3^- /Cl^- exchanger have been shown to have important roles in the regulation of the cytosolic pH of glomus cells (Buckler *et al.*, 1991b). Other than pH regulation, transmembrane HCO_3^- also appears to be important for hypoxic signaling. In the absence of extracellular HCO_3^-, moderate hypoxia failed to trigger CSN activity in the rat carotid body (Panisello & Donnelly, 1998). My findings indicate that extracellular HCO_3^- reduces mitochondrial Ca^{2+} uptake in glomus cells via a mechanism that is dependent on ROS, suggesting that the potentiation of hypoxic chemotransduction of the carotid body at physiological concentrations of extracellular HCO_3^- is related to a slowing in the rate of cytosolic Ca^{2+} clearance in glomus cells.
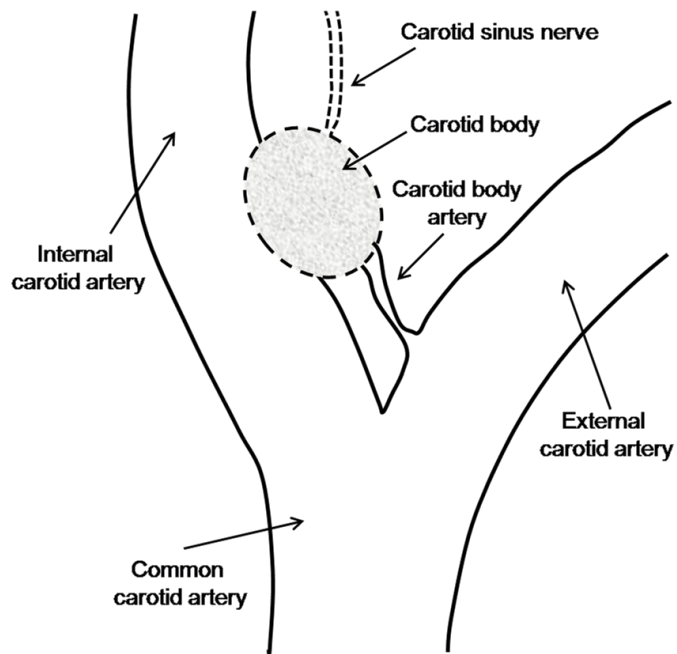
Fig. 1-1: A drawing of the location of the carotid body. The carotid body is a peripheral chemoreceptor which is located near the site where the common carotid artery bifurcates into the internal and external carotid arteries.
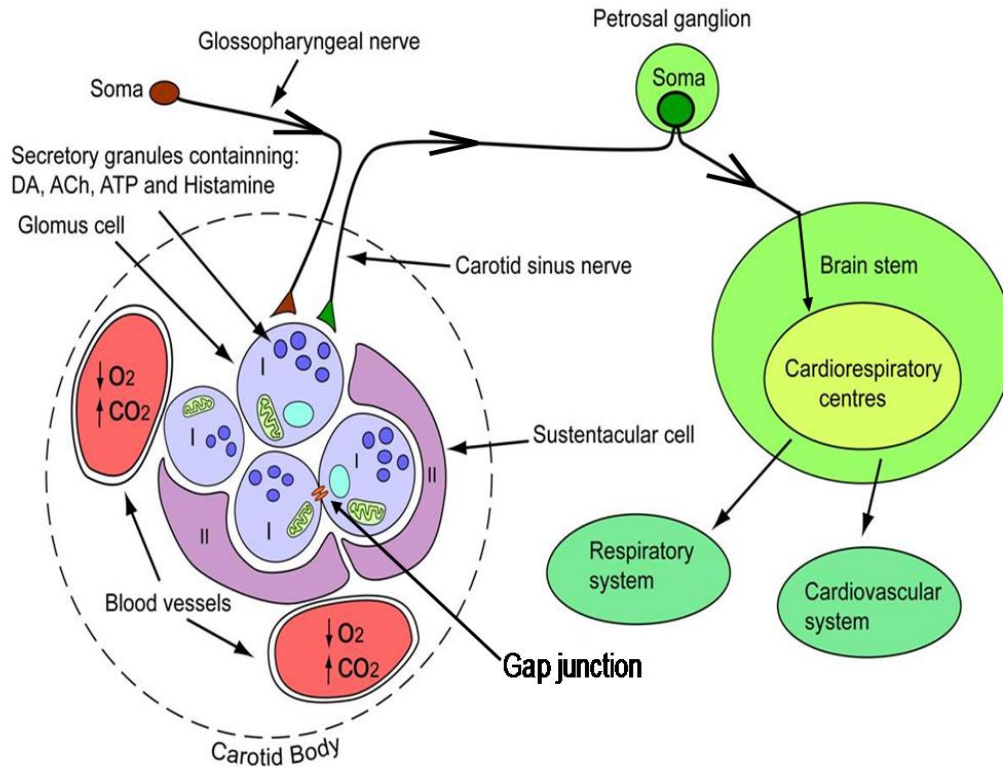
Fig. 1-2: Chemosensory transduction in the carotid body. There are four components in the carotid body: type I (glomus) cells, type II (sustentacular) cells, nerve endings (afferents of CSN and efferents of the glossopharyngeal nerve) and blood vessels. A decrease in arterial pO_2 or an increase in pCO_2 triggers transmitter release from glomus cells. Some of these transmitters excite the CSN which in turn triggers respiratory and cardiovascular reflexes via the cardiorespiratory center in the brain stem. This figure is modified from the Ph.D. thesis of a previous student, Fenglian Xu, in our laboratory.

Table 1-1 Ion channels in glomus cells

Channel type	Species	Reference
Na$^+$ channel		
Voltage-gated	Rabbit	(Lopez-Barneo *et al.*, 1988; Lopez-Lopez *et al.*, 1989)
	Rat *	(Stea & Nurse, 1991b; Fieber & McCleskey, 1993)
Background	Rat	(Carpenter & Peers, 2001)
VGCC		
L-, N-, P/Q-, and R-type	Rabbit	(Overholt & Prabhakar, 1997)
L- and N-type	Rat	(Fieber & McCleskey, 1993; Silva & Lewis, 1995; Peers *et al.*, 1996)
K$^+$ channels		
4-AP-sensitive, A-type	Rabbit	(Lopez-Lopez *et al.*, 1993; Perez-Garcia *et al.*, 2000; Sanchez *et al.*, 2002)
	Rat	(Vandier *et al.*, 1999)
Delayed rectifier	Rabbit	(Lopez-Lopez *et al.*, 1993)
	Rat	(Lopez-Lopez *et al.*, 1997)
BK	Rabbit	(Ganfornina & Lopez-Barneo, 1992)
	Rat	(Peers, 1990; Wyatt & Peers, 1995)
HERG-like	Rabbit	(Overholt *et al.*, 2000a; Overholt *et al.*, 2000b)
	Rat	(Kim *et al.*, 2005)
TASK-like	Rat	(Buckler, 1997; Buckler, 1999; Buckler *et al.*, 2000)
TREK	Rat	(Yamamoto *et al.*, 2002; Yamamoto & Taniguchi, 2006)
Cl$^-$ channel		
Large conductance voltage- independent and 9-AC-sensitive	Rat	(Stea & Nurse, 1989; Stea & Nurse, 1991a)
pH- and 9-AC-sensitive hyperpolarization-activated	Rat	(Petheo *et al.*, 2001)
Swelling- and cAMP-activated	Rat	(Carpenter & Peers, 1997)

*low density or absence

Table 1-2 O_2 sensors in glomus cells of the carotid body

O_2 sensors	Species	Reference
O_2-sensitive K^+ channels		
Delayed rectifier	Rabbit	(Lopez-Lopez *et al.*, 1989; Lopez-Lopez *et al.*, 1993)
A-type	Rabbit	Ganfornina & Lopez-Barneo, 1992;Lopez-Lopez *et al.*, 1993;Perez-Garcia *et al.*, 2000;Sanchez *et al.*, 2002
HERG-like	Rabbit	(Overholt *et al.*, 2000a; Overholt *et al.*, 2000b)
BK	Rat	(Buckler, 1997)
TASK-like	Rat	(Wyatt & Peers, 1995)
Heme-containing proteins		
cytochrome a3/a592	Cat/Rat	(Mills & Jobsis, 1972; Streller *et al.*, 2002)
NOX	Rat	(Wyatt *et al.*, 1994; Peng *et al.*, 2009)
	Mouse	(Sanders *et al.*, 2002; He *et al.*, 2005; He *et al.*, 2006)
HO-2	Rat	(Prabhakar *et al.*, 1995; Overholt *et al.*, 1996)
NOS	Mouse	(Kline *et al.*, 1998)
	Cat	(Wang *et al.*, 1994; Wang *et al.*, 1995)
	Rat	(Campanucci *et al.*, 2006)
AMPK	Rat	(Evans *et al.*, 2005; Evans *et al.*, 2006; Wyatt *et al.*, 2007; Peers *et al.*, 2010)
H_2S	Mouse	(Li *et al.*, 2010; Peng *et al.*, 2010)
	Rat	(Telezhkin *et al.*, 2010; Peng *et al.*, 2010; Buckler, 2012)

Reference List

Abudara V & Eyzaguirre C (1998). Modulation of junctional conductance between rat carotid body glomus cells by hypoxia, cAMP and acidity. *Brain Res* **792**, 114-125.

Adhikari S, Ray S, & Gachhui R (2000). Catalase activity of oxygenase domain of rat neuronal nitric oxide synthase. Evidence for product formation from L-arginine. *FEBS Lett* **475**, 35-38.

Agapito MT, Sanz-Alfayate G, Gomez-Nino A, Gonzalez C, & Obeso A (2009). General redox environment and carotid body chemoreceptor function. *Am J Physiol Cell Physiol* **296**, C620-C631.

Alcayaga J, Retamal M, Cerpa V, Arroyo J, & Zapata P (2003). Dopamine inhibits ATP-induced responses in the cat petrosal ganglion in vitro. *Brain Res* **966**, 283-287.

Alcayaga J, Varas R, Arroyo J, Iturriaga R, & Zapata P (1999). Responses to hypoxia of petrosal ganglia in vitro. *Brain Res* **845**, 28-34.

Allen AM (1998). Angiotensin AT1 receptor-mediated excitation of rat carotid body chemoreceptor afferent activity. *J Physiol* **510 (Pt 3)**, 773-781.

Bairam A, Neji H, De-Grandpre P, & Carroll JL (2000). Autoreceptor mechanism regulating carotid body dopamine release from adult and 10-day-old rabbits. *Respir Physiol* **120**, 27-34.

Bedard K & Krause KH (2007). The NOX family of ROS-generating NADPH oxidases: physiology and pathophysiology. *Physiol Rev* **87**, 245-313.

Benot AR & Lopez-Barneo J (1990). Feedback Inhibition of Ca^{2+} Currents by Dopamine in Glomus Cells of the Carotid Body. *Eur J Neurosci* **2**, 809-812.

Buckler KJ (1997). A novel oxygen-sensitive potassium current in rat carotid body type I cells. *J Physiol* **498 (Pt 3)**, 649-662.

Buckler KJ (1999). Background leak K^+-currents and oxygen sensing in carotid body type 1 cells. *Respir Physiol* **115**, 179-187.

Buckler KJ (2007). TASK-like potassium channels and oxygen sensing in the carotid body. *Respir Physiol Neurobiol* **157**, 55-64.

Buckler KJ (2010). Two-pore domain K(+) channels and their role in chemoreception. *Adv Exp Med Biol* **661**, 15-30.

Buckler KJ (2012). Effects of exogenous hydrogen sulphide on calcium signalling, background (TASK) K channel activity and mitochondrial function in chemoreceptor cells. *Pflugers Arch* **463**, 743-754.

Buckler KJ & Honore E (2005). The lipid-activated two-pore domain K^+ channel TREK-1 is resistant to hypoxia: implication for ischaemic neuroprotection. *J Physiol* **562**, 213-222.

Buckler KJ & Vaughan-Jones RD (1994a). Effects of hypercapnia on membrane potential and intracellular calcium in rat carotid body type I cells. *J Physiol* **478 (Pt 1)**, 157-171.

Buckler KJ & Vaughan-Jones RD (1994b). Effects of hypoxia on membrane potential and intracellular calcium in rat neonatal carotid body type I cells. *J Physiol* **476**, 423-428.

Buckler KJ, Vaughan-Jones RD, Peers C, Lagadic-Gossmann D, & Nye PC (1991a). Effects of extracellular pH, PCO_2 and. *J Physiol* **444**, 703-721.

Buckler KJ, Vaughan-Jones RD, Peers C, & Nye PC (1991b). Intracellular pH and its regulation in isolated type I carotid body cells of the neonatal rat. *J Physiol* **436**, 107-129.

Buckler KJ, Williams BA, & Honore E (2000). An oxygen-, acid- and anaesthetic-sensitive TASK-like background potassium channel in rat arterial chemoreceptor cells. *J Physiol* **525 Pt 1**, 135-142.

Buttigieg J & Nurse CA (2004). Detection of hypoxia-evoked ATP release from chemoreceptor cells of the rat carotid body. *Biochem Biophys Res Commun* **322**, 82-87.

Caley AJ, Gruss M, & Franks NP (2005). The effects of hypoxia on the modulation of human TREK-1 potassium channels. *J Physiol* **562**, 205-212.

Campanucci VA, Fearon IM, & Nurse CA (2003). A novel O_2-sensing mechanism in rat glossopharyngeal neurones mediated by a halothane-inhibitable background K^+ conductance. *J Physiol* **548**, 731-743.

Campanucci VA & Nurse CA (2005). Biophysical characterization of whole-cell currents in O_2-sensitive neurons from the rat glossopharyngeal nerve. *Neuroscience* **132**, 437-451.

Campanucci VA, Zhang M, Vollmer C, & Nurse CA (2006). Expression of multiple P2X receptors by glossopharyngeal neurons projecting to rat carotid body O_2-chemoreceptors: role in nitric oxide-mediated efferent inhibition. *J Neurosci* **26**, 9482-9493.

Carpenter E & Peers C (1997). Swelling- and cAMP-activated Cl^- currents in isolated rat carotid body type I cells. *J Physiol* **503 (Pt 3)**, 497-511.

Carpenter E & Peers C (2001). A standing Na^+ conductance in rat carotid body type I cells. *Neuroreport* **12**, 1421-1425.

Chandel NS & Schumacker PT (2000). Cellular oxygen sensing by mitochondria: old questions, new insight. *J Appl Physiol* **88**, 1880-1889.

Cheng PM & Donnelly DF (1995). Relationship between changes of glomus cell current and neural response of rat carotid body. *J Neurophysiol* **74**, 2077-2086.

Conde SV, Obeso A, & Gonzalez C (2007). Low glucose effects on rat carotid body chemoreceptor cells' secretory responses and action potential frequency in the carotid sinus nerve. *J Physiol* **585**, 721-730.

Cragg PA, Runold M, Kou YR, & Prabhakar NR (1994). Tachykinin antagonists in carotid body responses to hypoxia and substance P in the rat. *Respir Physiol* **95**, 295-310.

Dasso LL, Buckler KJ, & Vaughan-Jones RD (1997). Muscarinic and nicotinic receptors raise intracellular Ca^{2+} levels in rat carotid body type I cells. *J Physiol* **498 (Pt 2)**, 327-338.

Del RR, Moya EA, & Iturriaga R (2011). Differential expression of pro-inflammatory cytokines, endothelin-1 and nitric oxide synthases in the rat carotid body exposed to intermittent hypoxia. *Brain Res* **1395**, 74-85.

Del RR, Moya EA, Koenig CS, Fujiwara K, Alcayaga J, & Iturriaga R (2008). Modulatory effects of histamine on cat carotid body chemoreception. *Respir Physiol Neurobiol* **164**, 401-410.

Donnelly DF (1996). Chemoreceptor nerve excitation may not be proportional to catecholamine secretion. *J Appl Physiol* **81**, 657-664.

Doyle TP & Donnelly DF (1994). Effect of Na^+ and K^+ channel blockade on baseline and anoxia-induced catecholamine release from rat carotid body. *J Appl Physiol* **77**, 2606-2611.

Duchen MR & Biscoe TJ (1992a). Mitochondrial function in type I cells isolated from rabbit arterial chemoreceptors. *J Physiol* **450**, 13-31.

Duchen MR & Biscoe TJ (1992b). Relative mitochondrial membrane potential and $[Ca^{2+}]_i$ in type I cells isolated from the rabbit carotid body. *J Physiol* **450**, 33-61.

Evans AM, Hardie DG, Galione A, Peers C, Kumar P, & Wyatt CN (2006). AMP-activated protein kinase couples mitochondrial inhibition by hypoxia to

cell-specific Ca^{2+} signalling mechanisms in oxygen-sensing cells. *Novartis Found Symp* **272**, 234-252.

Evans AM, Mustard KJ, Wyatt CN, Peers C, Dipp M, Kumar P, Kinnear NP, & Hardie DG (2005). Does AMP-activated protein kinase couple inhibition of mitochondrial oxidative phosphorylation by hypoxia to calcium signaling in O_2-sensing cells? *J Biol Chem* **280**, 41504-41511.

Evans AM, Peers C, Wyatt CN, Kumar P, & Hardie DG (2012). Ion channel regulation by the LKB1-AMPK signalling pathway: The key to carotid body activation by hypoxia and metabolic homeostasis at the whole body level. *Adv Exp Med Biol* **758**, 81-90.

Fearon IM, Zhang M, Vollmer C, & Nurse CA (2003). GABA mediates autoreceptor feedback inhibition in the rat carotid body via presynaptic GABAB receptors and TASK-1. *J Physiol* **553**, 83-94.

Fidone S, Gonzalez C, & Yoshizaki K (1982). Effects of hypoxia on catecholamine synthesis in rabbit carotid body in vitro. *J Physiol* **333**, 81-91.

Fieber LA & McCleskey EW (1993). L-type calcium channels in type I cells of the rat carotid body. *J Neurophysiol* **70**, 1378-1384.

Fitzgerald RS, Shirahata M, Chang I, Kostuk E, & Kiihl S (2011). The impact of hydrogen sulfide (H(2)S) on neurotransmitter release from the cat carotid body. *Respir Physiol Neurobiol* **176**, 80-89.

Fitzgerald RS, Shirahata M, & Wang HY (1999). Acetylcholine release from cat carotid bodies. *Brain Res* **841**, 53-61.

Fletcher EC (2001). Invited review: Physiological consequences of intermittent hypoxia: systemic blood pressure. *J Appl Physiol* **90**, 1600-1605.

Fletcher EC, Lesske J, Behm R, Miller CC, III, Stauss H, & Unger T (1992). Carotid chemoreceptors, systemic blood pressure, and chronic episodic hypoxia mimicking sleep apnea. *J Appl Physiol* **72**, 1978-1984.

Fu XW, Wang D, Nurse CA, Dinauer MC, & Cutz E (2000). NADPH oxidase is an O_2 sensor in airway chemoreceptors: evidence from K^+ current modulation in wild-type and oxidase-deficient mice. *Proc Natl Acad Sci U S A* **97**, 4374-4379.

Fung ML, Lam SY, Chen Y, Dong X, & Leung PS (2001). Functional expression of angiotensin II receptors in type-I cells of the rat carotid body. *Pflugers Arch* **441**, 474-480.

Ganfornina MD & Lopez-Barneo J (1992). Potassium channel types in arterial chemoreceptor cells and their selective modulation by oxygen. *J Gen Physiol* **100**, 401-426.

Garcia-Fernandez M, Ortega-Saenz P, Castellano A, & Lopez-Barneo J (2007). Mechanisms of low-glucose sensitivity in carotid body glomus cells. *Diabetes* **56**, 2893-2900.

Gonzalez C, Agapito MT, Rocher A, Gomez-Nino A, Rigual R, Castaneda J, Conde SV, & Obeso A (2010). A revisit to O_2 sensing and transduction in the carotid body chemoreceptors in the context of reactive oxygen species biology. *Respir Physiol Neurobiol* **174**, 317-330.

Gonzalez C, Almaraz L, Obeso A, & Rigual R (1992). Oxygen and acid chemoreception in the carotid body chemoreceptors. *Trends Neurosci* **15**, 146-153.

Gonzalez C, Almaraz L, Obeso A, & Rigual R (1994). Carotid body chemoreceptors: from natural stimuli to sensory discharges. *Physiol Rev* **74**, 829-898.

Gonzalez C, Sanz-Alyayate G, Agapito MT, & Obeso A (2004). Effects of reducing agents on glutathione metabolism and the function of carotid body chemoreceptor cells. *Biol Chem* **385**, 265-274.

Hardie DG, Hawley SA, & Scott JW (2006). AMP-activated protein kinase--development of the energy sensor concept. *J Physiol* **574**, 7-15.

Hardie DG, Scott JW, Pan DA, & Hudson ER (2003). Management of cellular energy by the AMP-activated protein kinase system. *FEBS Lett* **546**, 113-120.

Hawley SA, Boudeau J, Reid JL, Mustard KJ, Udd L, Makela TP, Alessi DR, & Hardie DG (2003). Complexes between the LKB1 tumor suppressor, STRAD alpha/beta and MO25 alpha/beta are upstream kinases in the AMP-activated protein kinase cascade. *J Biol* **2**, 28.

He L, Dinger B, Gonzalez C, Obeso A, & Fidone S (2006). Function of NADPH oxidase and signaling by reactive oxygen species in rat carotid body type I cells. *Adv Exp Med Biol* **580**, 155-160.

He L, Dinger B, Sanders K, Hoidal J, Obeso A, Stensaas L, Fidone S, & Gonzalez C (2005). Effect of p47phox gene deletion on ROS production and oxygen sensing in mouse carotid body chemoreceptor cells. *Am J Physiol Lung Cell Mol Physiol* **289**, L916-L924.

Iturriaga R & Alcayaga J (1998). Effects of CO_2-HCO_3^- on catecholamine efflux from cat carotid body. *J Appl Physiol* **84**, 60-68.

Iturriaga R, Alcayaga J, & Zapata P (1996). Dissociation of hypoxia-induced chemosensory responses and catecholamine efflux in cat carotid body superfused in vitro. *J Physiol* **497 (Pt 2)**, 551-564.

Iturriaga R, Larrain C, & Zapata P (1994). Effects of dopaminergic blockade upon carotid chemosensory activity and its hypoxia-induced excitation. *Brain Res* **663**, 145-154.

Joseph V & Pequignot JM (2009). Breathing at high altitude. *Cell Mol Life Sci* **66**, 3565-3573.

Kahn BB, Alquier T, Carling D, & Hardie DG (2005). AMP-activated protein kinase: ancient energy gauge provides clues to modern understanding of metabolism. *Cell Metab* **1**, 15-25.

Kim C, Shvarev Y, Takeda S, Sakamoto A, Lindahl SG, & Eriksson LI (2006). Midazolam depresses carotid body chemoreceptor activity. *Acta Anaesthesiol Scand* **50**, 144-149.

Kim D, Cavanaugh EJ, Kim I, & Carroll JL (2009). Heteromeric TASK-1/TASK-3 is the major oxygen-sensitive background K^+ channel in rat carotid body glomus cells. *J Physiol* **587**, 2963-2975.

Kim DK, Oh EK, Summers BA, Prabhakar NR, & Kumar GK (2001). Release of substance P by low oxygen in the rabbit carotid body: evidence for the involvement of calcium channels. *Brain Res* **892**, 359-369.

Kim I, Boyle KM, & Carroll JL (2005). Postnatal development of E-4031-sensitive potassium current in rat carotid chemoreceptor cells. *J Appl Physiol* **98**, 1469-1477.

Kline DD, Yang T, Huang PL, & Prabhakar NR (1998). Altered respiratory responses to hypoxia in mutant mice deficient in neuronal nitric oxide synthase. *J Physiol* **511 (Pt 1)**, 273-287.

Koerner P, Hesslinger C, Schaefermeyer A, Prinz C, & Gratzl M (2004). Evidence for histamine as a transmitter in rat carotid body sensor cells. *J Neurochem* **91**, 493-500.

Kreneisz O, Benoit JP, Bayliss DA, & Mulkey DK (2009). AMP-activated protein kinase inhibits TREK channels. *J Physiol* **587**, 5819-5830.

Kumar GK, Kou YR, Overholt JL, & Prabhakar NR (2000). Involvement of substance P in neutral endopeptidase modulation of carotid body sensory responses to hypoxia. *J Appl Physiol* **88**, 195-202.

Kumar P (2009). Systemic effects resulting from carotid body stimulation-invited article. *Adv Exp Med Biol* **648**, 223-233.

Kumar P & Bin-Jaliah I (2007). Adequate stimuli of the carotid body: more than an oxygen sensor? *Respir Physiol Neurobiol* **157**, 12-21.

Lahiri S, Nishino T, Mokashi A, & Mulligan E (1980). Interaction of dopamine and haloperidol with O_2 and CO_2 chemoreception in carotid body. *J Appl Physiol* **49**, 45-51.

Lam SY & Leung PS (2002). A locally generated angiotensin system in rat carotid body. *Regul Pept* **107**, 97-103.

Lazarov N, Rozloznik M, Reindl S, Rey-Ares V, Dutschmann M, & Gratzl M (2006). Expression of histamine receptors and effect of histamine in the rat carotid body chemoafferent pathway. *Eur J Neurosci* **24**, 3431-3444.

Lesage F, Guillemare E, Fink M, Duprat F, Lazdunski M, Romey G, & Barhanin J (1996a). TWIK-1, a ubiquitous human weakly inward rectifying K^+ channel with a novel structure. *EMBO J* **15**, 1004-1011.

Lesage F, Reyes R, Fink M, Duprat F, Guillemare E, & Lazdunski M (1996b). Dimerization of TWIK-1 K^+ channel subunits via a disulfide bridge. *EMBO J* **15**, 6400-6407.

Leung PS, Fung ML, & Tam MS (2003). Renin-angiotensin system in the carotid body. *Int J Biochem Cell Biol* **35**, 847-854.

Li Q, Sun B, Wang X, Jin Z, Zhou Y, Dong L, Jiang LH, & Rong W (2010). A crucial role for hydrogen sulfide in oxygen sensing via modulating large conductance calcium-activated potassium channels. *Antioxid Redox Signal* **12**, 1179-1189.

Li YL, Xia XH, Zheng H, Gao L, Li YF, Liu D, Patel KP, Wang W, & Schultz HD (2006). Angiotensin II enhances carotid body chemoreflex control of sympathetic outflow in chronic heart failure rabbits. *Cardiovasc Res* **71**, 129-138.

Llados F & Zapata P (1978). Effects of dopamine analogues and antagonists on carotid body chemosensors in situ. *J Physiol* **274**, 487-499.

Lopez-Barneo J (2003). Oxygen and glucose sensing by carotid body glomus cells. *Curr Opin Neurobiol* **13**, 493-499.

Lopez-Barneo J, Lopez-Lopez JR, Urena J, & Gonzalez C (1988). Chemotransduction in the carotid body: K^+ current modulated by PO_2 in type I chemoreceptor cells. *Science* **241**, 580-582.

Lopez-Barneo J, Pardal R, & Ortega-Saenz P (2001). Cellular mechanism of oxygen sensing. *Annu Rev Physiol* **63**, 259-287.

Lopez-Lopez J, Gonzalez C, Urena J, & Lopez-Barneo J (1989). Low pO_2 selectively inhibits K channel activity in chemoreceptor cells of the mammalian carotid body. *J Gen Physiol* **93**, 1001-1015.

Lopez-Lopez JR, De Luis DA, & Gonzalez C (1993). Properties of a transient K^+ current in chemoreceptor cells of rabbit carotid body. *J Physiol* **460**, 15-32.

Lopez-Lopez JR, Gonzalez C, & Perez-Garcia MT (1997). Properties of ionic currents from isolated adult rat carotid body chemoreceptor cells: effect of hypoxia. *J Physiol* **499 (Pt 2)**, 429-441.

Lu Y, Whiteis C, Sluka KA, Chapleau MW, & Abboud FM (2012). Responses of glomus cells to hypoxia and acidosis are uncoupled, reciprocal, and linked to ASIC3 expression: selectivity of chemosensory transductions. *J Physiol* **591 (Pt 4)**, 919-932.

Maingret F, Honore E, Lazdunski M, & Patel AJ (2002). Molecular basis of the voltage-dependent gating of TREK-1, a mechano-sensitive K(+) channel. *Biochem Biophys Res Commun* **292**, 339-346.

McDonald DM (1983). Morphology of the rat carotid sinus nerve. I. Course, connections, dimensions and ultrastructure. *J Neurocytol* **12**, 345-372.

McDonald DM & Blewett RW (1981). Location and size of carotid body-like organs (paraganglia) revealed in rats by the permeability of blood vessels to Evans blue dye. *J Neurocytol* **10**, 607-643.

Mills E & Jobsis FF (1972). Mitochondrial respiratory chain of carotid body and chemoreceptor response to changes in oxygen tension. *J Neurophysiol* **35**, 405-428.

Monti-Bloch L, Abudara V, & Eyzaguirre C (1993). Electrical communication between glomus cells of the rat carotid body. *Brain Res* **622**, 119-131.

Montoro RJ, Urena J, Fernandez-Chacon R, Alvarez de TG, & Lopez-Barneo J (1996). Oxygen sensing by ion channels and chemotransduction in single glomus cells. *J Gen Physiol* **107**, 133-143.

Mulligan E, Lahiri S, & Storey BT (1981). Carotid body O_2 chemoreception and mitochondrial oxidative phosphorylation. *J Appl Physiol* **51**, 438-446.

Narkiewicz K & Somers VK (2003). Sympathetic nerve activity in obstructive sleep apnoea. *Acta Physiol Scand* **177**, 385-390.

Narkiewicz K, van de Borne PJ, Montano N, Dyken ME, Phillips BG, & Somers VK (1998). Contribution of tonic chemoreflex activation to sympathetic activity and blood pressure in patients with obstructive sleep apnea. *Circulation* **97**, 943-945.

Narkiewicz K, van de Borne PJ, Pesek CA, Dyken ME, Montano N, & Somers VK (1999). Selective potentiation of peripheral chemoreflex sensitivity in obstructive sleep apnea. *Circulation* **99**, 1183-1189.

Nurse CA (2010). Neurotransmitter and neuromodulatory mechanisms at peripheral arterial chemoreceptors. *Exp Physiol* **95**, 657-667.

Nurse CA & Piskuric NA (2012). Signal processing at mammalian carotid body chemoreceptors. *Semin Cell Dev Biol*.

Nurse CA & Zhang M (1999). Acetylcholine contributes to hypoxic chemotransmission in co-cultures of rat type 1 cells and petrosal neurons. *Respir Physiol* **115**, 189-199.

O'Kelly I, Lewis A, Peers C, & Kemp PJ (2000). O(2) sensing by airway chemoreceptor-derived cells. Protein kinase c activation reveals functional evidence for involvement of NADPH oxidase. *J Biol Chem* **275**, 7684-7692.

Obeso A, Gomez-Nino A, & Gonzalez C (1999). NADPH oxidase inhibition does not interfere with low PO_2 transduction in rat and rabbit CB chemoreceptor cells. *Am J Physiol* **276**, C593-C601.

Obeso A, Sanz-Alfayate G, Agapito MT, & Gonzalez C (2000). Significance of ROS in oxygen chemoreception in the carotid body chemoreception. Apparent lack of a role for NADPH oxidase. *Adv Exp Med Biol* **475**, 425-434.

Oomori Y, Nakaya K, Tanaka H, Iuchi H, Ishikawa K, Satoh Y, & Ono K (1994). Immunohistochemical and histochemical evidence for the presence of noradrenaline, serotonin and gamma-aminobutyric acid in chief cells of the mouse carotid body. *Cell Tissue Res* **278**, 249-254.

Ortega-Saenz P, Pardal R, Garcia-Fernandez M, & Lopez-Barneo J (2003). Rotenone selectively occludes sensitivity to hypoxia in rat carotid body glomus cells. *J Physiol* **548**, 789-800.

Ortega-Saenz P, Pascual A, Gomez-Diaz R, & Lopez-Barneo J (2006). Acute oxygen sensing in heme oxygenase-2 null mice. *J Gen Physiol* **128**, 405-411.

Overholt JL, Bright GR, & Prabhakar NR (1996). Carbon monoxide and carotid body chemoreception. *Adv Exp Med Biol* **410**, 341-344.

Overholt JL, Ficker E, Yang T, Shams H, Bright GR, & Prabhakar NR (2000a). Chemosensing at the carotid body. Involvement of a HERG-like potassium current in glomus cells. *Adv Exp Med Biol* **475**, 241-248.

Overholt JL, Ficker E, Yang T, Shams H, Bright GR, & Prabhakar NR (2000b). HERG-Like potassium current regulates the resting membrane potential in glomus cells of the rabbit carotid body. *J Neurophysiol* **83**, 1150-1157.

Overholt JL & Prabhakar NR (1997). Ca^{2+} current in rabbit carotid body glomus cells is conducted by multiple types of high-voltage-activated Ca^{2+} channels. *J Neurophysiol* **78**, 2467-2474.

Panisello JM & Donnelly DF (1998). Chemotransduction by carotid body chemoreceptors is dependent on bicarbonate currents. *Respir Physiol* **112**, 265-281.

Pardal R & Lopez-Barneo J (2002a). Carotid body thin slices: responses of glomus cells to hypoxia and K(+)-channel blockers. *Respir Physiol Neurobiol* **132**, 69-79.

Pardal R & Lopez-Barneo J (2002b). Low glucose-sensing cells in the carotid body. *Nat Neurosci* **5**, 197-198.

Patel AJ & Honore E (2001). Properties and modulation of mammalian 2P domain K$^+$ channels. *Trends Neurosci* **24**, 339-346.

Peers C (1990). Hypoxic suppression of K$^+$ currents in type I carotid body cells: selective effect on the Ca2(+)-activated K$^+$ current. *Neurosci Lett* **119**, 253-256.

Peers C & Buckler KJ (1995). Transduction of chemostimuli by the type I carotid body cell. *J Membr Biol* **144**, 1-9.

Peers C, Carpenter E, Hatton CJ, Wyatt CN, & Bee D (1996). Ca^{2+} channel currents in type I carotid body cells of normoxic and chronically hypoxic neonatal rats. *Brain Res* **739**, 251-257.

Peers C & Green FK (1991). Inhibition of Ca(2+)-activated K$^+$ currents by intracellular acidosis in isolated type I cells of the neonatal rat carotid body. *J Physiol* **437**, 589-602.

Peers C & Wyatt CN (2007). The role of maxiK channels in carotid body chemotransduction. *Respir Physiol Neurobiol* **157**, 75-82.

Peers C, Wyatt CN, & Evans AM (2010). Mechanisms for acute oxygen sensing in the carotid body. *Respir Physiol Neurobiol* **174**, 292-298.

Peng YJ, Nanduri J, Raghuraman G, Souvannakitti D, Gadalla MM, Kumar GK, Snyder SH, & Prabhakar NR (2010). H$_2$S mediates O$_2$ sensing in the carotid body. *Proc Natl Acad Sci U S A* **107**, 10719-10724.

Peng YJ, Nanduri J, Yuan G, Wang N, Deneris E, Pendyala S, Natarajan V, Kumar GK, & Prabhakar NR (2009). NADPH oxidase is required for the sensory plasticity of the carotid body by chronic intermittent hypoxia. *J Neurosci* **29**, 4903-4910.

Peng YJ, Overholt JL, Kline D, Kumar GK, & Prabhakar NR (2003). Induction of sensory long-term facilitation in the carotid body by intermittent hypoxia: implications for recurrent apneas. *Proc Natl Acad Sci U S A* **100**, 10073-10078.

Peng YJ & Prabhakar NR (2004). Effect of two paradigms of chronic intermittent hypoxia on carotid body sensory activity. *J Appl Physiol* **96**, 1236-1242.

Peng YJ, Raghuraman G, Khan SA, Kumar GK, & Prabhakar NR (2011). Angiotensin-II evokes sensory long-term facilitation of the carotid body via NADPH oxidase. *J Appl Physiol*.

Perez-Garcia MT, Lopez-Lopez JR, Riesco AM, Hoppe UC, Marban E, Gonzalez C, & Johns DC (2000). Viral gene transfer of dominant-negative Kv4 construct suppresses an O_2-sensitive K^+ current in chemoreceptor cells. *J Neurosci* **20**, 5689-5695.

Petheo GL, Molnar Z, Roka A, Makara JK, & Spat A (2001). A pH-sensitive chloride current in the chemoreceptor cell of rat carotid body. *J Physiol* **535**, 95-106.

Pizarro J, Ryan ML, Hedrick MS, Xue DH, Keith IM, & Bisgard GE (1995). Intracarotid substance P infusion inhibits ventilation in the goat. *Respir Physiol* **101**, 11-22.

Prabhakar NR (2000). Oxygen sensing by the carotid body chemoreceptors. *J Appl Physiol* **88**, 2287-2295.

Prabhakar NR (2006). O_2 sensing at the mammalian carotid body: why multiple O_2 sensors and multiple transmitters? *Exp Physiol* **91**, 17-23.

Prabhakar NR (2012a). Carbon monoxide (CO) and hydrogen sulfide (H(2)S) in hypoxic sensing by the carotid body. *Respir Physiol Neurobiol*.

Prabhakar NR (2012b). Hydrogen sulfide (H(2)S): a physiologic mediator of carotid body response to hypoxia. *Adv Exp Med Biol* **758**, 109-113.

Prabhakar NR, Dinerman JL, Agani FH, & Snyder SH (1995). Carbon monoxide: a role in carotid body chemoreception. *Proc Natl Acad Sci U S A* **92**, 1994-1997.

Prabhakar NR & Kumar GK (2010). Mechanisms of sympathetic activation and blood pressure elevation by intermittent hypoxia. *Respir Physiol Neurobiol* **174**, 156-161.

Prabhakar NR & Overholt JL (2000). Cellular mechanisms of oxygen sensing at the carotid body: heme proteins and ion channels. *Respir Physiol* **122**, 209-221.

Prabhakar NR & Semenza GL (2012). Gaseous messengers in oxygen sensing. *J Mol Med (Berl)* **90**, 265-272.

Prasad M, Fearon IM, Zhang M, Laing M, Vollmer C, & Nurse CA (2001). Expression of P2X2 and P2X3 receptor subunits in rat carotid body afferent neurones: role in chemosensory signalling. *J Physiol* **537**, 667-677.

Ramirez M, Gallego-Martin T, Olea E, Rocher A, Obeso A, & Gonzalez C (2012). Serotonin dynamics and actions in the rat carotid body: preliminary findings. *Adv Exp Med Biol* **758**, 255-263.

Riesco-Fagundo AM, Perez-Garcia MT, Gonzalez C, & Lopez-Lopez JR (2001). O(2) modulates large-conductance Ca(2+)-dependent K(+) channels of rat chemoreceptor cells by a membrane-restricted and CO-sensitive mechanism. *Circ Res* **89**, 430-436.

Rigual R, Gonzalez E, Gonzalez C, & Fidone S (1986). Synthesis and release of catecholamines by the cat carotid body in vitro: effects of hypoxic stimulation. *Brain Res* **374**, 101-109.

Rigual R, Lopez-Lopez JR, & Gonzalez C (1991). Release of dopamine and chemoreceptor discharge induced by low pH and high PCO_2 stimulation of the cat carotid body. *J Physiol* **433**, 519-531.

Rocher A, Geijo-Barrientos E, Caceres AI, Rigual R, Gonzalez C, & Almaraz L (2005). Role of voltage-dependent calcium channels in stimulus-secretion coupling in rabbit carotid body chemoreceptor cells. *J Physiol* **562**, 407-420.

Rong W, Gourine AV, Cockayne DA, Xiang Z, Ford AP, Spyer KM, & Burnstock G (2003). Pivotal role of nucleotide P2X2 receptor subunit of the ATP-gated ion channel mediating ventilatory responses to hypoxia. *J Neurosci* **23**, 11315-11321.

Ross FA, Rafferty JN, Dallas ML, Ogunbayo O, Ikematsu N, McClafferty H, Tian L, Widmer H, Rowe IC, Wyatt CN, Shipston MJ, Peers C, Hardie DG, & Evans AM (2011). Selective expression in carotid body type I cells of a single splice variant of the large conductance calcium- and voltage-activated potassium channel confers regulation by AMP-activated protein kinase. *J Biol Chem* **286**, 11929-11936.

Sanchez D, Lopez-Lopez JR, Perez-Garcia MT, Sanz-Alfayate G, Obeso A, Ganfornina MD, & Gonzalez C (2002). Molecular identification of Kvα subunits that contribute to the oxygen-sensitive K^+ current of chemoreceptor cells of the rabbit carotid body. *J Physiol* **542**, 369-382.

Sanders KA, Sundar KM, He L, Dinger B, Fidone S, & Hoidal JR (2002). Role of components of the phagocytic NADPH oxidase in oxygen sensing. *J Appl Physiol* **93**, 1357-1364.

Sanz-Alfayate G, Obeso A, Agapito MT, & Gonzalez C (2001). Reduced to oxidized glutathione ratios and oxygen sensing in calf and rabbit carotid body chemoreceptor cells. *J Physiol* **537**, 209-220.

Shibahara S, Muller R, Taguchi H, & Yoshida T (1985). Cloning and expression of cDNA for rat heme oxygenase. *Proc Natl Acad Sci U S A* **82**, 7865-7869.

Shirahata M, Balbir A, Otsubo T, & Fitzgerald RS (2007). Role of acetylcholine in neurotransmission of the carotid body. *Respir Physiol Neurobiol* **157**, 93-105.

Shirahata M, Fitzgerald RS, & Sham JS (1997). Acetylcholine increases intracellular calcium of arterial chemoreceptor cells of adult cats. *J Neurophysiol* **78**, 2388-2395.

Shirahata M, Hirasawa S, Okumura M, Mendoza JA, Okumura A, Balbir A, & Fitzgerald RS (2004). Identification of M1 and M2 muscarinic acetylcholine receptors in the cat carotid body chemosensory system. *Neuroscience* **128**, 635-644.

Shirahata M, Ishizawa Y, Rudisill M, Schofield B, & Fitzgerald RS (1998). Presence of nicotinic acetylcholine receptors in cat carotid body afferent system. *Brain Res* **814**, 213-217.

Silva MJ & Lewis DL (1995). L- and N-type Ca^{2+} channels in adult rat carotid body chemoreceptor type I cells. *J Physiol* **489 (Pt 3)**, 689-699.

Stea A & Nurse CA (1989). Chloride channels in cultured glomus cells of the rat carotid body. *Am J Physiol* **257**, C174-C181.

Stea A & Nurse CA (1991a). Contrasting effects of HEPES vs HCO3(-)-buffered media on whole-cell currents in cultured chemoreceptors of the rat carotid body. *Neurosci Lett* **132**, 239-242.

Stea A & Nurse CA (1991b). Whole-cell and perforated-patch recordings from O_2-sensitive rat carotid body cells grown in short- and long-term culture. *Pflugers Arch* **418**, 93-101.

Streller T, Huckstorf C, Pfeiffer C, & Acker H (2002). Unusual cytochrome a592 with low PO_2 affinity correlates as putative oxygen sensor with rat carotid body chemoreceptor discharge. *FASEB J* **16**, 1277-1279.

Summers BA, Overholt JL, & Prabhakar NR (1999). Nitric oxide inhibits L-type Ca^{2+} current in glomus cells of the rabbit carotid body via a cGMP-independent mechanism. *J Neurophysiol* **81**, 1449-1457.

Summers BA, Overholt JL, & Prabhakar NR (2000). Augmentation of L-type calcium current by hypoxia in rabbit carotid body glomus cells: evidence for a PKC-sensitive pathway. *J Neurophysiol* **84**, 1636-1644.

Summers BA, Overholt JL, & Prabhakar NR (2002). CO(2) and pH independently modulate L-type Ca(2+) current in rabbit carotid body glomus cells. *J Neurophysiol* **88**, 604-612.

Sun MK & Reis DJ (1994). Dopamine or transmitter release from rat carotid body may not be essential to hypoxic chemoreception. *Am J Physiol* **267**, R1632-R1639.

Tan ZY, Lu Y, Whiteis CA, Benson CJ, Chapleau MW, & Abboud FM (2007). Acid-sensing ion channels contribute to transduction of extracellular acidosis in rat carotid body glomus cells. *Circ Res* **101**, 1009-1019.

Telezhkin V, Brazier SP, Cayzac S, Muller CT, Riccardi D, & Kemp PJ (2009). Hydrogen sulfide inhibits human BK(Ca) channels. *Adv Exp Med Biol* **648**, 65-72.

Telezhkin V, Brazier SP, Cayzac SH, Wilkinson WJ, Riccardi D, & Kemp PJ (2010). Mechanism of inhibition by hydrogen sulfide of native and recombinant BKCa channels. *Respir Physiol Neurobiol* **172**, 169-178.

Thompson CM, Troche K, Jordan HL, Barr BL, & Wyatt CN (2010). Evidence for functional, inhibitory, histamine H3 receptors in rat carotid body Type I cells. *Neurosci Lett* **471**, 15-19.

Trapp S, Aller MI, Wisden W, & Gourine AV (2008). A role for TASK-1 (KCNK3) channels in the chemosensory control of breathing. *J Neurosci* **28**, 8844-8850.

Tse A, Yan L, Lee AK, & Tse FW (2012). Autocrine and paracrine actions of ATP in rat carotid body. *Can J Physiol Pharmacol* **90**, 705-711.

Urena J, Fernandez-Chacon R, Benot AR, Alvarez de Toledo GA, & Lopez-Barneo J (1994). Hypoxia induces voltage-dependent Ca^{2+} entry and quantal dopamine secretion in carotid body glomus cells. *Proc Natl Acad Sci U S A* **91**, 10208-10211.

Vandier C, Conway AF, Landauer RC, & Kumar P (1999). Presynaptic action of adenosine on a 4-aminopyridine-sensitive current in the rat carotid body. *J Physiol* **515 (Pt 2)**, 419-429.

Varas R, Wyatt CN, & Buckler KJ (2007). Modulation of TASK-like background potassium channels in rat arterial chemoreceptor cells by intracellular ATP and other nucleotides. *J Physiol* **583**, 521-536.

Verna A, Roumy M, & Leitner LM (1975). Loss of chemoreceptive properties of the rabbit carotid body after destruction of the glomus cells. *Brain Res* **100**, 13-23.

Vicario I, Rigual R, Obeso A, & Gonzalez C (2000). Characterization of the synthesis and release of catecholamine in the rat carotid body in vitro. *Am J Physiol Cell Physiol* **278**, C490-C499.

Wang HY & Fitzgerald RS (2002). Muscarinic modulation of hypoxia-induced release of catecholamines from the cat carotid body. *Brain Res* **927**, 122-137.

Wang ZZ, Stensaas LJ, Bredt DS, Dinger B, & Fidone SJ (1994). Localization and actions of nitric oxide in the cat carotid body. *Neuroscience* **60**, 275-286.

Wang ZZ, Stensaas LJ, Dinger BG, & Fidone SJ (1995). Nitric oxide mediates chemoreceptor inhibition in the cat carotid body. *Neuroscience* **65**, 217-229.

Weir EK & Archer SL (1995). The mechanism of acute hypoxic pulmonary vasoconstriction: the tale of two channels. *FASEB J* **9**, 183-189.

Williams BA & Buckler KJ (2004). Biophysical properties and metabolic regulation of a TASK-like potassium channel in rat carotid body type 1 cells. *Am J Physiol Lung Cell Mol Physiol* **286**, L221-L230.

Williams SE, Wootton P, Mason HS, Bould J, Iles DE, Riccardi D, Peers C, & Kemp PJ (2004). Hemoxygenase-2 is an oxygen sensor for a calcium-sensitive potassium channel. *Science* **306**, 2093-2097.

Wyatt CN & Buckler KJ (2004). The effect of mitochondrial inhibitors on membrane currents in isolated neonatal rat carotid body type I cells. *J Physiol* **556**, 175-191.

Wyatt CN, Mustard KJ, Pearson SA, Dallas ML, Atkinson L, Kumar P, Peers C, Hardie DG, & Evans AM (2007). AMP-activated protein kinase mediates carotid body excitation by hypoxia. *J Biol Chem* **282**, 8092-8098.

Wyatt CN & Peers C (1993). Nicotinic acetylcholine receptors in isolated type I cells of the neonatal rat carotid body. *Neuroscience* **54**, 275-281.

Wyatt CN & Peers C (1995). Ca(2+)-activated K^+ channels in isolated type I cells of the neonatal rat carotid body. *J Physiol* **483 (Pt 3)**, 559-565.

Wyatt CN, Weir EK, & Peers C (1994). Diphenylene iodonium blocks K^+ and Ca^{2+} currents in type I cells isolated from the neonatal rat carotid body. *Neurosci Lett* **172**, 63-66.

Xu F, Tse FW, & Tse A (2007). Pituitary adenylate cyclase-activating polypeptide (PACAP) stimulates the oxygen sensing type I (glomus) cells of rat carotid bodies via reduction of a background TASK-like K^+ current. *J Neurochem* **101**, 1284-1293.

Xu F, Xu J, Tse FW, & Tse A (2006). Adenosine stimulates depolarization and rise in cytoplasmic $[Ca^{2+}]$ in type I cells of rat carotid bodies. *Am J Physiol Cell Physiol* **290**, C1592-C1598.

Xu J, Tse FW, & Tse A (2003). ATP triggers intracellular Ca^{2+} release in type II cells of the rat carotid body. *J Physiol* **549**, 739-747.

Xu J, Xu F, Tse FW, & Tse A (2005). ATP inhibits the hypoxia response in type I cells of rat carotid bodies. *J Neurochem* **92**, 1419-1430.

Yamamoto Y, Kummer W, Atoji Y, & Suzuki Y (2002). TASK-1, TASK-2, TASK-3 and TRAAK immunoreactivities in the rat carotid body. *Brain Res* **950**, 304-307.

Yamamoto Y & Taniguchi K (2006). Immunolocalization of tandem pore domain K$^+$ channels in the rat carotid body. *Adv Exp Med Biol* **580**, 9-14.

Zhang M, Buttigieg J, & Nurse CA (2007). Neurotransmitter mechanisms mediating low-glucose signalling in cocultures and fresh tissue slices of rat carotid body. *J Physiol* **578**, 735-750.

Zhang M, Clarke K, Zhong H, Vollmer C, & Nurse CA (2009). Postsynaptic action of GABA in modulating sensory transmission in co-cultures of rat carotid body via GABA(A) receptors. *J Physiol* **587**, 329-344.

Zhang M, Fearon IM, Zhong H, & Nurse CA (2003). Presynaptic modulation of rat arterial chemoreceptor function by 5-HT: role of K$^+$ channel inhibition via protein kinase C. *J Physiol* **551**, 825-842.

Zhang M & Nurse CA (2000). Does endogenous 5-HT mediate spontaneous rhythmic activity in chemoreceptor clusters of rat carotid body? *Brain Res* **872**, 199-203.

Zhang M & Nurse CA (2004). CO_2/pH chemosensory signaling in co-cultures of rat carotid body receptors and petrosal neurons: role of ATP and ACh. *J Neurophysiol* **92**, 3433-3445.

Zhang M, Zhong H, Vollmer C, & Nurse CA (2000). Co-release of ATP and ACh mediates hypoxic signalling at rat carotid body chemoreceptors. *J Physiol* **525 Pt 1**, 143-158.

Zhong H, Zhang M, & Nurse CA (1997). Synapse formation and hypoxic signalling in co-cultures of rat petrosal neurones and carotid body type 1 cells. *J Physiol* **503 (Pt 3)**, 599-612.

Chapter 2

Materials and Methods

2.1 Chemicals

Indo-1 K^+ salt, indo-1 acetoxymethyl ester (AM) and rhod-2 AM were obtained from Molecular Probes (Eugene, OR). Sodium cyanide (NaCN), sodium dithionite ($Na_2S_2O_4$), acetazolamide, cyclopiozonic acid (CPA), ruthenium red, N-methylglucamine (NMG^+), N-acetyl-L-cysteine (NAC), reduced form of L-glutathione (GSH), amphotericin B, bovine serum albumin (BSA), ethylene glycol tetraacetic acid (EGTA), and all the enzymes for cell dissociation (including collagenase type IV, DNase type V and trypsin type XIII) were purchased from Sigma-Aldrich Ltd. (Oakville, ON, Canada). Carbonyl cyanide m-chlorophenylhydrazone (CCCP), 2,5-di(tert-butyl)-1,4-benzohydroquinone (BHQ) and, 8-(4-chloro-phenylthio)-adenosine 3',5'-cyclic monophosphate (8-CPT-cAMP) were from Calbiochem (San Diego, CA, USA). Fetal bovine serum, Dulbecco's modified Eagle's medium (DMEM) F-12, penicillin G and streptomycin were obtained from Gibco (Grand Island, NY, USA).

2.2 Solutions

The standard HEPES-buffered bath solution contained (in mM): 2.5 $CaCl_2$, 1 $MgCl_2$, 8 glucose, 10 HEPES, 150 NaCl, 4.5 KCl, pH 7.4. The standard HCO_3^--buffered bath solution contained (in mM): 117 NaCl, 4.5 KCl, 23 $NaHCO_3$, 5 sucrose, 5 glucose, 2.5 $CaCl_2$, and 1 $MgCl_2$ (pH 7.4 when bubbled continuously with 5% CO_2). For experiments in which CO_2 bubbling was omitted from HCO_3^--buffered solution, 10 mM HEPES was added to maintain the pH at 7.4. For experiments involving the removal of extracellular Na^+ in the standard HEPES-

buffered solution, Na^+ was replaced by N-methyl-glucamine (NMG^+). For experiments involving hypoxia, cells were perfused with the standard HEPES-buffered solution containing 1 mM $Na_2S_2O_4$ and bubbled with 100% N_2. For whole-cell recording, the pipette solution contained (in mM): 120 Cs-aspartate, 20 TEA-Cl, 20 Cs-HEPES, 2.5 $MgCl_2$, 5 Na_2ATP and 0.1 Na_4GTP (pH 7.4). For experiments involving mitochondrial Ca^{2+} signal recording with rhod-2 AM, the whole-cell pipette solution contained (in mM): 120 K-aspartate, 20 K-HEPES, 20 KCl, 2.5 $MgCl_2$, 5 Na_2ATP and 0.1 Na_4GTP (pH 7.4). For experiments with perforated-patch recording, the pipette solution contained (in mM): 140 K-gluconate, 10 K-HEPES, 5 $MgCl_2$ and 1 EGTA (pH 7.2) and amphotericin B (200 µg/ml) was added to the pipette solution.

In most experiments, the bath was continuously perfused with solution and the flow rate was around 3-4 ml/min. In some experiments, a glass pipette was positioned in the vicinity (~several mm) of the cells for a faster perfusion rate. Bars shown in the figures indicate the time when the distribution valve for the bath solution was switched from one reservoir to another. The delay in the response to specific drugs was primarily due to the time for the exchange of solution in the bath as well as a 30 cm tubing which connected the output of the distribution valve and the bath.

2.3 Animals

Male Sprague-Dawley rats (6-7 weeks old) were obtained from the Bioscience Animal facility at the University of Alberta. All rats were housed and

treated according to the standards set by the Canadian Council on Animal Care. All procedures received prior approval from the Health Sciences Animal Care and Use Committee of the University of Alberta. Rats were housed two per cage under a 12-hour light/dark cycle at room temperature, and were provided with food and water *ad libitum*.

2.4 Cell preparation and short-term culture

Details of the preparation of carotid cells were as described previously (Xu *et al.*, 2003). Briefly, rats were first euthanized in accordance with the standards of the Canadian Council on Animal Care. The carotid bifurcation was removed and placed in ice-cold 100% O_2-equilibrated Tyrode's solution (in mM): 140 NaCl, 5 KCl, 2 $CaCl_2$, 1.1 $MgCl_2$, 5 glucose and 10 HEPES (titrated with NaOH to pH 7.4). Following the dissection of the carotid bodies from the surrounding tissue under a dissecting microscope, the carotid bodies were incubated in 0.5 ml of the Ca^{2+}- and Mg^{2+}-free Tyrode's solution (the divalent ions were replaced by an additional 5 mM of NaCl) containing collagenase (type IV, 2 mg/ml), DNase (type V, 0.5 mg/ml) for 23 min at 37 ^{o}C. The carotid bodies were then triturated with a fire-polished glass pipette and incubated at 37 ^{o}C for another 7 min. The tissues were further triturated with the fire-polished glass pipette and 2.5 ml of the Ca^{2+}- and Mg^{2+}-free Tyrode's solution was then added. The tissue suspension was centrifuged (2000 rpm for 5 min). Following the removal of the supernatant, the tissue pellet was resuspended in 0.5 ml of the Ca^{2+}- and Mg^{2+}-free Tyrode's solution containing trypsin (type XIII, 0.2 mg/ml) and then incubated for 12 min

at 37 ^{o}C. The tissue suspension was triturated with a very finely fire-polished glass pipette to obtain single cells. The enzyme (trypsin) for cell dissociation was removed by repeating the following procedure twice: 3 ml of DMEM containing 0.1% BSA was added to the cell suspension and then centrifuged (2000 rpm for 5 min). After the last wash, the cell pellet was resuspended in DMEM. A droplet of 6 µl of the cell suspension was plated onto the center of each glass coverslip which was previously put in a 35 mm plastic culture dish. After the cells were in the 37 ^{o}C incubator for ~45 min, a medium containing F-12/Dulbecco's modified Eagle's medium (1:1), 5% fetal bovine serum, 50 U/ml penicillin G and 50 µg/ml streptomycin was then added to flood the bottom of each culture dish. Except for the hypoxia experiments in Fig. 3-10, all experiments were performed in cells maintained in standard culture conditions (37 ^{o}C, 5% CO_2) for 1 day. In our experience, the ability of rat glomus cells to respond to hypoxia declined with the duration of culture (Xu *et al.*, 2005). Therefore, for experiments involving hypoxia, I employed cells that were cultured for 2-6 hrs. We have shown previously that glomus cells, but not the sustentacular (type II) cells, express VGCCs (Xu *et al.*, 2003); therefore, I identified individual glomus cells from the mixed carotid cell preparations based on the ability to evoke a rise in $[Ca^{2+}]_i$ with membrane depolarization.

2.5 Electrophysiology

All experiments were performed at room temperature (20-23 ^{o}C). In most experiments, single glomus cells were recorded with the whole-cell patch clamp

configuration with an EPC-9 patch clamp amplifier (List-electronic, Darmstadt, Germany) that was controlled by an IBM-compatible PC loaded with the Patchmaster data acquisition program (HEKA Electronik, Lambrecht/Pfalz, Germany). Since it has been reported that glomus cells failed to respond to hypoxia when recorded in the whole-cell configuration (Wyatt & Peers, 1995; Buckler *et al.*, 2000), I employed the perforated-patch clamp technique in experiments involving hypoxia (Fig. 3-10). In all other experiments, cells were voltage clamped at -70 mV and a voltage step (500 ms) to 0 mV was applied to activate VGCCs and a transient rise in $[Ca^{2+}]_i$. An example of this procedure is shown in Fig. 3-2. For experiments involving membrane-capacitance measurement, the built-in lock-in amplifier software of the EPC-9 Pulse software was employed. A 1-kHz, 10-mV peak-to-peak sinusoid voltage command was employed in the "sine wave plus direct current" method to calculate the cell membrane capacitance. The recording pipettes were made from hematocrit glass (VWR scientific Canada Ltd., London, ON, Canada) and their resistance was 3-5 $M\Omega$ after filling with the pipette solution. The pipette resistance was 10-20 $M\Omega$ during whole-cell recording and was 20-30 $M\Omega$ during perforated-patch recording. A -10 mV correction for junction potential was applied in all experiments.

2.6 Measurement of $[Ca^{2+}]_i$

In most experiments, $[Ca^{2+}]_i$ measurement was made with the Ca^{2+}-sensitive dye, indo-1 (K^+ salt; 25 μM), which was included in the whole-cell pipette solution and loaded into the cytoplasm. In chapter 3, for experiments involving

60

hypoxia (Fig. 3-10), cells were loaded with indo-1 AM (2.5 µM) for 12 min at 37 ^{o}C and then washed in standard bath solution for at least 10 min before the start of recording. Details of the instrumentation and procedures of $[Ca^{2+}]_i$ measurement were as described previously (Lee & Tse, 2005; Hughes *et al.*, 2006). Briefly, indo-1 was excited by 365 nm light from a HBO 100-W mercury lamp via a 40×, 1.3 NA UV Fluor oil immersion objective lens (Nikon). Emission fluorescence at 405 ± 35 nm and 495 ± 45 nm was collected with two photomultiplier tubes (Hamamatsu H3460-04) for 20 ms every 200 ms. The output of the photomultiplier tubes was converted to TTL pulses and counted by a CYCTIM-10 counter card (Cyber Research Inc., Branford, CT, USA) installed in an IBM-compatible PC. For experiments involving whole-cell loading of indo-1, the fluorescence of the pipette and the cell before the establishment of whole-cell configuration was used for background subtraction. For experiments involving indo-1 AM loading, there was no correction for cell autofluorescence. $[Ca^{2+}]_i$ was calculated from the ratio (R) of the fluorescence at 405 and 495 nm according to the equation (Grynkiewicz *et al.*, 1985): $[Ca^{2+}] = K^* \times (R - R_{min}) / (R_{max} - R)$. R_{min} is the fluorescence ratio of Ca^{2+}-free indicator and R_{max} is the ratio of Ca^{2+}-bound indicator. K^* is a constant that was determined empirically. Calibrations for indo-1 were determined from single cells introduced with one of the three pipette solutions in whole-cell recording mode as described previously (Tse & Tse, 1998). R_{min} was measured in cells loaded with (in mM): 52 K-aspartate, 10 KCl, 50 K-EGTA, 50 K-HEPES and 0.1 indo-1, pH 7.4; and R_{max} was measured in cells loaded with (in mM): 136 K-aspartate, 15 $CaCl_2$, 50 K-HEPES and 0.1 indo-1, pH

7.4. K^* was calculated from the equation above using R values obtained from cells loaded with (in mM): 60 K-aspartate, 50 K-HEPES, 20 K-EGTA, 15 $CaCl_2$, 0.1 indo-1, pH 7.4, which had a calculated free $[Ca^{2+}]$ of 212 nM at 22 ^{o}C (Blinks *et al.*, 1982). The values for R_{min}, R_{max} and K^* were 0.26, 2.92 and 1.80 μM, respectively.

2.7 Measurement of mitochondrial Ca^{2+} signal using rhod-2 fluorescence

Cells were incubated with 4 μM rhod-2 AM for 20-25 min at room temperature. At the end of the incubation, punctate fluorescent staining within the cell was observed, suggesting the localization of the dye to the mitochondria. Cells were then washed with dye-free standard bath solution and recorded with the whole-cell or perforated-patch clamp technique. Rhod-2 was excited at 535 nm, and emission fluorescence at wavelengths greater than 590 nm was collected with a photomultiplier tube (Hamamatsu H3460-04) for 20 ms every 500 ms. The output of the photomultiplier tube was converted to TTL pulses and counted by a CYCTIM-10 counter card (Cyber Research Inc., Branford, CT, USA) installed in an IBM-compatible PC.

2.8   Measurement of mitochondrial membrane potential using tetramethylrhodamine ethyl ester (TMRE) fluorescence

TMRE (10 μM) was loaded into the cell via the whole-cell pipette and the cell was voltage clamped at -70 mV. In my experimental conditions, punctate

fluorescent staining within the cell was observed after ~5 min of the establishment of whole-cell configuration, suggesting the partitioning of TMRE into the mitochondria. TMRE was excited at 535 nm, and its emission fluorescence (from the entire cell) was collected at wavelengths greater than 590 nm using a long-pass filter with a photomultiplier tube (Hamamatsu H3460-04) for 20 ms every 500 ms. The output of the photomultiplier tube, in photon counting mode, was converted to TTL pulses and counted by a CYCTIM-10 counter card (Cyber Research Inc., Branford, CT, USA) installed in an IBM-compatible PC.

2.9 Statistical analysis

The Origin program v.8 (OriginLab Corp., Northampton, MA) was employed for plotting and statistical procedures. The time constant of Ca^{2+} clearance was estimated by fitting the decay of the Ca^{2+} signal with a single exponential function. The two-sample Student's t test was used to compare mean values between two populations of cells. Any difference with p <0.05 was considered statistically significant and was marked with an asterisk in the figures. All values shown were means ± SEM.

Reference List

Blinks JR, Wier WG, Hess P, & Prendergast FG (1982). Measurement of Ca^{2+} concentrations in living cells. *Prog Biophys Mol Biol* **40**, 1-114.

Buckler KJ, Williams BA, & Honore E (2000). An oxygen-, acid- and anaesthetic-sensitive TASK-like background potassium channel in rat arterial chemoreceptor cells. *J Physiol* **525 Pt 1**, 135-142.

Grynkiewicz G, Poenie M, & Tsien RY (1985). A new generation of Ca^{2+} indicators with greatly improved fluorescence properties. *J Biol Chem* **260**, 3440-3450.

Hughes E, Lee AK, & Tse A (2006). Dominant role of sarcoendoplasmic reticulum Ca^{2+}-ATPase pump in Ca^{2+} homeostasis and exocytosis in rat pancreatic beta-cells. *Endocrinology* **147**, 1396-1407.

Lee AK & Tse A (2005). Dominant role of mitochondria in calcium homeostasis of single rat pituitary corticotropes. *Endocrinology* **146**, 4985-4993.

Tse A & Tse FW (1998). alpha-adrenergic stimulation of cytosolic Ca^{2+} oscillations and exocytosis in identified rat corticotrophs. *J Physiol* **512 (Pt 2)**, 385-393.

Wyatt CN & Buckler KJ (2004). The effect of mitochondrial inhibitors on membrane currents in isolated neonatal rat carotid body type I cells. *J Physiol* **556**, 175-191.

Wyatt CN & Peers C (1995). Ca(2+)-activated K^+ channels in isolated type I cells of the neonatal rat carotid body. *J Physiol* **483 (Pt 3)**, 559-565.

Xu J, Tse FW, & Tse A (2003). ATP triggers intracellular Ca^{2+} release in type II cells of the rat carotid body. *J Physiol* **549**, 739-747.

Xu J, Xu F, Tse FW, & Tse A (2005). ATP inhibits the hypoxia response in type I cells of rat carotid bodies. *J Neurochem* **92**, 1419-1430.

Chapter 3

Ca^{2+} uptake into mitochondria is the major cytosolic Ca^{2+} clearance mechanism in rat glomus cells

3.1 Introduction

3.1.1 Role of mitochondria in the hypoxic chemotransduction of the carotid body

In rat glomus cells, hypoxia inhibits oxygen-sensitive K^+ channels (BK and TASK-like K^+ channels) (Wyatt & Peers, 1995; Buckler, 1997), resulting in depolarization and activation of VGCCs (Prabhakar, 2000). The rise in $[Ca^{2+}]_i$ causes the release of neurotransmitters, resulting in the stimulation of the CSN and the triggering of respiratory and cardiovascular reflexes (Lopez-Barneo et al., 2009). Mitochondria have been suggested to play important roles in hypoxic chemotransduction in the carotid bodies (Donnelly & Carroll, 2005; Gonzalez *et al.*, 2010; Peers *et al.*, 2010). The mitochondria in glomus cells have been postulated to be highly sensitive to hypoxia; moderate hypoxia has been shown to cause depolarization in mitochondrial membrane potential in glomus cells but not in other cell types (Duchen & Biscoe, 1992). Inhibitors of mitochondrial functions (mitochondrial uncouplers or blockers of specific complexes in the respiratory chain) caused depolarization in glomus cells, resulting in $[Ca^{2+}]_i$ elevations (Duchen & Biscoe, 1992; Wyatt & Buckler, 2004), transmitter release (Ortega-Saenz et al., 2003) and stimulation of CSN (Mulligan et al., 1981). The link between mitochondrial inhibition and glomus cell excitation is not completely understood; various mechanisms, including an ATP-dependent regulation of TASK-like K^+ channels (Wyatt & Buckler, 2004) as well as the activation of AMPK (which in turn suppresses the opening of BK and TASK-like K^+ channels)

66

(Evans *et al.*, 2005; Wyatt *et al.*, 2007), have been proposed (Gonzalez *et al.*, 2010; Peers *et al.*, 2010).

3.1.2 Role of mitochondria in the regulation of Ca^{2+} signals

An important role of mitochondria in the regulation of Ca^{2+} signals has been demonstrated in a number of cell types, including sympathetic neurons (Friel, 2000), adrenal chromaffin cells (Herrington et al., 1996) and pituitary corticotropes (Lee & Tse, 2005). In pituitary corticotropes for example, inhibition of mitochondrial function by mitochondrial uncouplers was shown to cause elevation in basal $[Ca^{2+}]_i$ and slowed the decay of the depolarization-triggered Ca^{2+} signal by ~3-fold (Lee & Tse, 2005). This raises the possibility that, other than its effect on cellular excitability, mitochondrial inhibition may affect $[Ca^{2+}]_i$ in glomus cells via changes in Ca^{2+} homeostasis.

3.1.3 The shaping of the Ca^{2+} signal

As summarized in Fig. 3-1, in most cell types, the shape of Ca^{2+} signal can be regulated by multiple mechanisms (Berridge et al., 2003). Extracellular Ca^{2+} entry can occur via the activation of VGCC, capacitative Ca^{2+} entry (CCE) or via a passive Ca^{2+} leak at the plasma membrane. Ca^{2+} can be released from the intracellular compartments such as the endoplasmic/sarcoplasmic reticulum (ER/SR) via the opening of channels linked to the inositol 1,4,5-trisphosphate receptor (IP_3R) or ryanodine receptor (RyR), or via a small passive Ca^{2+} leak.

Ca^{2+} can also be released from the mitochondria via the permeability transition pore (PTP) and mitochondrial Na^{+}/Ca^{2+} exchanger (mNCX). Regardless of how Ca^{2+} enters the cytosol, a large fraction of the cytosolic Ca^{2+} load is reversibly bound to multiple cytosolic Ca^{2+} binding sites. Only a small fraction (~1-5%) of the Ca^{2+} load shows up as free Ca^{2+} and contributes to the rising phase of the Ca^{2+} transient (Zhou & Neher, 1993). The decay phase of the Ca^{2+} transient is regulated by multiple Ca^{2+} clearance mechanisms. Ca^{2+} can be extruded to the extracellular space by plasma membrane Ca^{2+} ATPase (PMCA) pump and Na^{+}/Ca^{2+} exchanger (NCX). Ca^{2+} can also be sequestered to the ER/SR by the sarco(endo)plasmic reticulum Ca^{2+} ATPase (SERCA) pump or into the mitochondria via the mitochondrial Ca^{2+} transporters, such as the uniporter (Berridge et al., 2003).

3.1.4 Goals of project 1

In rat glomus cells, it is well established that the rising phase of the hypoxia-evoked Ca^{2+} signal is caused by extracellular Ca^{2+} entry through VGCCs (Prabhakar, 2000). In addition, activation of muscarinic receptors by ACh in glomus cells causes Ca^{2+} release from an IP_3-sensitive store (Dasso *et al.*, 1997). However, the cytosolic Ca^{2+} clearance mechanisms that determine the time course of the decay of the Ca^{2+} signal in glomus cells are unclear. In this study, I examined the relative contribution of several major cytosolic Ca^{2+} clearance mechanisms (NCX, SERCA pump, PMCA pump, and mitochondria) in the regulation of Ca^{2+} homeostasis in glomus cells. I found that mitochondrial Ca^{2+}

uptake played a dominant role in cytosolic Ca^{2+} clearance in rat glomus cells. Since hypoxia causes mitochondrial depolarization (Duchen & Biscoe, 1992) and mitochondrial inhibitors have been shown to cause depolarization in glomus cells via the inhibition of oxygen-sensitive K^+ channels (Wyatt & Buckler, 2004), I examined whether hypoxia could affect the time course of the cytosolic Ca^{2+} clearance in glomus cells whose membrane potential was whole-cell voltage clamped. I also examined whether the exocytosis (which reflects transmitter release) of glomus cells was affected by the change in the duration of the depolarization-triggered Ca^{2+} signal when the mitochondrial function was inhibited.

3.2 Results

3.2.1 *Time course of cytosolic Ca^{2+} clearance during whole-cell patch clamp recording (in standard HEPES-buffered bath solution)*

For all experiments described in this chapter, each individual glomus cell was voltage clamped at -70 mV. Each stimulus of the cell involved a 500 ms voltage step to 0 mV which activated VGCCs and elicited a transient rise in $[Ca^{2+}]_i$. An example of a control cell (in standard HEPES-buffered bath solution) is shown in Fig. 3-2. At <3 min of whole-cell recording the holding current was very small (<7 pA). Over the next few minutes the holding current gradually increased by ~30 pA. Identical depolarizing voltage steps were delivered at ~3, ~7 and ~10 min

69

after the establishment of the whole-cell configuration (Fig. 3-2A). Note that following the termination of the depolarizing voltage step, the VGCC closed rapidly (Fig. 3-2B). Therefore, under my experimental conditions, the decay phase of the Ca^{2+} signal reflects the removal of cytosolic Ca^{2+} via various Ca^{2+} clearance mechanisms. As shown in Fig. 3-2B & C, the 2nd depolarization typically evoked a smaller Ca^{2+} current and a smaller Ca^{2+} signal when compared with those evoked by the 1st depolarization, probably reflecting a time-dependent rundown of VGCC with a longer duration of whole-cell recording. Note that with the 3rd depolarization, the amplitude of the Ca^{2+} signal was similar to that evoked by the 2nd depolarization but the current during the voltage pulse became outward (Fig. 3-2B & C). Because of the rundown of VGCC and the gradual development of an outward current with longer durations of whole-cell recording, the amplitude or time integral of the Ca^{2+} current was not analysed in my experiments except those in Appendix 2.

In rat glomus cells, mitochondrial inhibitors have been reported to suppress the background TASK-like K^{+} channels, resulting in depolarization (Wyatt & Buckler, 2004). Therefore, the control of cell membrane potential via voltage clamp (holding potential at -70 mV) as shown in Fig. 3-2 will prevent this excitatory effect of mitochondrial inhibitors in the experiments described in section 3.2.2. Moreover, I also included 5 mM ATP in the whole-cell pipette solution to reduce any decrease in cellular ATP content during my experiments.

As shown in Fig. 3-2C, the time course of the decay of the Ca^{2+} transients could be described by a single exponential function. Therefore, I estimated the

70

rate of cytosolic Ca^{2+} clearance from the time constant (τ) of the single exponential function fitted to the decay phase of each Ca^{2+} transient. In the example shown in Fig. 3-2, the τ for the decay phase of each of the three Ca^{2+} transients was 3.2, 4.8 and 4.8 s, respectively. In 5 cells examined, the mean value of the $[Ca^{2+}]_i$ decay τ in the 2nd depolarization was 5.3 ± 0.9 s, not significantly different from that obtained in the 1st depolarization (4.2 ± 0.6 s). The mean value of the $[Ca^{2+}]_i$ decay τ in the 3rd depolarization was 5.5 ± 1.3 s (n = 3), also not significantly different from that obtained in the 1st or 2nd depolarization. In these cells, the basal $[Ca^{2+}]_i$ before the 2nd and 3rd depolarization were 138 ± 11 nM (n = 5) and 146 ± 2 nM (n = 3) respectively. These values were not significantly different from the value of 116 ± 10 nM (n = 5) before the 1st depolarization. Therefore, despite a time-dependent increase in the amplitude of holding current over the duration of whole-cell recording in the control cells (Fig. A-1A and Table A-1a in Appendices), there was no significant change in $[Ca^{2+}]_i$ decay or basal $[Ca^{2+}]_i$ among the three depolarizations.

Although there were some variations in the basal $[Ca^{2+}]_i$ (25-250 nM; Fig. 3-3A) and the amplitude of the depolarization-triggered Ca^{2+} transients (0.5-4 µM; Fig. 3-3B) among individual glomus cells, neither the basal $[Ca^{2+}]_i$ (Fig. 3-3A) nor the amplitude of the Ca^{2+} transient (Fig. 3-3B) had any major influence on the time course of the $[Ca^{2+}]_i$ decay. Note that because of the variability in the amplitude of the Ca^{2+} transients among cells, a comparison of this parameter is meaningful only if the amplitude of each Ca^{2+} transient can be normalized with the total Ca^{2+} entry of each depolarizing voltage pulse (calculated from the time

integral of the Ca^{2+} current). However, as shown in Fig. 3-2B, the total Ca^{2+} entry could not be estimated accurately in my experiments because of the gradual development of an outward current when the cell was recorded in the whole-cell mode for a few minutes (even with Cs^+ and TEA in the pipette solution). Therefore, for the rest of my thesis, my analysis is restricted to the time course of the $[Ca^{2+}]_i$ decay.

3.2.2 *Effects of mitochondrial inhibition on the Ca^{2+} signal*

I first examined the effect of CCCP which dissipates the mitochondrial proton gradient and thus collapses the mitochondrial membrane potential. Fig. 3-4A shows an example of the effect of CCCP on the Ca^{2+} signal of a glomus cell. At ~3 min after the establishment of whole-cell configuration while the cell was bathed in standard extracellular solution, a depolarizing voltage step was delivered, resulting in a transient rise of $[Ca^{2+}]_i$. Upon the return of $[Ca^{2+}]_i$ to basal level, the bath solution was switched to one containing CCCP (2 µM). Shortly after the application of CCCP (~40 s in this example), a 2nd depolarizing voltage step was delivered. Note that in the presence of CCCP, the decay of the Ca^{2+} transient was dramatically slower. Fig. 3-4B shows the superimposed Ca^{2+} transients (scaled to matching amplitudes) evoked before and in the presence of CCCP (same cell as in Fig. 3-4A). In this example, before the application of CCCP, the $[Ca^{2+}]_i$ decay τ was 3.2 s and it increased ~8-fold to 25.5 s in the presence of CCCP. Upon the removal of CCCP for ~3.5 min, the $[Ca^{2+}]_i$ decay τ decreased to 9.9 s. In 5 cells examined with this experimental protocol (i.e. the

delivery of a 2nd depolarization shortly after the application of CCCP), the mean value of the $[Ca^{2+}]_i$ decay τ before CCCP was 3.2 ± 0.5 s and it increased by ~6-fold to 18.8 ± 2.7 s in the presence of CCCP (Fig. 3-4C). The removal of CCCP partially restored the rate of Ca^{2+} removal (7.6 ± 1.3 s; Fig. 3-4C). Fig. 3-4D shows that a longer exposure (~2-3 min) to CCCP (2 µM) caused a gradual rise in basal $[Ca^{2+}]_i$. When the CCCP-induced rise in basal $[Ca^{2+}]_i$ reached a plateau, a 2nd depolarizing voltage step was delivered to evoke a Ca^{2+} transient (at ~7-8 min after the establishment of whole-cell configuration). In cells examined with this experimental protocol (i.e. the delivery of a 2nd depolarization after the CCCP-induced basal $[Ca^{2+}]_i$ elevation reached a plateau), CCCP at 2 or 10 µM elevated basal $[Ca^{2+}]_i$ by ~140 nM (Fig. 3-4E) and slowed $[Ca^{2+}]_i$ decay by 2.4 or 3.1-fold (Fig. 3-4F). These results suggest that mitochondria play a significant role in the clearance of cytosolic Ca^{2+} in rat glomus cells.

To further examine the role of mitochondria, I employed cyanide which is an inhibitor of the activity of complex IV in the respiratory chain. The example in Fig. 3-5A shows that in the presence of cyanide (5 mM), there was a gradual rise in basal $[Ca^{2+}]_i$ and a slowing in the decay of the depolarization-triggered Ca^{2+} signal (Fig. 3-5B). In 5 cells examined with this experimental protocol, cyanide elevated basal $[Ca^{2+}]_i$ by 143 ± 26 nM (Fig. 3-5C) and increased the $[Ca^{2+}]_i$ decay τ by ~2.1-fold (from 4.8 ± 0.6 s to 9.9 ± 1.4 s; Fig. 3-5D). I also tested whether the delivery of a 2nd depolarization before the onset of the cyanide-evoked rise in basal $[Ca^{2+}]_i$ could affect the $[Ca^{2+}]_i$ decay. In 5 cells examined with this experimental protocol, the $[Ca^{2+}]_i$ decay τ was increased by ~1.9-fold in the

presence of cyanide and the $[Ca^{2+}]_i$ decay accelerated upon the removal of cyanide (Fig. 3-5E). Since both CCCP and cyanide elevated basal $[Ca^{2+}]_i$ in glomus cells when the cells were voltage clamped at -70 mV, this rise in basal $[Ca^{2+}]_i$ could not be due to VGCC-mediated Ca^{2+} entry. It has been suggested that mitochondrial inhibitors may cause Ca^{2+} release from mitochondria in glomus cells (Duchen & Biscoe, 1992; Wyatt & Buckler, 2004). However, in a Ca^{2+}-free bath solution (which also contained 1 mM EGTA), the application of cyanide did not evoke any detectable rise in $[Ca^{2+}]_i$ ($\Delta[Ca^{2+}]_i$ = -15 ± 9 nM; n = 5). Thus, mitochondrial inhibitors did not evoke any intracellular Ca^{2+} release and the rise in basal $[Ca^{2+}]_i$ was dependent on the presence of extracellular Ca^{2+}.

3.2.3 Effects of inhibition of the SERCA pump, PMCA pump or NCX on Ca^{2+} signals

In endocrine cells such as pancreatic β cells (Hughes et al., 2006) and pituitary gonadotropes (Tse et al., 1994), Ca^{2+} uptake into the ER via the SERCA pump is the dominant mechanism for cytosolic Ca^{2+} removal. To examine the role of the SERCA pump in glomus cells, I employed 2,5-di(tert-butyl)-1,4-benzohydroquinone (BHQ) to inhibit SERCA pump activities. As shown in the example in Fig. 3-6A, application of BHQ (20 µM) caused a rise in basal $[Ca^{2+}]_i$. The decay of the depolarization-triggered Ca^{2+} signal was slightly slower in the presence of BHQ (e.g. Fig. 3-6B). In 6 cells investigated, BHQ elevated basal $[Ca^{2+}]_i$ by 71 ± 13 nM (Fig. 3-6C) and slowed the decay of the depolarization-triggered Ca^{2+} signal by 1.6 ± 0.1-fold (7.1 ± 1.0 s versus 4.6 ± 0.4 s; Fig. 3-6D).

In the absence of extracellular Ca^{2+}, BHQ failed to trigger any detectable rise in basal $[Ca^{2+}]_i$ (n = 4), indicating that the BHQ-mediated rise in basal $[Ca^{2+}]_i$ was dependent on extracellular Ca^{2+}. I also tested another SERCA pump inhibitor, cyclopiazonic acid (CPA). Similar to BHQ, the application of CPA (50 µM) elevated basal $[Ca^{2+}]_i$ by 87 ± 21 nM and slowed the $[Ca^{2+}]_i$ decay by ~1.8-fold (5.5 ± 0.6 s versus 3.1 ± 0.4 s; n = 4; Fig. 3-6E). These findings suggest that the SERCA pump plays some role in cytosolic Ca^{2+} clearance in rat glomus cells.

I next examined whether the PMCA pump also contributed to the regulation of Ca^{2+} dynamics in glomus cells. Since the extrusion of cytosolic Ca^{2+} by the PMCA pump depends on Ca^{2+}/H^+ exchange (Xu et al., 2000), the lowering of extracellular $[H^+]$ (e.g. bath solution of pH 8.8) can reduce PMCA pump activities (Wennemuth *et al.*, 2003; Gover *et al.*, 2007). As shown in Fig. 3-7A, the decay of the depolarization-triggered Ca^{2+} signal was slowed slightly when the cell was exposed to a bath solution of pH 8.8. On average, the rate of cytosolic Ca^{2+} removal was slowed by 1.7 ± 0.1-fold (7.1 ± 0.8 s versus 4.3 ± 0.4 s; Fig. 3-7B) but there was no significant change in basal $[Ca^{2+}]_i$ (Fig. 3-7C). I also investigated whether the inhibition of cytosolic Ca^{2+} extrusion via NCX affected Ca^{2+} homeostasis in glomus cells. As shown in the example in Fig. 3-7D, the removal of extracellular Na^+ resulted in a small slowing in the $[Ca^{2+}]_i$ decay. In 5 cells investigated, NCX inhibition slowed the rate of cytosolic Ca^{2+} removal by 1.7 ± 0.2-fold (7.4 ± 1.1 s versus 4.4 ± 0.3 s; Fig. 3-7E) but did not cause any significant change in basal $[Ca^{2+}]_i$ (Fig. 3-7F). These findings suggest that both

PMCA pump and NCX play some role in cytosolic Ca^{2+} clearance in rat glomus cells.

3.2.4 A dominant role of mitochondria in cytosolic Ca^{2+} clearance

For the experiments shown above (Figs. 3-4 to 3-7), the effects of various inhibitors of the Ca^{2+} clearance mechanisms were compared in the same cells before (~3 min after whole-cell configuration) and in the presence of inhibitors (~7 min after whole-cell configuration). As described in Section 3.2.1, I found no significant difference in basal $[Ca^{2+}]_i$ or the time constant of $[Ca^{2+}]_i$ decay between the 1st and 2nd depolarization in control cells. Nevertheless, the $[Ca^{2+}]_i$ decay τ tended to increase slightly (~1.3-fold) at the 2nd depolarization. Therefore, to quantify the relative effects of the different inhibitors, I compared the Ca^{2+} signals in the presence of different inhibitors with their time-matched controls (Fig. 3-8). When compared to time-matched controls (at ~7 min of whole-cell recording), significant elevations in basal $[Ca^{2+}]_i$ could still be detected with inhibition of the SERCA pump or mitochondrial function (Fig. 3-8A). Similarly, significant slowing in cytosolic Ca^{2+} clearance was detected with all the inhibitors tested (Fig. 3-8B). Note that the effects of the mitochondrial inhibitors (CCCP and cyanide) were most dramatic. For experiments in which the 2nd depolarization was delivered after the CCCP or cyanide-mediated rise in basal $[Ca^{2+}]_i$ had reached a plateau, the decay of the Ca^{2+} signal was slowed by >2-fold. On the other hand, inhibition of SERCA pump, NCX or PMCA pump slowed cytosolic Ca^{2+} removal by only ~20-30%.

76

A previous study in corticotropes has shown that mitochondrial Ca^{2+} uptake can be progressively inhibited by loading ruthenium red into the cytosol via the whole-cell pipette (Lee & Tse, 2005). To examine whether ruthenium red has a similar effect on glomus cells, I included ruthenium red (10 µM) in the whole-cell pipette solution. The depolarization-triggered Ca^{2+} transients were elicited at 2 min intervals starting at ~1 min after the establishment of whole-cell configuration. As shown in Fig. 3-9A, after the establishment of whole-cell configuration, there was a gradual slowing in the $[Ca^{2+}]_i$ decay when ruthenium red was loaded into the cell via the whole-cell pipette. In comparison, there was less slowing in the $[Ca^{2+}]_i$ decay for the time-matched controls (e.g. Fig. 3-9B). For cells recorded with ruthenium red in the pipette solution, the rate of $[Ca^{2+}]_i$ decay (at ~3 min after the establishment of whole-cell configuration) was ~1.6-fold slower ($\tau = 7.8 \pm 0.5$ s; n = 5) than the time-matched control ($\tau = 5.1 \pm 0.6$ s, n = 4; Fig. 3-9D). Thus, Ca^{2+} uptake via the mitochondria is a major cytosolic Ca^{2+} clearance mechanism in glomus cells.

3.2.5 Influence of hypoxia on cytosolic Ca^{2+} clearance

Since hypoxia has been shown to cause mitochondrial depolarization in glomus cells (Duchen & Biscoe, 1992) and mitochondrial inhibitors slowed cytosolic Ca^{2+} clearance (Figs. 3-4 and 3-5), I examined whether hypoxia affected the Ca^{2+} dynamics in glomus cells. Fig. 3-10A shows the depolarization-triggered Ca^{2+} transients before and at 3, 5 or 7 min of hypoxia. The cell was voltage clamped at -70 mV (with the perforated-patch clamp technique) to prevent any

depolarization induced by hypoxia (Buckler, 1997; Buckler & Vaughan-Jones, 1998). Under hypoxic conditions, there was a slowing in the decay of the Ca^{2+} transients and the basal $[Ca^{2+}]_i$ also stayed slightly elevated (~30 nM; Fig. 3-10A). Upon return to normoxic conditions, the basal $[Ca^{2+}]_i$ returned to pre-hypoxic level. A similar small elevation (<30 nM) in basal $[Ca^{2+}]_i$ was detected in 2 other cells (out of 5) during hypoxia. Because of the small amplitude of the basal $[Ca^{2+}]_i$ rise, it was not further investigated. Fig. 3-10B shows the superimposed Ca^{2+} transients (scaled to matching amplitudes) evoked before and after 5 min of hypoxia (same cell as in Fig. 3-10A). Note that in this cell, exposure to the hypoxic condition for 5 min slowed the $[Ca^{2+}]_i$ decay by ~2-fold (τ = 6.0 s versus 3.0 s). In 5 cells examined, the decay of Ca^{2+} transient was slowed by 1.6-1.9-fold when exposed to hypoxia for 3-7 min and recovered partially upon the return to normoxic conditions (Fig. 3-10C). The slowing in cytosolic Ca^{2+} clearance observed with hypoxia is smaller than that induced by CCCP (Fig. 3-4) but comparable to that mediated by cyanide (Fig. 3-5). Thus, my result is consistent with the notion that during hypoxia, the depolarization in mitochondrial membrane potential impairs Ca^{2+} uptake and causes a slowing in cytosolic Ca^{2+} clearance.

3.2.6 Influence of mitochondrial inhibition on exocytotic response

My above findings indicate that mitochondrial inhibition slowed the decay of the depolarization-triggered Ca^{2+} signal in glomus cells. Since the hypoxia-evoked transmitter release from glomus cells is dependent on voltage-gated Ca^{2+} entry, Dr.

Andy Lee in our laboratory examined how the change in the shape of the Ca^{2+} signal after mitochondrial inhibition might affect secretion by monitoring $[Ca^{2+}]_i$ simultaneously with exocytosis (membrane capacitance measurement). An example of this experiment is shown in Fig. 3-11A. The cell was whole-cell voltage clamped at -70 mV and a 500 ms voltage step to 0 mV was first delivered in control condition (standard bath solution) to trigger a Ca^{2+} transient. The rise in $[Ca^{2+}]_i$ was accompanied by an increase in cell membrane capacitance, reflecting exocytosis. Note that the cell membrane capacitance continued to increase as long as $[Ca^{2+}]_i$ remained above ~1 µM and the cumulative increase in capacitance was ~25 fF. The same cell was then exposed to CCCP (2 µM). Similar to the results described in Fig. 3-4, CCCP slowed the decay of the depolarization-triggered Ca^{2+} signal. In Fig. 3-11A, the amplitude of the depolarization-triggered Ca^{2+} signal before and in the presence of CCCP was similar. Note that with the slowing of cytosolic Ca^{2+} clearance by CCCP, the depolarization-triggered Ca^{2+} signal stayed above 1 µM for a longer duration (~19 s versus ~5 s before CCCP) and resulted in more exocytosis. The cumulative increase in cell membrane capacitance evoked by the 2nd depolarization in the presence of CCCP was ~70 fF, almost 3-fold larger than the control. In this example, as well as other cells in this experiment, there was a partial recovery in the rate of Ca^{2+} clearance upon the removal of CCCP but the amplitude of the Ca^{2+} transient was reduced by ~50% and no exocytosis was triggered. In 5 cells examined, a single 500 ms voltage step increased the cell membrane capacitance by 9 ± 5 fF in control conditions (Fig. 3-11B). The secretory granules in glomus cells have a diameter of ~100 nm and the

exocytosis of a single granule of this size should contribute ~0.3 fF increase in cell membrane capacitance (Klyachko & Jackson, 2002). If the above assumption is correct, an increase in the cell membrane capacitance by 9 fF should reflect that ~30 glomus granules were released by the Ca^{2+} signal triggered by a 500 ms voltage step under control conditions. In the presence of CCCP, the same voltage step increased the cell membrane capacitance by 50 ± 11 fF (Fig. 3-11B), releasing ~160 granules. The increase in exocytotic response in CCCP was associated with an increase in the duration of the depolarization-triggered Ca^{2+} signal. As shown in Fig. 3-11C, the average duration of the Ca^{2+} signal at $[Ca^{2+}]_i$ ≥1 µM in these 5 cells before CCCP was 4.0 ± 0.6 s and it increased ~6-fold to 23.8 ± 5.5 s in CCCP. Note that there was no significant difference in the amplitude of the Ca^{2+} transient before and after CCCP in these cells (Fig. 3-11D). Overall, our findings suggest that an increase in the duration of the Ca^{2+} signal was the major mechanism underlying the enhancement of the depolarization-triggered exocytotic response by CCCP.

3.3 Discussion

In this study, I investigated the role of mitochondria in the regulation of Ca^{2+} dynamics in glomus cells with two mitochondrial inhibitors. My results show that cyanide, which inhibits mitochondria by acting at the electron transport chain, caused a small elevation in basal $[Ca^{2+}]_i$ (~140 nM) in glomus cells (Fig. 3-5C) and slowed the decay of the Ca^{2+} transient by ~2.1-fold (Fig. 3-5D). The effect of cyanide on the $[Ca^{2+}]_i$ decay was not influenced by the increase in basal $[Ca^{2+}]_i$;

when the depolarizing voltage step was delivered before the onset of the cyanide-mediated rise in basal $[Ca^{2+}]_i$, cyanide still slowed the $[Ca^{2+}]_i$ decay by ~1.9-fold (Fig. 3-5E). The mitochondrial uncoupler CCCP also caused a small elevation in basal $[Ca^{2+}]_i$ (~140 nM) and a slowing in the rate of cytosolic Ca^{2+} clearance (Fig. 3-4). Interestingly, the slowing in $[Ca^{2+}]_i$ decay by CCCP was more robust if the depolarization was delivered shortly (30-40 s) after the application of CCCP (i.e. before the onset of the CCCP-mediated rise in basal $[Ca^{2+}]_i$). Under this condition, CCCP (2 μM) slowed the $[Ca^{2+}]_i$ decay by ~6-fold (Fig. 3-4C). In contrast, when the depolarization was delivered after the CCCP-mediated rise in basal $[Ca^{2+}]_i$ reached a plateau (typically ~2-3 min in CCCP), the slowing in $[Ca^{2+}]_i$ decay by CCCP at 2 or 10 μM was only ~2.4 and 3.1-fold respectively (Fig. 3-4F). It is not clear why the slowing in $[Ca^{2+}]_i$ decay by CCCP (but not cyanide) was affected by the duration of exposure to the inhibitor. One possible explanation is that mitochondrial depolarization develops rapidly in the presence of CCCP but the continuous supply of ATP (5 mM) via the whole-cell pipette may fuel the reversal of the ATP synthase and result in a partial recovery of the mitochondrial membrane potential. Nevertheless, the dramatic slowing in $[Ca^{2+}]_i$ decay by CCCP or cyanide before the development of basal $[Ca^{2+}]_i$ rise is consistent with the scenario that the CCCP or cyanide-mediated mitochondrial depolarization reduces the driving force across the inner membrane of mitochondria and thus inhibits mitochondrial Ca^{2+} uptake.

The dominant role of mitochondria in cytosolic Ca^{2+} clearance is further supported by my finding that intracellular ruthenium red also slowed the $[Ca^{2+}]_i$

81

decay (Fig. 3-9). It has been known for a long time that Ca^{2+} can be taken up into mitochondria by the mitochondrial uniporter which has a low affinity for Ca^{2+} (Kd $\geq$10 μM) (Santo-Domingo & Demaurex, 2010). Although the mitochondrial uniporter has a low affinity for Ca^{2+}, it is likely that some mitochondria near the plasma membrane experience a much higher local [Ca^{2+}] following the VGCC-mediated extracellular Ca^{2+} influx and thus robustly activate the uniporter (Carafoli, 2010). However, it has recently been reported that mitochondria also possess at least two other forms of Ca^{2+} uptake mechanisms including a rapid mode of Ca^{2+} uptake (RaM) which activates transiently at the beginning of the repetitive Ca^{2+} pulses, and the Ca^{2+}/H^+ antiporter which exchanges 1 Ca^{2+} for 1 H^+. Both RaM and Ca^{2+}/H^+ antiporter have high affinities for Ca^{2+} (Kd >100 nM) (Jiang *et al.*, 2009; Santo-Domingo & Demaurex, 2010). Since ruthenium red can inhibit all three Ca^{2+} uptake mechanisms (Santo-Domingo & Demaurex, 2010), it is not possible to determine the relative contribution of the three mitochondrial Ca^{2+} uptake mechanisms in the removal of cytosolic Ca^{2+} in rat glomus cells. Consistent with the notion that Ca^{2+} uptake into mitochondria is the major mechanism of cytosolic Ca^{2+} clearance in glomus cells, the inhibition of other Ca^{2+} transport mechanisms (SERCA pump, PMCA pump or NCX) only slowed the cytosolic Ca^{2+} clearance by ~20-30% (Fig. 3-8B).

A dominant role of mitochondrial Ca^{2+} uptake in regulating cytosolic Ca^{2+} clearance has also been reported in chromaffin cells (Herrington et al., 1996), sympathetic neurons (Friel, 2000) and pituitary corticotropes (Lee & Tse, 2005). In chromaffin cells (Herrington et al., 1996) and sympathetic neurons (Friel,

82

2000), the $[Ca^{2+}]_i$ decay was monophasic only when depolarization elevated $[Ca^{2+}]_i$ to <0.5 μM. At higher rises of $[Ca^{2+}]_i$, the $[Ca^{2+}]_i$ decay in chromaffin cells and sympathetic neurons was complex: the initial fast decline phase (τ of ~3 s) was followed by a plateau phase and then a slow return to basal level (Herrington et al., 1996; Friel, 2000). The plateau phase of the $[Ca^{2+}]_i$ decay was attributed to the efflux of mitochondrial Ca^{2+} to the cytosol (Babcock et al., 1997; Friel, 2000). Consistent with this, in chromaffin cells and sympathetic neurons, CCCP slowed the decay of the initial decline phase, abolished the plateau phase and accelerated the slow return of $[Ca^{2+}]_i$ to basal level (Herrington et al., 1996; Friel, 2000). In glomus cells, however, the time course of the decay of the Ca^{2+} transient (with peak $[Ca^{2+}]_i$ ranging from 0.5 to 4 μM) could be well described by a single exponential function with a τ value of ~4 s (e.g. Fig. 3-3B). The absence of a plateau phase in the depolarization-triggered Ca^{2+} transients of glomus cells suggests that mitochondrial Ca^{2+} efflux is not significant during the time course of $[Ca^{2+}]_i$ decay. Consistent with this, CCCP or cyanide slowed the decay of the Ca^{2+} transient in glomus cells but the decay remained monophasic (e.g. Fig. 3-4B). The $[Ca^{2+}]_i$ decay kinetics of glomus cells resembles those of pituitary corticotropes whose Ca^{2+} transient (regardless of its amplitude) also decayed monotonically with a time constant of ~5-6 s (Lee & Tse, 2005). A similar slowing in $[Ca^{2+}]_i$ decay (~3-fold) by CCCP or cyanide was also reported in corticotropes (Lee & Tse, 2005). Thus, it is possible that in glomus cells as well as corticotropes, the efflux of Ca^{2+} from the mitochondria to the cytosol occurs at a much slower rate than in chromaffin cells and sympathetic neurons. Alternatively, Ca^{2+} efflux from

the mitochondria may be locally taken up into the adjacent ER or other cellular compartments and thus was undetected by the cytosolic Ca^{2+} indicator.

In glomus cells, CCCP or cyanide caused a gradual elevation in basal $[Ca^{2+}]_i$ (~140 nM; Figs. 3-4 and 3-5) which was not associated with an increase in holding current (Fig. A-1A and Table A-1a in Appendices). CCCP also elevated basal $[Ca^{2+}]_i$ in chromaffin cells and the effect of CCCP was attributed to mitochondrial Ca^{2+} release (Babcock et al., 1997). However, as described in Section 3.2.2, in the absence of extracellular Ca^{2+}, cyanide did not evoke any rise in basal $[Ca^{2+}]_i$, suggesting a dependence on extracellular Ca^{2+}. Both CCCP and cyanide reduce mitochondrial ATP synthesis. Although in my experiments, ATP (5 mM) was continuously supplied to the cell via the whole-cell pipette, it remains a possibility that the local ATP generation by mitochondria may be needed to fully support the function of some Ca^{2+} pumps. Consistent with this, in rat sensory neurons, the activities of the SERCA pump, but not the PMCA pump, was found to be dependent on mitochondrial generated ATP (Jackson & Thayer, 2006). My results show that the inhibition of PMCA pump did not cause any significant elevation in basal $[Ca^{2+}]_i$ (Fig. 3-7C) but SERCA pump inhibition caused a small rise in basal $[Ca^{2+}]_i$ (~70 nM; Fig. 3-6C). SERCA pump inhibition has been reported to elevate basal $[Ca^{2+}]_i$ in many cell types and this effect is attributed to the depletion of ER Ca^{2+} stores and the activation of capacitative Ca^{2+} entry (Parekh, 2006). Since the BHQ-mediated Ca^{2+} rise in glomus cells required the presence of extracellular Ca^{2+} (Section 3.2.3), it is likely that capacitative Ca^{2+} entry is involved. While this raises the possibility that the CCCP or cyanide-

mediated rise in basal $[Ca^{2+}]_i$ in glomus cell is secondary to an impairment of SERCA pump function which in turn activates capacitative Ca^{2+} entry, several lines of evidence argue against this scenario. First, the $[Ca^{2+}]_i$ rise evoked by BHQ or CPA was only 70-90 nM, about 50% of that evoked by CCCP or cyanide (~140 nM). Second, in a previous study in corticotropes, our laboratory has shown that the cyanide-mediated increase in basal $[Ca^{2+}]_i$ was not associated with an increase in extracellular Ca^{2+} influx (Lee & Tse, 2005). Third, inhibition of mitochondria was shown to reduce capacitative Ca^{2+} entry via a Ca^{2+}-dependent inactivation of calcium release-activated calcium (CRAC) channels (Parekh, 2008). Thus, mitochondrial inhibition is anticipated to reduce capacitative Ca^{2+} entry. Finally, in the presence of BHQ, cyanide could still evoke a rise in basal $[Ca^{2+}]_i$ in glomus cells (my unpublished observation). Therefore, it is unlikely that an impairment of SERCA pump can account for the mitochondrial inhibitor-mediated rise in basal $[Ca^{2+}]_i$. I found that the removal of extracellular Ca^{2+} reduced the basal $[Ca^{2+}]_i$ of glomus cells by ~90 nM, suggesting the presence of a basal Ca^{2+} influx. I speculate that mitochondrial Ca^{2+} uptake contributes to balance this basal Ca^{2+} influx, possibly with a scenario similar to that of the mitochondrial uptake of Ca^{2+} during the activation of capacitative Ca^{2+} entry and the subsequent release of mitochondrial Ca^{2+} to the ER (Parekh, 2008). Such a mechanism can help to replenish the Ca^{2+} stores in the ER, which prevents the ER stress induced by Ca^{2+} depletion in the lumen of the ER and the subsequent cell damage (Mekahli *et al.*, 2011). With mitochondrial inhibition, the basal Ca^{2+} influx is no longer balanced and results in a small elevation of basal $[Ca^{2+}]_i$.

Dr. Andy Lee found that in glomus cells, exocytosis continued to occur even when the depolarization-triggered Ca^{2+} signal was decaying (Fig. 3-11A). In contrast, in rat pancreatic β cells, exocytosis typically stopped with the termination of VGCC-mediated Ca^{2+} entry even when $[Ca^{2+}]_i$ remained elevated (Hughes et al., 2006). This observation in β cells was attributed to the tight coupling between the VGCCs and secretory granules such that the dissipation of local Ca^{2+} gradient following the closing of VGCCs terminated the exocytotic response (Barg *et al.*, 2002; Hughes *et al.*, 2006). Thus, in glomus cells, exocytosis may be less dependent on the local Ca^{2+} gradient near the VGCCs, and a sustained elevation in cytosolic $[Ca^{2+}]$ can continue to trigger exocytosis. In this scenario, the duration of the Ca^{2+} signal is expected to have a strong impact on the amount of exocytosis. Consistent with this, when the clearance of cytosolic Ca^{2+} was slowed by the mitochondrial inhibitor, the increase in the duration of the depolarization-triggered Ca^{2+} signal was associated with an enhancement of the exocytotic response (Fig. 3-11). The ability of glomus cells to undergo sustained release of neurotransmitters while $[Ca^{2+}]_i$ is elevated beyond ~1 μM for many seconds after the activation of VGCCs may be an important adaptive mechanism for prolonged episodes of hypoxia.

In a physiological context, hypoxia triggers $[Ca^{2+}]_i$ elevation in glomus cells via depolarization and activation of VGCCs. Under hypoxic conditions, there was also a slowing in the rate of cytosolic Ca^{2+} clearance (Fig. 3-10). This is consistent with the scenario that hypoxia causes mitochondrial depolarization (Duchen & Biscoe, 1992) which decreases mitochondrial Ca^{2+} uptake. The slowing of

cytosolic Ca^{2+} clearance resulted in an enhancement of neurotransmitter release. The multiplicity of the influences of mitochondria on glomus cell Ca^{2+} signaling and exocytosis underscores the importance of mitochondria in hypoxic chemotransduction in the carotid bodies.

3.4 Acknowledgements
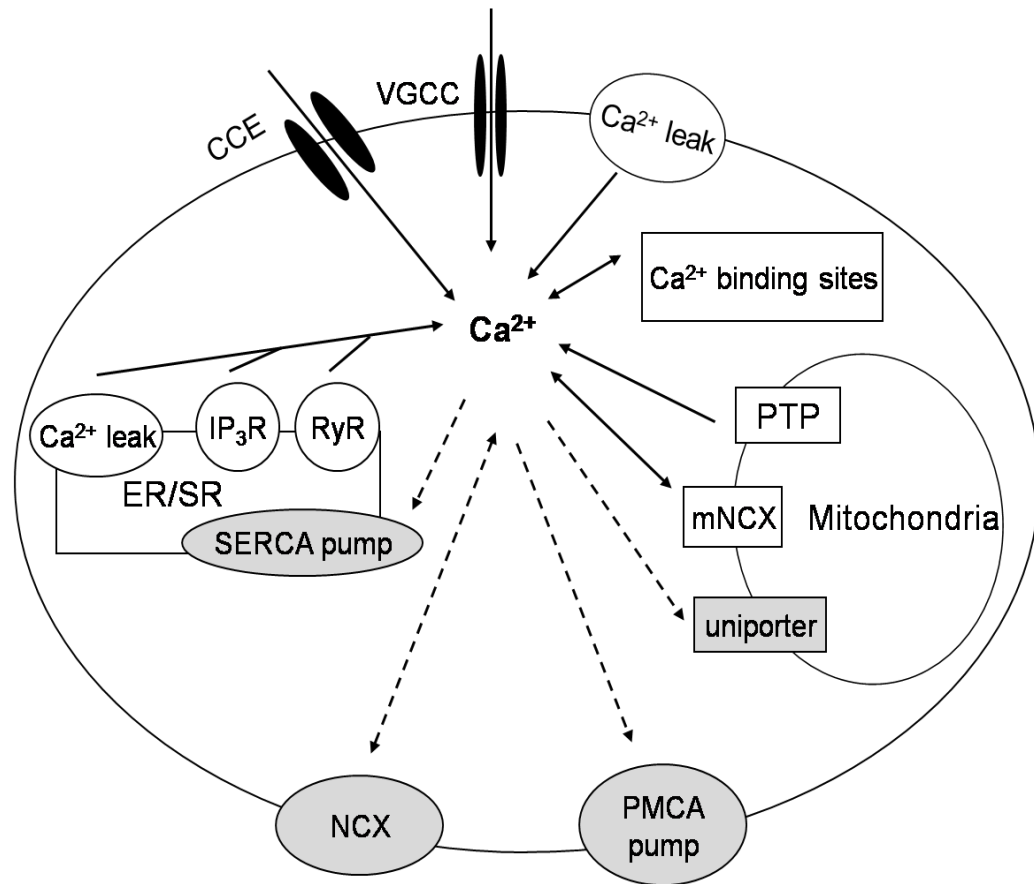
Figure 3-1 Ca^{2+} dynamics and homeostasis. Extracellular Ca^{2+} entry can occur via the activation of VGCC, CCE or via a passive Ca^{2+} leak. Ca^{2+} can be released from ER/SR (via IP_3R, RyR channels or passive Ca^{2+} leak), as well as mitochondria (via PTP or mNCX). Most of the Ca^{2+} is bound to the endogenous Ca^{2+} binding sites. Only a small fraction shows up as free Ca^{2+} and contributes to the rising phase of the Ca^{2+} transient. Ca^{2+} can be extruded to the extracellular space by plasma membrane NCX and PMCA pump. Some Ca^{2+} is sequestered into the ER/SR via the SERCA pump or into the mitochondria via the uniporter.
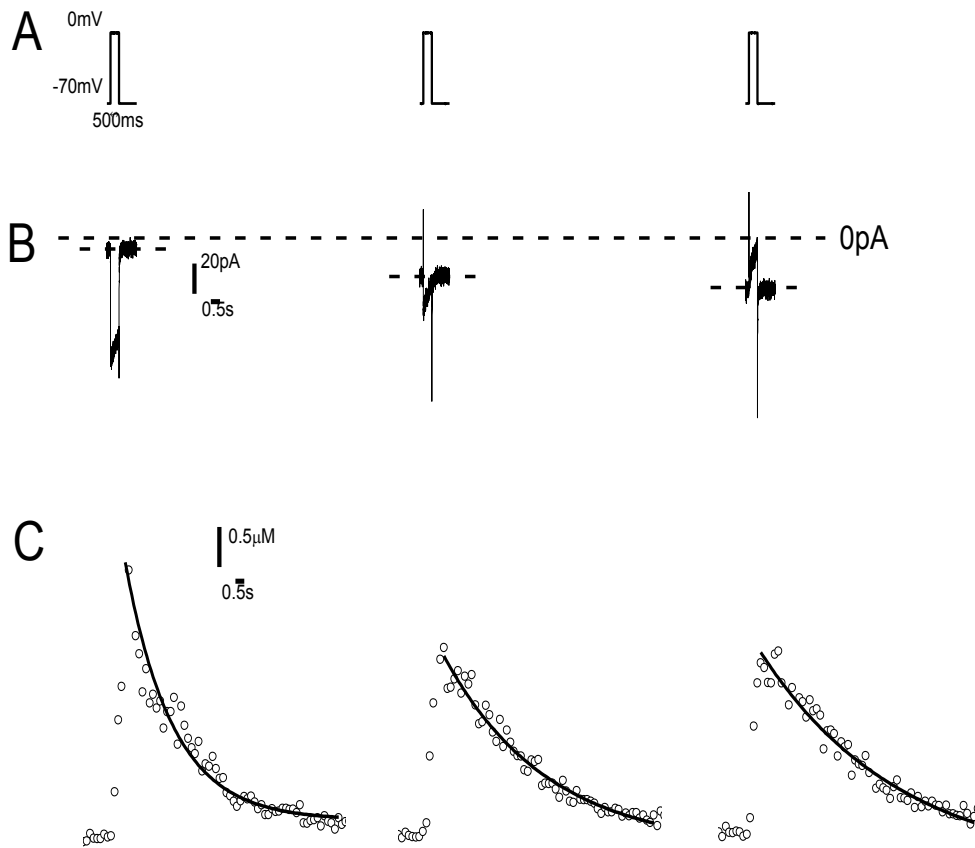
Figure 3-2 Depolarization-triggered Ca^{2+} signals during whole-cell patch clamp recording (in HEPES-buffered external solution) in glomus cells. (A) A control cell was voltage clamped at -70 mV and a depolarizing voltage step (500 ms) to 0 mV was applied to elicit Ca^{2+} entry through VGCCs at about 3, 7 and 10 min after the establishment of whole-cell configuration. (B) The Ca^{2+} current (K^+ currents are blocked by Cs^+ and TEA in the pipette solution) evoked by each depolarization. Note that the current evoked by the 3rd depolarization was outward although the amplitude of the Ca^{2+} signal was similar to that evoked by the 2nd depolarization. (C) The corresponding Ca^{2+} transients (circles) were recorded with indo-1 at every 200 ms. The decay phase of the Ca^{2+} transient could be well described by a single exponential function (solid lines).
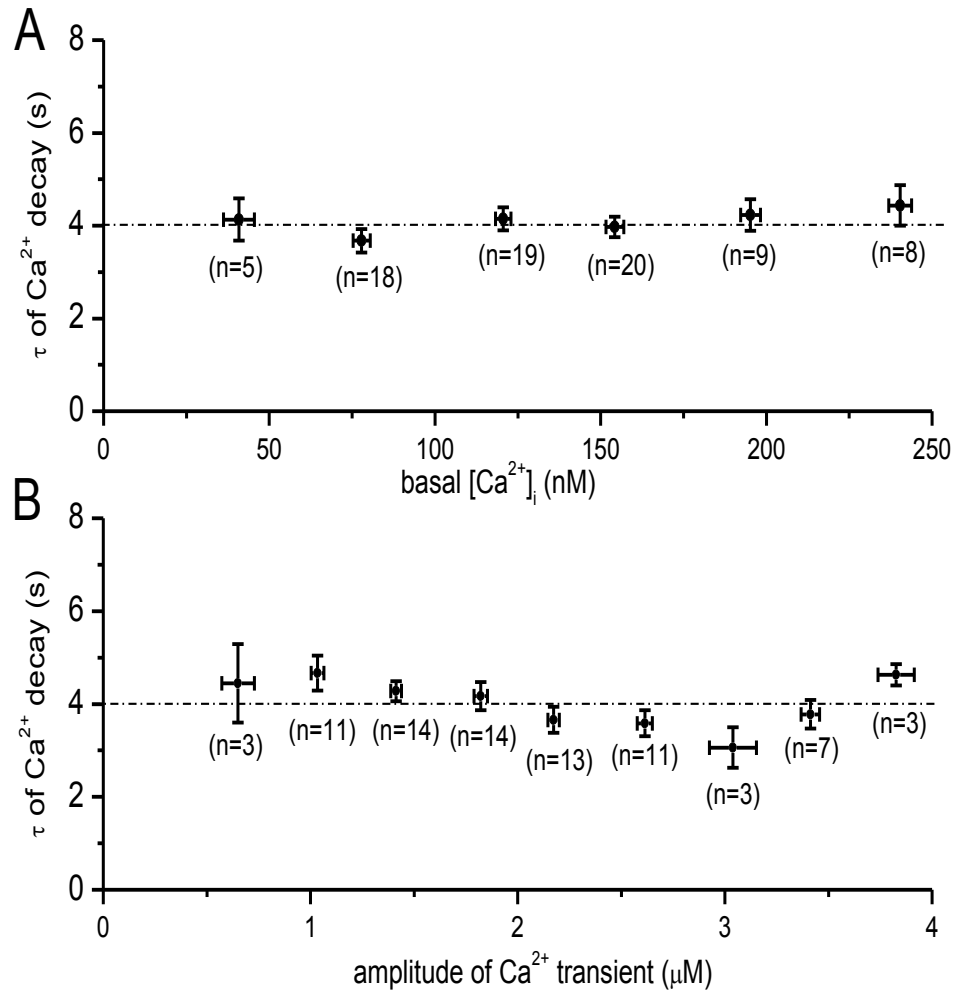
89

Figure 3-3 The basal $[Ca^{2+}]_i$ (A) and the amplitude of the depolarization-triggered Ca^{2+} transient (B) had little effect on $[Ca^{2+}]_i$ decay τ. The dashed lines shown in (A) and (B) depict the value of τ averaged from all the cells (n = 79). The error bars shown in this figure and all other figures of this thesis represent SEM.
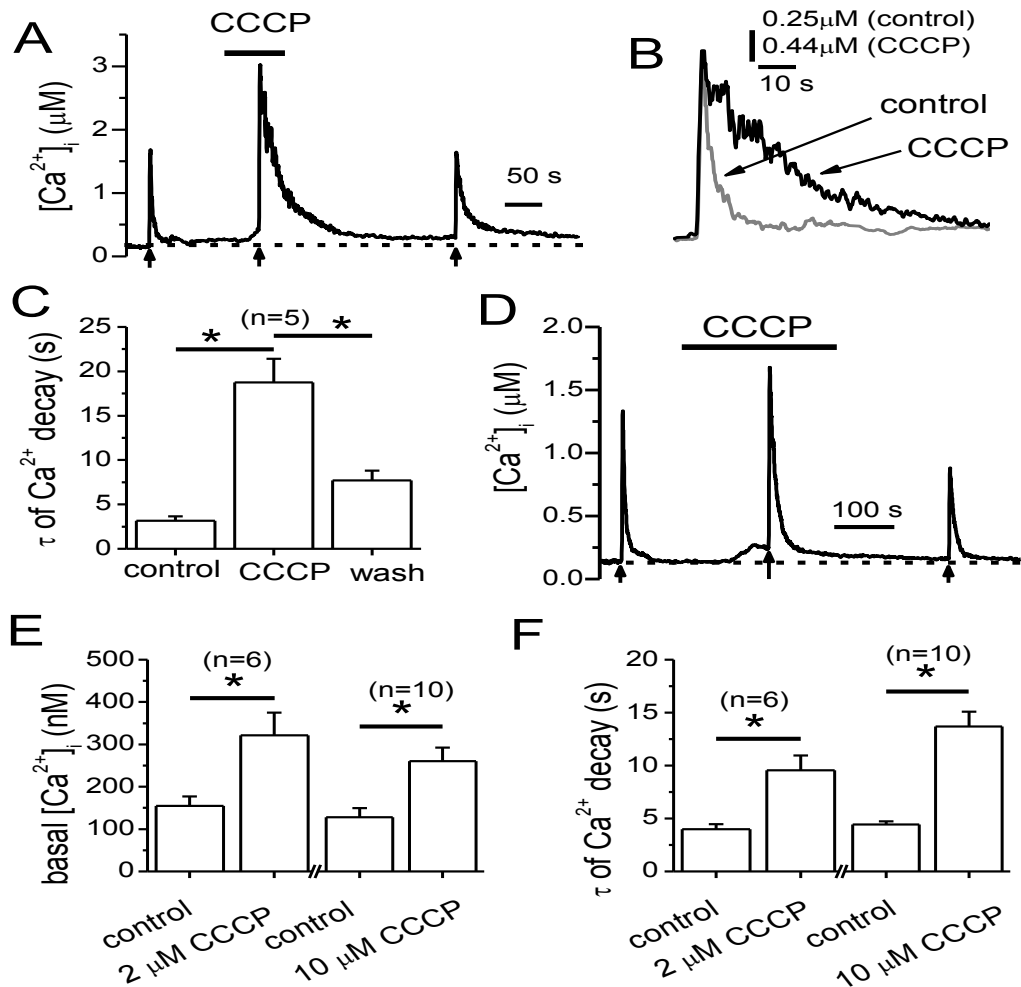
Figure 3-4 Effects of the mitochondrial inhibitor CCCP on the Ca^{2+} dynamics of glomus cell. (A) A short application of CCCP (2 μM) caused a dramatic slowing in the decay of the depolarization-triggered Ca^{2+} signal. The cell was voltage clamped at -70 mV. At the time indicated by each arrow, a voltage step (500 ms) to 0 mV was delivered to evoke voltage-gated Ca^{2+} entry. The dashed line denotes the initial resting $[Ca^{2+}]_i$. (B) Superimposed traces of the Ca^{2+} transients before and in CCCP (same cell as in A). For comparison, the amplitude of the Ca^{2+} transient in control was scaled up to match that in CCCP. (C) Slowing in the $[Ca^{2+}]_i$ decay by CCCP (2 μM; before the triggering of a rise in basal $[Ca^{2+}]_i$). Plot of the mean values of the time constant (τ) of the exponential fit to the $[Ca^{2+}]_i$ decay before, shortly (30-40 s) after the application of CCCP (2 μM) and after CCCP removal. (D) A longer exposure (2-3 min) to CCCP (2 μM) caused a rise in basal $[Ca^{2+}]_i$. A depolarizing voltage step was delivered when the CCCP-evoked rise in basal $[Ca^{2+}]_i$ reached a plateau. (E) The rise in basal $[Ca^{2+}]_i$ evoked by 2 or 10 μM CCCP. (F) Slowing of the $[Ca^{2+}]_i$ decay by 2 or 10 μM CCCP. In this experiment, the 2nd depolarization was delivered after the CCCP-evoked rise in basal $[Ca^{2+}]_i$ reached a plateau (same cells as in (E)).
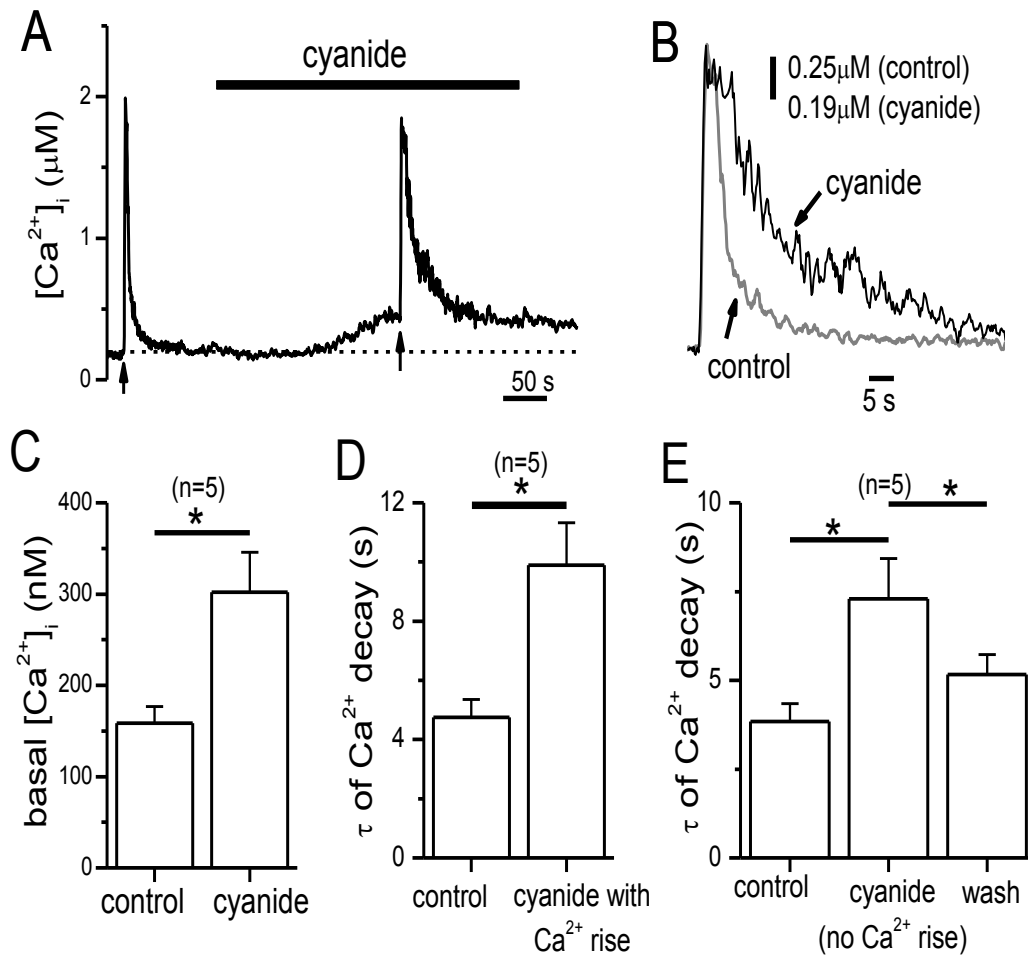
91

Figure 3-5 The effects of CCCP on Ca^{2+} signal could be mimicked by cyanide. (A) In the presence of cyanide (5 mM), there was a gradual elevation in basal $[Ca^{2+}]_i$. When the cyanide-evoked rise in basal $[Ca^{2+}]_i$ reached a plateau, a depolarizing step was delivered to trigger a Ca^{2+} transient. Note the slowing in the decay of the Ca^{2+} transient in the presence of cyanide. (B) Superimposed traces of the Ca^{2+} transients before and in the presence of cyanide (same cell as in A). (C) and (D) The mean elevation in basal $[Ca^{2+}]_i$ evoked by cyanide (5 mM) and the slowing of $[Ca^{2+}]_i$ decay in the same cells. In this experiment, the 2nd depolarization was delivered after the cyanide-evoked rise in basal $[Ca^{2+}]_i$ reached a plateau. (E) Plots of the τ values of $[Ca^{2+}]_i$ decay before, in cyanide (5 mM) and after its removal. In this experiment, the 2nd depolarization was delivered before the onset of the cyanide-evoked rise in basal $[Ca^{2+}]_i$.

92
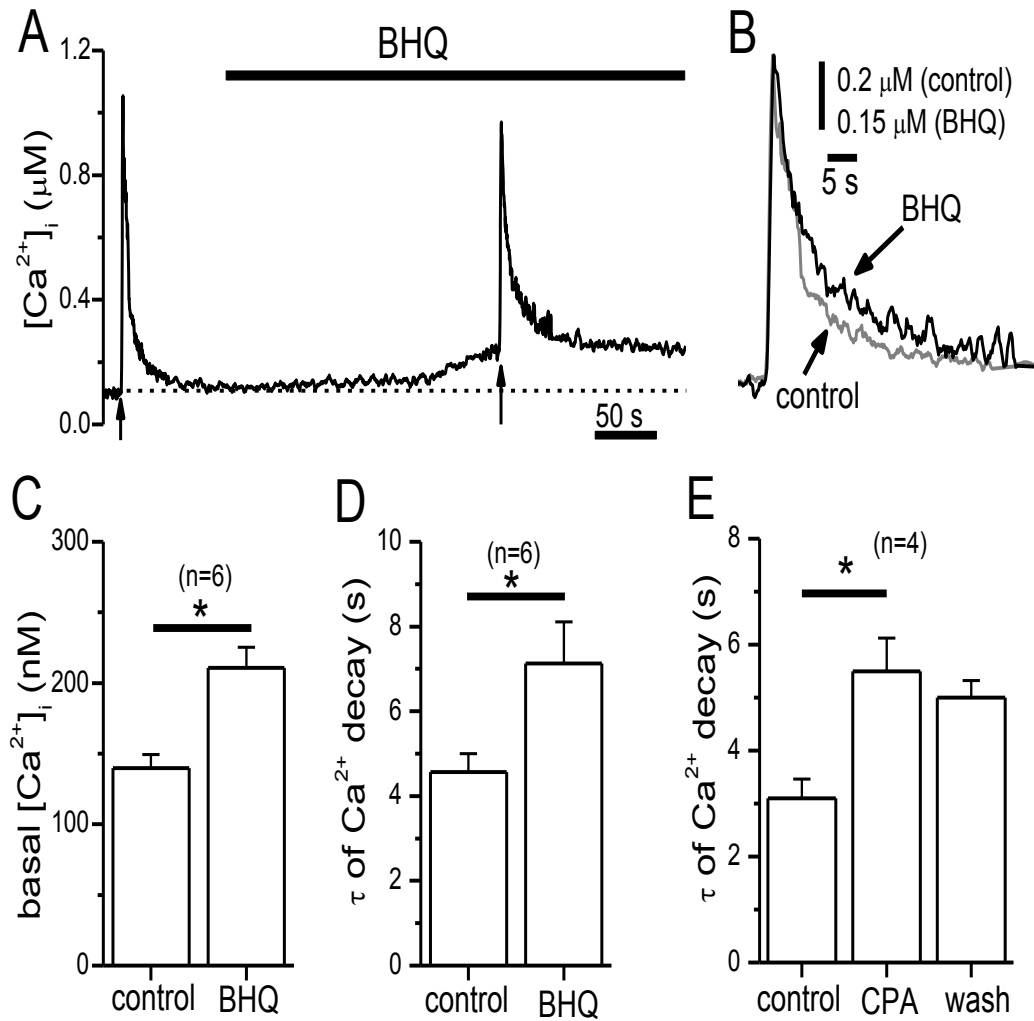
Figure 3-6 Effects of SERCA pump inhibition on Ca^{2+} dynamics. (A) Application of BHQ (20 μM) caused a small rise in basal $[Ca^{2+}]_i$ and a slowing in the decay of the depolarization-triggered Ca^{2+} signal. (B) Superimposed traces of Ca^{2+} transients before and in BHQ (same cell as in (A)). (C) and (D) The mean increase in basal $[Ca^{2+}]_i$ and the τ values of the Ca^{2+} decay induced by BHQ. (E) Application of another SERCA pump inhibitor cyclopiazonic acid (CPA, 50 μM) also caused a slowing in $[Ca^{2+}]_i$ decay.
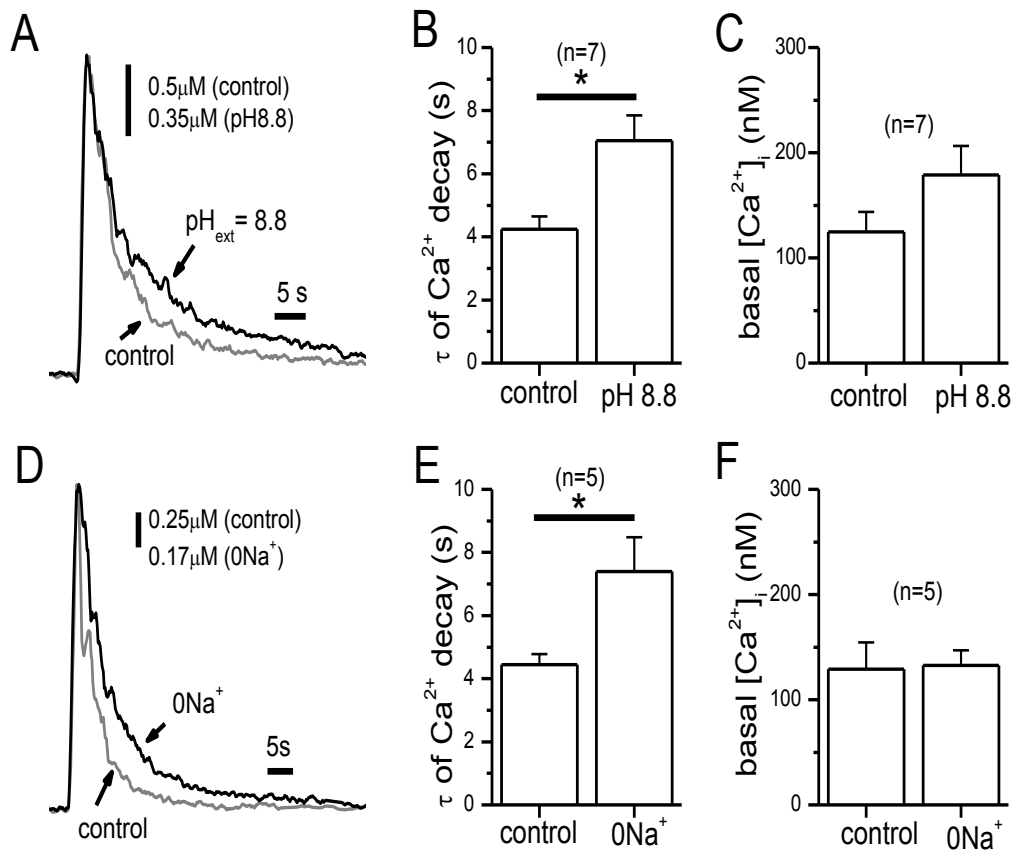
Fig. 3-7 Inhibition of the PMCA pump or NCX caused a small slowing in the $[Ca^{2+}]_i$ decay but did not affect basal $[Ca^{2+}]_i$. (A) Superimposed traces of the depolarization-triggered Ca^{2+} transients from a cell before and following the suppression of PMCA pump activities (by increasing the extracellular pH to 8.8 ($pH_{ext} = 8.8$)). (B) and (C) The reduction of PMCA pump activities caused a significant slowing in the $[Ca^{2+}]_i$ decay but had no significant effect on basal $[Ca^{2+}]_i$. (D) Superimposed traces of the depolarization-triggered Ca^{2+} transients from a cell before and after removal of extracellular Na^+ ($0Na^+$). (E) and (F) NCX inhibition caused a significant slowing in the $[Ca^{2+}]_i$ decay but there was no change in basal $[Ca^{2+}]_i$.

94
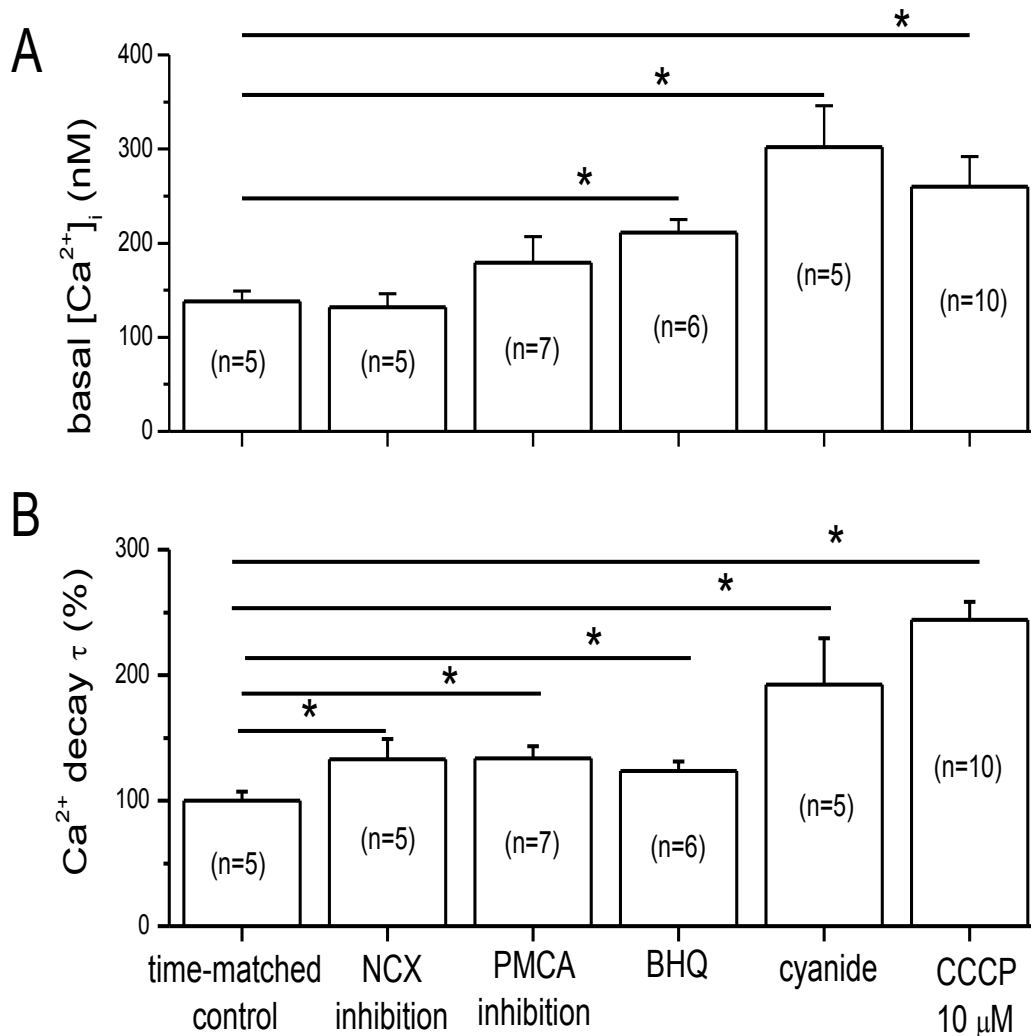
Figure 3-8 Effects of various inhibitors of the Ca^{2+} clearance mechanisms when compared with time-matched controls (at ~7 min of whole-cell recording). (A) The basal $[Ca^{2+}]_i$ was regulated by the SERCA pump and mitochondria. The values of the basal $[Ca^{2+}]_i$ in the absence (control) or presence of different inhibitors were compared. (B) Mitochondria have the largest contribution to cytosolic Ca^{2+} clearance. The decay of the Ca^{2+} transient was slowed by only 20-30% with the inhibition of the SERCA pump, PMCA pump or NCX but mitochondrial inhibitors slowed cytosolic Ca^{2+} removal by >2-fold. The mean τ values of the $[Ca^{2+}]_i$ decay in the presence of different inhibitors were normalized to the mean value obtained from time-matched control cells.

Figure 3-9 Inhibition of the mitochondrial Ca^{2+} uptake slowed the decay of the depolarization-triggered Ca^{2+} transient. (A) In this example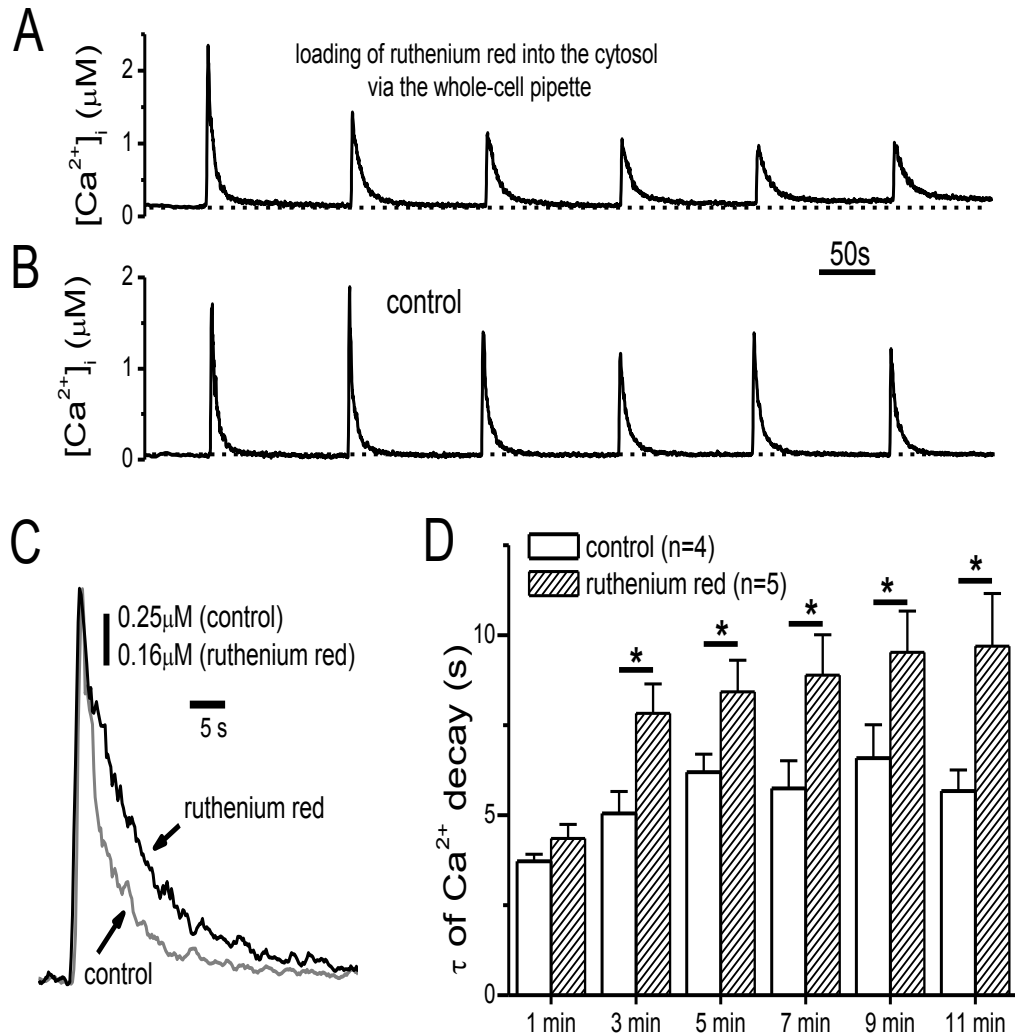, ruthenium red (10 μM) was loaded into the cytosol via the whole-cell pipette. The depolarizing voltage step was delivered at approximately 1, 3, 5, 7, 9 and 11 min after the establishment of whole-cell configuration. Note the gradual slowing in $[Ca^{2+}]_i$ decay as ruthenium red was loaded into the cell. (B) In a time-matched control cell, there was less slowing in the $[Ca^{2+}]_i$ decay with increasing duration of whole-cell dialysis. Same experimental protocol as in (A) except that the whole-cell pipette solution did not contain any ruthenium red. (C) Superimposed traces of the Ca^{2+} transient (evoked at ~3 min of whole-cell recording) from the cell in (A) and (B). Note that the Ca^{2+} decay was slower in the cell which was loaded with ruthenium red into the cytosol. (D) Summary of the changes in the mean τ value of the $[Ca^{2+}]_i$ decay in cells loaded with ruthenium red when compared with time-matched controls. Significant slowing in the decay τ could be detected at ~3 min of whole-cell loading of ruthenium red.

96
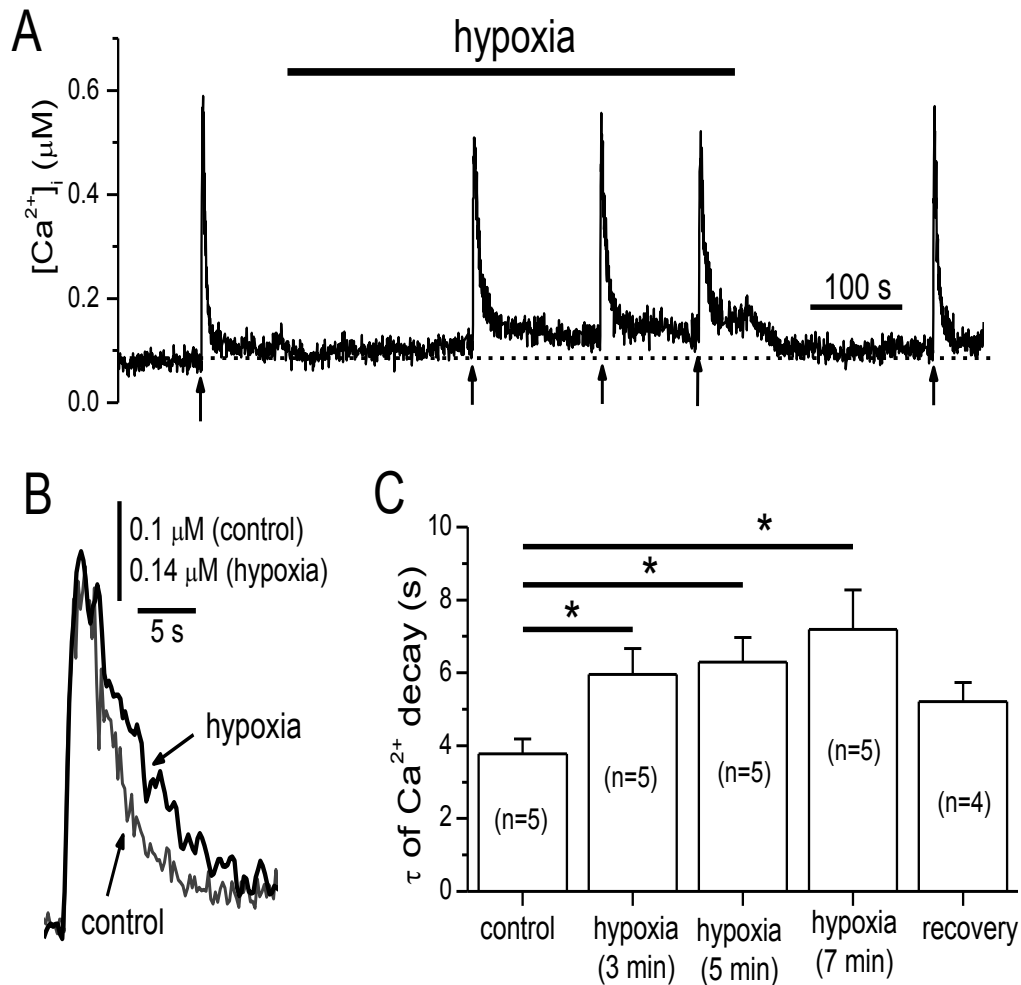
Figure 3-10 Hypoxia slowed the decay of the depolarization-triggered Ca^{2+} signal. (A) Hypoxia was induced by perfusing the cells with a bath solution containing sodium dithionite (1 mM) and bubbled with 100% N_2. The cell was voltage clamped at -70 mV with the perforated-patch clamp technique. Depolarization-triggered Ca^{2+} transients were evoked before and at 3, 5 or 7 min during hypoxia. (B) Superimposed Ca^{2+} transients (scaled to matching amplitudes) evoked before and after 5 min of hypoxia (same cell as in A). Note the slowing in the time course of $[Ca^{2+}]_i$ decay under hypoxic conditions. (C) Mean τ values of $[Ca^{2+}]_i$ decay before, when exposed to hypoxia for 3, 5 or 7 min and upon return to normoxia.
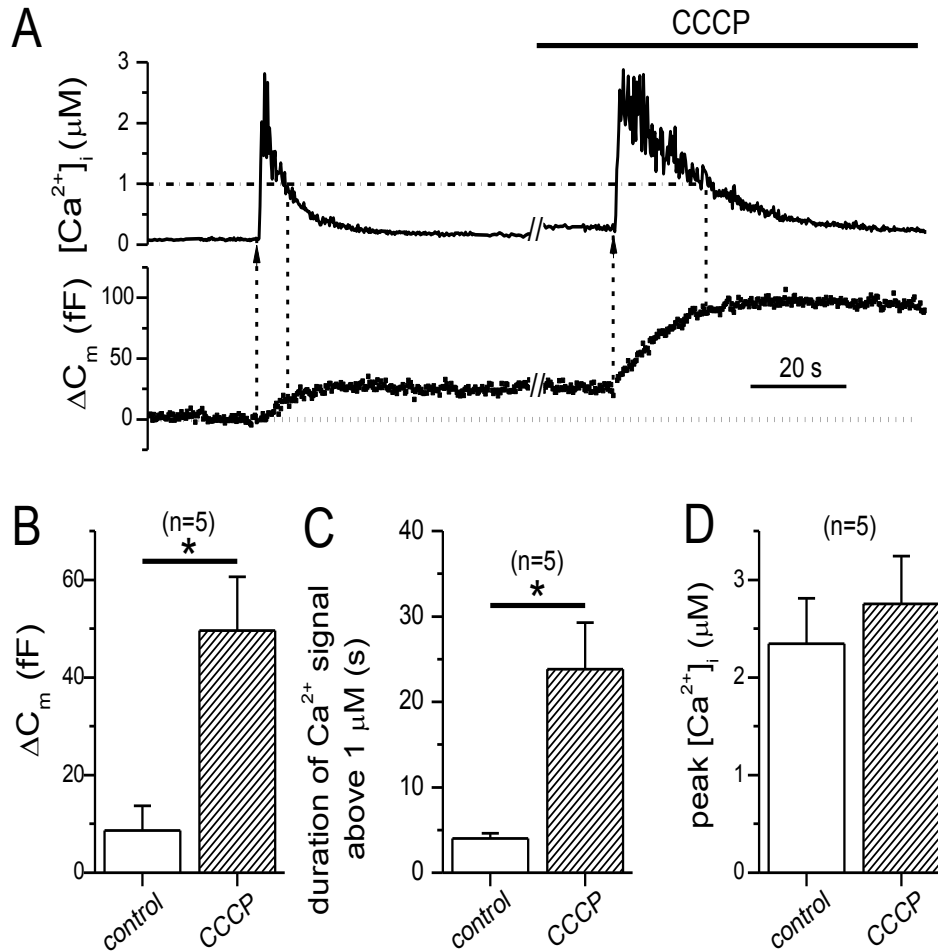
Figure 3-11 Effect of mitochondrial inhibition on the depolarization-triggered exocytosis. (A) An example of simultaneous measurement of $[Ca^{2+}]_i$ and exocytosis in a glomus cell. The depolarization-triggered Ca^{2+} signal was accompanied by an increase in cell membrane capacitance (C_m), reflecting exocytosis. Note that the increase in C_m stopped when $[Ca^{2+}]_i$ decayed below 1 μM. In the presence of CCCP (2 μM), the same depolarization triggered a Ca^{2+} signal whose duration (time at which $[Ca^{2+}]_i$ was ≥1 μM) was ~4-fold longer and it was accompanied by a much larger increase in Cm. (B) The depolarization-triggered exocytotic response in the presence of CCCP was significantly larger than the controls. (C) CCCP increased the duration at which $[Ca^{2+}]_i$ was ≥1 μM by ~6-fold. The average duration of the depolarization-triggered Ca^{2+} signal ($[Ca^{2+}]_i$ above 1 μM) before and in the presence of CCCP. (D) The increase in exocytotic response was not due to a change in the amplitude of the depolarization-triggered Ca^{2+} signal. There was no significant difference in the mean value of the amplitude of the depolarization-triggered Ca^{2+} signal before and in the presence of CCCP. Experiments were conducted by Dr. Andy Lee.

Babcock DF, Herrington J, Goodwin PC, Park YB, & Hille B (1997). Mitochondrial participation in the intracellular Ca^{2+} network. *J Cell Biol* **136**, 833-844.

Barg S, Eliasson L, Renstrom E, & Rorsman P (2002). A subset of 50 secretory granules in close contact with L-type Ca^{2+} channels accounts for first-phase insulin secretion in mouse beta-cells. *Diabetes* **51 Suppl 1**, S74-S82.

Berridge MJ, Bootman MD, & Roderick HL (2003). Calcium signalling: dynamics, homeostasis and remodelling. *Nat Rev Mol Cell Biol* **4**, 517-529.

Buckler KJ (1997). A novel oxygen-sensitive potassium current in rat carotid body type I cells. *J Physiol* **498 (Pt 3)**, 649-662.

Buckler KJ & Vaughan-Jones RD (1998). Effects of mitochondrial uncouplers on intracellular calcium, pH and membrane potential in rat carotid body type I cells. *J Physiol* **513 (Pt 3)**, 819-833.

Carafoli E (2010). The fateful encounter of mitochondria with calcium: how did it happen? *Biochim Biophys Acta* **1797**, 595-606.

Dasso LL, Buckler KJ, & Vaughan-Jones RD (1997). Muscarinic and nicotinic receptors raise intracellular Ca^{2+} levels in rat carotid body type I cells. *J Physiol* **498 (Pt 2)**, 327-338.

Donnelly DF & Carroll JL (2005). Mitochondrial function and carotid body transduction. *High Alt Med Biol* **6**, 121-132.

Duchen MR & Biscoe TJ (1992). Relative mitochondrial membrane potential and $[Ca^{2+}]_i$ in type I cells isolated from the rabbit carotid body. *J Physiol* **450**, 33-61.

Evans AM, Mustard KJ, Wyatt CN, Peers C, Dipp M, Kumar P, Kinnear NP, & Hardie DG (2005). Does AMP-activated protein kinase couple inhibition of mitochondrial oxidative phosphorylation by hypoxia to calcium signaling in O_2-sensing cells? *J Biol Chem* **280**, 41504-41511.

Friel DD (2000). Mitochondria as regulators of stimulus-evoked calcium signals in neurons. *Cell Calcium* **28**, 307-316.

Gonzalez C, Agapito MT, Rocher A, Gomez-Nino A, Rigual R, Castaneda J, Conde SV, & Obeso A (2010). A revisit to O_2 sensing and transduction in the carotid body chemoreceptors in the context of reactive oxygen species biology. *Respir Physiol Neurobiol* **174**, 317-330.

Gover TD, Moreira TH, Kao JP, & Weinreich D (2007). Calcium regulation in individual peripheral sensory nerve terminals of the rat. *J Physiol* **578**, 481-490.

Herrington J, Park YB, Babcock DF, & Hille B (1996). Dominant role of mitochondria in clearance of large Ca^{2+} loads from rat adrenal chromaffin cells. *Neuron* **16**, 219-228.

Hughes E, Lee AK, & Tse A (2006). Dominant role of sarcoendoplasmic reticulum Ca^{2+}-ATPase pump in Ca^{2+} homeostasis and exocytosis in rat pancreatic beta-cells. *Endocrinology* **147**, 1396-1407.

Jackson JG & Thayer SA (2006). Mitochondrial modulation of Ca^{2+}-induced Ca^{2+}-release in rat sensory neurons. *J Neurophysiol* **96**, 1093-1104.

Jiang D, Zhao L, & Clapham DE (2009). Genome-wide RNAi screen identifies Letm1 as a mitochondrial Ca^{2+}/H^{+} antiporter. *Science* **326**, 144-147.

Klyachko VA & Jackson MB (2002). Capacitance steps and fusion pores of small and large-dense-core vesicles in nerve terminals. *Nature* **418**, 89-92.

Lee AK & Tse A (2005). Dominant role of mitochondria in calcium homeostasis of single rat pituitary corticotropes. *Endocrinology* **146**, 4985-4993.

Lopez-Barneo J, Ortega-Saenz P, Pardal R, Pascual A, Piruat JI, Duran R, & Gomez-Diaz R (2009). Oxygen sensing in the carotid body. *Ann N Y Acad Sci* **1177**, 119-131.

Mekahli D, Bultynck G, Parys JB, De SH, & Missiaen L (2011). Endoplasmic-reticulum calcium depletion and disease. *Cold Spring Harb Perspect Biol* **3**.

Mulligan E, Lahiri S, & Storey BT (1981). Carotid body O_2 chemoreception and mitochondrial oxidative phosphorylation. *J Appl Physiol* **51**, 438-446.

Ortega-Saenz P, Pardal R, Garcia-Fernandez M, & Lopez-Barneo J (2003). Rotenone selectively occludes sensitivity to hypoxia in rat carotid body glomus cells. *J Physiol* **548**, 789-800.

Parekh AB (2006). On the activation mechanism of store-operated calcium channels. *Pflugers Arch* **453**, 303-311.

Parekh AB (2008). Mitochondrial regulation of store-operated CRAC channels. *Cell Calcium* **44**, 6-13.

Peers C, Wyatt CN, & Evans AM (2010). Mechanisms for acute oxygen sensing in the carotid body. *Respir Physiol Neurobiol* **174**, 292-298.

Prabhakar NR (2000). Oxygen sensing by the carotid body chemoreceptors. *J Appl Physiol* **88**, 2287-2295.

Santo-Domingo J & Demaurex N (2010). Calcium uptake mechanisms of mitochondria. *Biochim Biophys Acta* **1797**, 907-912.

Tse A, Tse FW, & Hille B (1994). Calcium homeostasis in identified rat gonadotrophs. *J Physiol* **477 (Pt 3)**, 511-525.

Wennemuth G, Babcock DF, & Hille B (2003). Calcium clearance mechanisms of mouse sperm. *J Gen Physiol* **122**, 115-128.

Wyatt CN & Buckler KJ (2004). The effect of mitochondrial inhibitors on membrane currents in isolated neonatal rat carotid body type I cells. *J Physiol* **556**, 175-191.

Wyatt CN, Mustard KJ, Pearson SA, Dallas ML, Atkinson L, Kumar P, Peers C, Hardie DG, & Evans AM (2007). AMP-activated protein kinase mediates carotid body excitation by hypoxia. *J Biol Chem* **282**, 8092-8098.

Wyatt CN & Peers C (1995). Ca(2+)-activated K^+ channels in isolated type I cells of the neonatal rat carotid body. *J Physiol* **483 (Pt 3)**, 559-565.

Xu W, Wilson BJ, Huang L, Parkinson EL, Hill BJ, & Milanick MA (2000). Probing the extracellular release site of the plasma membrane calcium pump. *Am J Physiol Cell Physiol* **278**, C965-C972.

Zhou Z & Neher E (1993). Mobile and immobile calcium buffers in bovine adrenal chromaffin cells. *J Physiol* **469**, 245-273.

Chapter 4

Influence of bicarbonate ion (HCO_3^-) on mitochondrial Ca^{2+} transport in rat carotid glomus cells

4.1 Introduction

4.1.1 Mechanisms of transmembrane HCO_3^- transport in glomus cells

As summarized in Fig. 4-1, glomus cells express several HCO_3^- transporters, including the Na^+/HCO_3^- cotransporter, HCO_3^-/Cl^- exchanger (Buckler *et al.*, 1991), Na^+-dependent HCO_3^-/Cl^- exchanger (Rocher *et al.*, 1991), as well as an anion channel (Stea & Nurse, 1989) which is permeable to both Cl^- and HCO_3^-. The Na^+/HCO_3^- cotransporter and the HCO_3^-/Cl^- exchanger have been shown to have important roles in the regulation of the cytosolic pH of glomus cells (Buckler *et al.*, 1991). Under physiological conditions, the concentration of HCO_3^- in the extracellular fluid ($[HCO_3^-]_{ext}$) is expected to be close to that of the plasma (~23 mM). Although the cytosolic concentration of HCO_3^- ($[HCO_3^-]_i$) is not precisely measured, it is possible that extracellular HCO_3^- can be transported into the cell via the Na^+/HCO_3^- cotransporter and Na^+-dependent HCO_3^-/Cl^- exchanger (Fig. 4-1). Extracellular HCO_3^- can also pass through the anion channels in glomus cells. Glomus cells also express the enzyme carbonic anhydrase (Nurse, 1990; Yamamoto *et al.*, 2003). CO_2 in the bath diffuses into the cell and is converted by carbonic anhydrase into HCO_3^- and H^+. With a rise in $[HCO_3^-]_i$, excess HCO_3^- can be extruded from the cell via the HCO_3^-/Cl^- exchanger. Part of the excess H^+ in the cytosol is extruded via the Na^+/H^+ exchanger.

103

4.1.2 Extracellular HCO$_3$$^-$ is important for hypoxic chemotransduction in the carotid body

In addition to cytosolic pH regulation, extracellular HCO$_3$$^-$ was found to be important for hypoxic chemotransduction of the carotid body. In both cat (Iturriaga & Lahiri, 1991; Shirahata & Fitzgerald, 1991) and rat (Panisello & Donnelly, 1998) carotid bodies, the hypoxia-triggered CSN discharge and the hypoxia-mediated catecholamine release from glomus cells were reduced by the removal of extracellular HCO$_3$$^-$. The mechanism underlying the enhancement of the hypoxic response of glomus cells by extracellular HCO$_3$$^-$ is not completely understood. There is some evidence that modulation of the activity of the ion channels is involved. In rabbit glomus cells, moderate hypoxia in the presence of physiological [HCO$_3$$^-$]$_{ext}$ (25 mM; while the extracellular fluid was bubbled with 5% CO$_2$) was found to enhance the L-type Ca^{2+} current by ~20% via a PKC-dependent pathway, but this enhancing effect was abolished in the absence of extracellular HCO$_3$$^-$ (Summers *et al.*, 2000). The effect of extracellular HCO$_3$$^-$ on VGCCs was postulated to be related to cytosolic acidification because hypoxia could enhance VGCCs in rabbit glomus cells when the pH of the extracellular solution (without HCO$_3$$^-$) was lowered from 7.4 to 7.0 (Summers *et al.*, 2000). On the other hand, the voltage-activated K$^+$ current of rat glomus cells was reduced by ~22% upon switching from a HCO$_3$$^-$-free extracellular solution ([HCO$_3$$^-$]$_{ext}$ = 0) to one containing physiological [HCO$_3$$^-$]$_{ext}$ (Stea & Nurse, 1991). Thus, extracellular HCO$_3$$^-$ may increase the electrical excitability of glomus cells via an inhibition of voltage-dependent K$^+$ current. The above changes in the activity of

the ion channels can increase the Ca^{2+} signal and thus potentiate the response of glomus cells to hypoxia in the presence of physiological $[HCO_3^-]_{ext}$.

4.1.3 Goals of project 2

In my first project (Chapter 3), Dr. Andy Lee found that a slowing in the rate of cytosolic Ca^{2+} clearance (or an increase in the duration of the Ca^{2+} signal) enhanced transmitter release from glomus cells (Fig. 3-11). Therefore, in this study, I tested the hypothesis that the potentiation of hypoxic chemotransduction in physiological $[HCO_3^-]_{ext}$ is related to a change in the rate of cytosolic Ca^{2+} clearance in glomus cells. I found that the clearance of cytosolic Ca^{2+} was slower in the presence of physiological $[HCO_3^-]_{ext}$. Based on this finding, I further examined whether this effect involved specific HCO_3^- transporter mechanisms that are known to be expressed in glomus cells. Lastly, since the effects of physiological $[HCO_3^-]_{ext}$ on the Ca^{2+} signal resembled the effects of mitochondrial inhibitors, I investigated whether physiological $[HCO_3^-]_{ext}$ slowed cytosolic Ca^{2+} clearance in glomus cells by affecting mitochondrial Ca^{2+} uptake or mitochondrial membrane potential. These experiments involved direct measurement of either the mitochondrial Ca^{2+} signal via a mitochondrial Ca^{2+} sensitive dye, rhod-2 AM, or changes in the mitochondrial membrane potential via a voltage-sensitive dye, TMRE. All the experiments shown in this chapter were conducted by me.

4.2 Results

4.2.1 Effects of physiological [HCO$_3^-$]$_{ext}$ on the Ca^{2+} signals

To examine whether physiological [HCO$_3^-$]$_{ext}$ affects Ca^{2+} homeostasis in glomus cells, I compared the rate of the decay of the depolarization-triggered Ca^{2+} transients in cells bathed first in a HCO$_3^-$-free solution and then in 23 mM [HCO$_3^-$]$_{ext}$. Cells were whole-cell voltage clamped at -70 mV and at certain intervals a depolarizing voltage step (500 ms) to 0 mV was delivered to activate VGCCs. An example of such an experiment is shown in Fig. 4-2A. When the bath solution was switched from a HCO$_3^-$-free solution (buffered with HEPES) to one containing 23 mM [HCO$_3^-$]$_{ext}$ (bubbled with 5% CO$_2$), there was an elevation in the basal [Ca^{2+}]$_i$ and a slowing in the decay of the depolarization-triggered Ca^{2+} transient. Fig. 4-2B shows the superimposed Ca^{2+} transients (scaled to matching amplitudes) evoked in the HCO$_3^-$-free solution and then in the presence of 23 mM [HCO$_3^-$]$_{ext}$ (same cell as in Fig. 4-2A). As described in Chapter 3, the time course of the decay of the depolarization-triggered Ca^{2+} signal can be described by an exponential function with a time constant of τ. In this example, the [Ca^{2+}]$_i$ decay τ was 2.4 s in HCO$_3^-$-free solution and it increased to 6.9 s in the presence of 23 mM [HCO$_3^-$]$_{ext}$ for ~1.5 min (with local perfusion). Upon the removal of extracellular HCO$_3^-$ for ~3 min, the [Ca^{2+}]$_i$ decay τ decreased to 5.0 s. In 8 cells examined, the presence of physiological [HCO$_3^-$]$_{ext}$ slowed the decay τ by 2.8 $\pm$ 0.3-fold (10.9 $\pm$ 1.8 s vs. 3.9 $\pm$ 0.4 s; Fig. 4-2C) and elevated the basal [Ca^{2+}]$_i$ by 98 $\pm$ 18 nM (Fig. 4-2D). These effects of extracellular HCO$_3^-$ resemble those of the mitochondrial inhibitors (CCCP and cyanide) shown in Chapter 3 (Fig. 3-4 and 3-5). In the absence of extracellular Ca^{2+} (the bath solution also contained 1

mM EGTA), extracellular HCO_3^- did not evoke any detectable rise in basal $[Ca^{2+}]_i$ and similar results were found in 4 cells. Thus, similar to the effects of mitochondrial inhibitors described in Chapter 3, the extracellular HCO_3^--induced elevation in basal $[Ca^{2+}]_i$ was dependent on the presence of extracellular Ca^{2+}.

4.2.2 The slowing of cytosolic Ca^{2+} clearance by extracellular HCO_3^- is concentration-dependent

To determine the concentration dependence of the effect of extracellular HCO_3^- on cytosolic Ca^{2+} clearance in glomus cells, I compared the decay τ of the depolarization-triggered Ca^{2+} signal when the extracellular solution was switched from a HCO_3^--free solution to one containing 2 or 10 mM HCO_3^-. In these experiments, I omitted CO_2 bubbling in the bath and 10 mM HEPES was added to buffer the bath solution to a pH of 7.4. Fig. 4-3A shows an example of a glomus cell when the bath solution was switched from a HCO_3^--free solution to one containing 2 mM HCO_3^-. Note that in the presence of 2 mM $[HCO_3^-]_{ext}$ for >3 min (with bath perfusion), the glomus cell did not exhibit any increase in basal $[Ca^{2+}]_i$ and there was only a minor change in the time course of the decay of the depolarization-triggered Ca^{2+} signal (τ of 5.3 s in 2 mM $[HCO_3^-]_{ext}$ vs. 3.7 s in HCO_3^--free). In 5 cells examined, the mean value of the decay τ in the presence of 2 mM $[HCO_3^-]_{ext}$ was 5.5 ± 0.4 s, not significantly different from the mean decay τ value obtained from the same cells in the absence of extracellular HCO_3^- (4.0 ± 0.4 s; Fig. 4-3B). On the other hand, a significant slowing in the $[Ca^{2+}]_i$ decay was detected for cells exposed to 10 mM $[HCO_3^-]_{ext}$ (18.4 ± 1.4 s vs. 5.3 ± 0.9 s in

HCO_3^--free; n = 3; Fig. 4-3B). Similarly in 4 cells tested with 23 mM $[HCO_3^-]_{ext}$ without CO_2 bubbling, the decay of the depolarization-triggered Ca^{2+} signal was 3.9 ± 0.3 s in the HCO_3^--free bath solution and significantly increased to 10.6 ± 2.5 s in 23 mM $[HCO_3^-]_{ext}$ (Fig. 4-3B). These results suggest that the slowing of cytosolic Ca^{2+} clearance in glomus cells is dependent on the concentration of extracellular HCO_3^-. My result also shows that the omission of CO_2 bubbling did not affect the slowing of $[Ca^{2+}]_i$ decay by 23 mM $[HCO_3^-]_{ext}$. This raises the possibility that the conversion of CO_2 by carbonic anhydrase may have a minor role in the slowing of cytosolic Ca^{2+} clearance. Consistent with this notion, inhibition of carbonic anhydrase with 10 μM acetazolamide did not prevent the effect of physiological $[HCO_3^-]_{ext}$ on cytosolic Ca^{2+} clearance; the decay τ in the presence of acetazolamide and 23 mM $[HCO_3^-]_{ext}$ (with CO_2 bubbling) was 9.4 ± 2.2 s vs. 3.6 ± 0.5 s in HCO_3^--free (n = 4).

4.2.3 The slowing of cytosolic Ca^{2+} clearance by physiological $[HCO_3^-]_{ext}$ is not dependent on extracellular Na^+ influx or cytosolic acidification

Since Na^+ is co-transported with HCO_3^- via the Na^+/HCO_3^- cotransporter and Na^+-dependent HCO_3^-/Cl^- exchanger, a rise in $[HCO_3^-]_i$ is expected to be accompanied by a rise in $[Na^+]_i$. This raises the possibility that an increase in $[Na^+]_i$ may stimulate the reverse mode of NCX (Fig. 4-4), resulting in a rise in basal $[Ca^{2+}]_i$ and a slowing in cytosolic Ca^{2+} clearance. The elevation of $[Na^+]_i$ may also reduce the activity of the Na^+/H^+ exchanger, leading to cytosolic acidification (Fig. 4-4). As described later in section 4.2.5, cytosolic acidification

may result in a reduction in Ca^{2+} uptake via the mitochondrial Ca^{2+}/H^+ antiporter and thus a slowing of cytosolic Ca^{2+} clearance. To test the above possibilities, I examined the effect of HCO_3^- when all extracellular Na^+ was replaced by NMG^+ in the HCO_3^--buffered bath solution (bubbled with 5% CO_2). An example of such an experiment is shown in Fig. 4-5A. When the bath solution was switched from a HCO_3^--free solution to a Na^+-free, HCO_3^--buffered bath solution (with 23 mM HCO_3^- and 5% CO_2 bubbling), an elevation in the basal $[Ca^{2+}]_i$ and a robust slowing in the decay of the depolarization-triggered Ca^{2+} signal was observed. In this example, the $[Ca^{2+}]_i$ decay τ was 4.4 s in the absence of extracellular HCO_3^- and it increased to 29.0 s when the bath solution was switched to the Na^+-free, HCO_3^--buffered solution for >3 min (with bath perfusion). In 4 cells similarly examined, the Na^+-free, HCO_3^--buffered solution slowed the decay τ by 5.2 ± 0.7-fold (25.6 ± 3.5 s vs. 4.9 ± 0.2 s; Fig. 4-5B). This result indicates that the slowing of the $[Ca^{2+}]_i$ decay by HCO_3^- does not require the influx of extracellular Na^+. Furthermore, the rise in basal $[Ca^{2+}]_i$ induced by HCO_3^- was also robust in the absence of extracellular Na^+ (209 ± 30 nM; n = 4). Thus, neither the reverse mode of NCX nor a reduction of Na^+/H^+ exchanger activity contributes to the effect of extracellular HCO_3^- on Ca^{2+} signal in glomus cells.

Other than a reduction in Na^+/H^+ exchanger activity, cytosolic $[H^+]$ in glomus cells can be elevated (i.e. resulting in a drop in cytosolic pH (pH_i)) when CO_2 is converted by carbonic anhydrase into H^+ and HCO_3^- (Fig. 4-1). In intact glomus cells, the presence of extracellular HCO_3^- (23 mM) and 5% CO_2 bubbling has been shown to cause a decrease in pH_i (by ~0.3 unit) (Buckler et al., 1991). In my

study, the pH_i in single glomus cells was maintained via a whole-cell pipette solution which was buffered to 7.4 (with 20 mM HEPES). However, the possibility that some cytosolic acidification might occur in the presence of extracellular HCO_3^- could not be ruled out. Therefore, I examined whether cytosolic acidification can cause a slowing in cytosolic Ca^{2+} clearance. In this experiment, the pH of the whole-cell pipette solution was reduced from 7.4 to 7.0. As shown in the example in Fig. 4-6A, when the cell was bathed in a HCO_3^--free bath solution, the $[Ca^{2+}]_i$ decay τ was 3.6 s. After the cell was exposed to a HCO_3^--buffered bath solution, the $[Ca^{2+}]_i$ decay τ increased to 11.2 s. In 5 cells recorded with a whole-cell pipette solution of pH 7.0 in a HCO_3^--free bath solution, the $[Ca^{2+}]_i$ decay τ was 4.0 ± 0.4 s, similar to the cells recorded with a whole-cell pipette solution of pH 7.4 ($\tau = 3.9 \pm 0.4$ s; Fig. 4-2C). For cells recorded with a pH 7.0 whole-cell pipette solution, 23 mM of extracellular HCO_3^- slowed the decay of the depolarization-triggered Ca^{2+} signal by 3.1 ± 0.2-fold ($\tau = 12.3 \pm 1.0$ s; Fig. 4-6B), similar to the effect of HCO_3^- on cells recorded with a pH 7.4 whole-cell pipette solution (2.8 ± 0.3-fold; Fig. 4-2C). Therefore, it is unlikely that cytosolic acidification has an important role in the HCO_3^--mediated slowing in cytoslic Ca^{2+} clearance.

4.2.4 Influence of physiological $[HCO_3^-]_{ext}$ on mitochondrial Ca^{2+} uptake

My results in Chapter 3 have shown that Ca^{2+} uptake into mitochondria plays a dominant role in the removal of cytosolic Ca^{2+} in glomus cells. Since the effects of physiological $[HCO_3^-]_{ext}$ on the Ca^{2+} signal resemble the effects of

mitochondrial inhibitors (described in section 4.2.1), I investigated whether physiological $[HCO_3^-]_{ext}$ slows cytosolic Ca^{2+} clearance in glomus cells by affecting mitochondrial Ca^{2+} uptake. Individual glomus cells were first incubated with a mitochondrial Ca^{2+} sensitive dye, rhod-2 AM (Kd for Ca^{2+} = 570 nM). Following the accumulation of rhod-2 in the mitochondria (indicated by the appearance of punctuate fluorescent staining in the cytosol), the cell was whole-cell voltage clamped at -70 mV. This step is expected to cause the small amount of rhod-2 in the cytosol (i.e. not accumulated in the mitochondria) to be lost via the whole-cell pipette. An example of mitochondrial Ca^{2+} signal measurement from a glomus cell in the presence of a HCO_3^--free bath solution is shown in Fig. 4-7A. Following a short (500 ms) depolarizing voltage step (to 0 mV) to activate VGCCs, there was a rapid increase in the rhod-2 fluorescence, reflecting a rise in mitochondrial $[Ca^{2+}]$. The rapid increase in the rhod-2 fluorescence was followed by a slow decay, reflecting the much slower removal of Ca^{2+} from the mitochondria. As shown in Fig. 4-7A, the 2nd and 3rd depolarizing voltage steps delivered at ~3 and ~6 min after the 1st depolarizing step could still evoke robust increases in the rhod-2 fluorescence. Because the intensity of the rhod-2 fluorescence was variable among cells, in all my rhod-2 experiments, I compared the increase in the rhod-2 fluorescence evoked by the 2nd depolarization to that evoked by the 1st depolarization in the same cell. Note that there was a gradual rundown in the amplitude of the depolarization-triggered increase in the rhod-2 fluorescence. In 4 cells examined in HCO_3^--free bath solution, the amplitude of the rhod-2 fluorescence increase triggered by the 2nd depolarization was ~16%

111

smaller than that evoked by the 1st depolarization (Fig. 4-7D). Consistent with the notion that the depolarization-evoked increase in the rhod-2 fluorescence reflects an increase in mitochondrial $[Ca^{2+}]$, Fig. 4-7B shows that the depolarization-evoked increase in the rhod-2 fluorescence was largely abolished in the presence of the mitochondrial uncoupler (CCCP; 2 μM). In 4 cells examined, CCCP reduced the depolarization-evoked increase in the rhod-2 fluorescence by ~84% (Fig. 4-7D). The data in Chapter 3 have shown that CCCP (2 μM) does not affect the peak of the depolarization-evoked $[Ca^{2+}]_i$ transient (Fig. 3-11). Therefore, the reduction in the depolarization-evoked increase in the rhod-2 fluorescence by CCCP in Fig. 4-7B is not caused by the inhibition of extracellular Ca^{2+} entry through VGCCs by CCCP. The example in Fig. 4-7C shows that in the presence of physiological $[HCO_3^-]_{ext}$, depolarization triggered a much smaller increase in the rhod-2 fluorescence, suggesting a reduction in mitochondrial Ca^{2+} uptake. Similar to the slowing of cytosolic $[Ca^{2+}]_i$ decay by $[HCO_3^-]_{ext}$ (Fig. 4-2), the inhibitory action of $[HCO_3^-]_{ext}$ on mitochondrial Ca^{2+} uptake is reversible. As shown in Fig. 4-7C, the delivery of the 3rd depolarization following the removal of extracellular HCO_3^-, was able to evoke a larger increase in the rhod-2 fluorescence when compared with that evoked by the 2nd depolarization in the presence of extracellular HCO_3^-. On average, in the presence of 23 mM $[HCO_3^-]_{ext}$, the depolarization-evoked increase in the rhod-2 fluorescence was reduced by ~68% (Fig. 4-7D). As shown in Fig. 4-2, a robust depolarization-evoked $[Ca^{2+}]_i$ transient could be detected in the presence of 23 mM $[HCO_3^-]_{ext}$ (it was smaller than the first depolarization-evoked $[Ca^{2+}]_i$ transient in the HCO_3^--free solution

112

because of the rundown of VGCCs during the whole-cell recording (Fig. 3-2)). Therefore, in Fig. 4-7C, the reduction in the depolarization-evoked increase in the rhod-2 fluorescence by HCO_3^- is not caused by an inhibitory effect of HCO_3^- on the extracellular Ca^{2+} entry through VGCCs. The finding in Fig. 4-7C suggests that the slowing of cytosolic Ca^{2+} clearance in glomus cells in the presence of physiological $[HCO_3^-]_{ext}$ is due to a reduction in mitochondrial Ca^{2+} uptake.

4.2.5 Role of mitochondrial Ca^{2+}/H^+ antiporter

As described in Chapter 3, Ca^{2+} uptake into the mitochondria may be mediated via multiple mechanisms, including the uniporter, Ca^{2+}/H^+ antiporter and RaM, all of which can be inhibited by ruthenium red (Santo-Domingo & Demaurex, 2010). Among the above mechanisms, it has been reported that the activity of Ca^{2+}/H^+ antiporter can be enhanced by cytosolic alkalinisation but reduced by cytosolic acidification (Jiang *et al.*, 2009). Whether the Ca^{2+}/H^+ antiporter is present in most cell types is controversial (Santo-Domingo & Demaurex, 2010). Since the activity of Ca^{2+}/H^+ antiporter is reduced by cytosolic acidification and mitochondrial Ca^{2+} uptake regulates cytosolic Ca^{2+} clearance in glomus cells, a slowing of cytosolic Ca^{2+} clearance with cytosolic acidification will implicate an important role of Ca^{2+}/H^+ antiporter in glomus cells. However, my experiments in section 4.2.3 have already shown that the lowering of pH_i to 7.0 did not affect the rate of cytosolic Ca^{2+} clearance. Nevertheless, I further tested the possible involvement of Ca^{2+}/H^+ antiporter by examining whether an enhancement in the activity of Ca^{2+}/H^+ antiporter with cytosolic alkalinisation can

reduce the inhibitory action of extracellular HCO_3^- on mitochondrial Ca^{2+} uptake. In this experiment, I recorded single glomus cells with a whole-cell pipette solution buffered to pH 8.0. As shown in the example in Fig. 4-8A, physiological $[HCO_3^-]_{ext}$ could still cause a strong suppression on the depolarization-evoked mitochondrial Ca^{2+} uptake when the cytosolic pH was buffered to 8.0. In 4 cells with pH_i of 8.0, the mean reduction in mitochondrial Ca^{2+} uptake by extracellular HCO_3^- was ~60%, similar to the inhibition on cells with pH_i of 7.4 (Fig. 4-8B). Therefore, it is unlikely that the inhibitory action of extracellular HCO_3^- on mitochondrial Ca^{2+} uptake in glomus cells involves a suppression of mitochondrial Ca^{2+}/H^+ antiporter.

4.2.6 *The inhibitory action of HCO_3^- on mitochondrial Ca^{2+} uptake involves reactive oxygen species (ROS)*

Mitochondria are the main source of ROS production in the cell and the common members of cellular ROS include superoxide anions, hydrogen peroxide and hydroxyl radicals. ROS can modulate the function of multiple proteins in mitochondria (Mari *et al.*, 2012). This raises the possibility that the function of some mitochondrial Ca^{2+} uptake mechanisms can be modulated by ROS. To test the hypothesis that ROS contributes to the inhibitory action of physiological $[HCO_3^-]_{ext}$ on mitochondrial Ca^{2+} uptake, I examined whether the reduction of cellular ROS level affects the action of extracellular HCO_3^- on glomus cells. In the first experiment, glomus cells were pretreated with the reduced form of L-glutathione (GSH; 2 mM) for 25 min. In the continued presence of GSH, the

114

glomus cell was voltage clamped at -70 mV in the perforated-patch mode. As shown in the example in Fig. 4-9A, physiological $[HCO_3^-]_{ext}$ failed to suppress the depolarization-evoked increase in mitochondrial Ca^{2+} signal in this glomus cell pretreated with GSH. For 7 cells pretreated with GSH, the inhibitory action of HCO_3^- on mitochondrial Ca^{2+} uptake was essentially abolished (<1%; Fig. 4-9D). This effect of GSH could be mimicked by another ROS scavenger, N-acetyl-L-cysteine (NAC). Fig. 4-9B shows an example of a glomus cell pretreated with 2 mM NAC (same procedure as GSH). Note that in the NAC pretreated cells, depolarization evoked a robust increase in mitochondrial Ca^{2+} signal in the presence of physiological $[HCO_3^-]_{ext}$ (Fig. 4-9B). In 10 cells pretreated with NAC, the mean reduction in mitochondrial Ca^{2+} signal by physiological $[HCO_3^-]_{ext}$ was $23 \pm 6\%$ (Fig. 4-9D). In contrast, for untreated cells also voltage clamped in the perforated-patch mode, physiological $[HCO_3^-]_{ext}$ reduced the depolarization-evoked increase in mitochondrial Ca^{2+} signal by $59 \pm 3\%$ (n = 9; Figs. 4-9C & D). These findings indicate that the inhibitory action of HCO_3^- on mitochondrial Ca^{2+} uptake is dependent on the cellular level of ROS.

One possible link between HCO_3^- and cellular ROS level is the enzyme, soluble adenylyl cyclase (sAC). In many cell types, HCO_3^- was found to activate sAC, resulting in the generation of cAMP (Wuttke *et al.*, 2001; Litvin *et al.*, 2003). In rat carotid body, sAC has been identified and the cellular level of cAMP was elevated by the presence of physiological $[HCO_3^-]_{ext}$ (Nunes *et al.*, 2009). Other than the cytosol, sAC is present in multiple intracellular organelles including the mitochondria (Zippin *et al.*, 2003). In HeLa cells, it has been reported that the

activation of mitochondrial sAC-cAMP-PKA signaling pathway by HCO_3^- could enhance mitochondrial respiration, resulting in a decrease in mitochondrial ROS production (Acin-Perez *et al.*, 2009). However, in permeabilized rat myocytes, PKA activation was found to increase mitochondrial ROS production (Nagasaka *et al.*, 2007). Therefore, it is possible that depending on the cell types, PKA activation may increase or decrease mitochondrial ROS production. In the literature, the role of sAC is frequently examined with KH7, a selective inhibitor of sAC (Kumar *et al.*, 2009). However, I found that KH7 interfered with the loading of rhod-2 into glomus cells. Therefore, I examined whether the elevation of cAMP in glomus cells could mimic the effect of HCO_3^- on mitochondrial Ca^{2+} uptake. In this experiment, I employed a membrane permeable cAMP analog, 8-CPT-cAMP, which has been shown to induce mitochondrial PKA activation (Acin-Perez *et al.*, 2009). As shown in the example in Fig. 4-10A, application of 8-(4-chlorophenylthio)-adenosine 3',5'-cyclic monophosphate (8-CPT-cAMP; 0.5 mM) in a HCO_3^--free bath solution did not cause any significant reduction in the depolarization-evoked mitochondrial Ca^{2+} signal. In 4 cells examined, the depolarization-evoked increase in the rhod-2 fluorescence in the presence of 8-CPT-cAMP was only ~10% smaller than that evoked by the 1st depolarization in the same cells before exposure to 8-CPT-cAMP (Fig. 4-10B). This finding indicates that the inhibitory action of HCO_3^- on mitochondrial Ca^{2+} uptake cannot be mimicked by an elevation of cAMP. Therefore, it is unlikely that the activation of mitochondrial sAC-cAMP-PKA signaling pathway has a significant role in the action of HCO_3^- on mitochondrial Ca^{2+} uptake in glomus cells.

116

4.2.7 Mitochondrial depolarization has a minor role in the inhibitory action of
HCO_3^- on mitochondrial Ca^{2+} uptake

It is well known that the inhibitors of mitochondria such as cyanide and CCCP cause mitochondrial depolarization and thus reduce the driving force for Ca^{2+} uptake into the mitochondria (Duchen & Biscoe, 1992b; Buckler & Vaughan-Jones, 1998). Since the effects of physiological $[HCO_3^-]_{ext}$ on the Ca^{2+} signal of glomus cells resemble the effects of mitochondrial inhibitors (as described in sections 4.2.1 and 4.2.4), I examined whether the inhibition of mitochondrial Ca^{2+} uptake by HCO_3^- in glomus cells was due to mitochondrial depolarization. In this experiment, the change in mitochondrial potential (Ψ_m) was monitored with TMRE. TMRE is a cationic dye that accumulates within the mitochondria due to the negative potential in the mitochondrial matrix (Duchen *et al.*, 1998; Chalmers & McCarron, 2008). With a high concentration of TMRE accumulated in the mitochondria, the fluorescence of TMRE autoquenches there. Following mitochondrial depolarization, some TMRE will leave the mitochondria and the reduction in mitochondrial concentration of TMRE results in dequenching (or an increase in fluorescence) as long as the concentration of TMRE in the mitochondria is not significantly depleted (Duchen *et al.*, 1998; Chalmers & McCarron, 2008). In my study, TMRE (10 µM) was loaded into the cell via the whole-cell pipette. This method has at least two advantages over a short incubation of the cells with TMRE. Firstly, TMRE can be continuously supplied into the cell. Without a continuous supply of TMRE into the cell, there may be a gradual loss of TMRE from the cell during the time course of recording (e.g. due

to photobleaching or diffusion out of the cell). This loss is particularly problematic in experiments that involve repetitive mitochondrial depolarizations because re-accumulation of TMRE into the mitochondria may not occur following mitochondrial repolarization. Secondly, uptake of Ca^{2+} that enters the cell via VGCC into the mitochondria causes mitochondrial depolarization. Mitochondrial inhibition in glomus cells causes cell depolarization and VGCC activation (Wyatt & Buckler, 2004). Therefore, voltage clamping the cell membrane potential at -70 mV with the whole-cell pipette will prevent any depolarization of the plasma membrane and the resultant activation of VGCC in glomus cells which are known to accompany mitochondrial inhibition.

An example of the TMRE signal in a glomus cell is shown in Fig. 4-11A. Following the accumulation of TMRE in the mitochondria, the bath solution was switched from HCO_3^--free to one containing 23 mM $[HCO_3^-]_{ext}$. In the presence of HCO_3^-, the TMRE fluorescence increased gradually and reached a plateau, reflecting the dequenching of TMRE during mitochondrial depolarization. Following the removal of extracellular HCO_3^-, the TMRE fluorescence returned to the basal level, suggesting that the HCO_3^--evoked mitochondrial depolarization was reversible (Fig. 4-11A). When the same cell was subsequently challenged with cyanide (5 mM), the increase in TMRE fluorescence was much larger than that mediated by extracellular HCO_3^-, indicating that cyanide evoked a larger mitochondrial depolarization (Fig. 4-11A). In the presence of cyanide, the rapid increase in TMRE fluorescence was followed by a slow decay (Fig. 4-11A). The cause of the slow decay is not completely understood. One possible explanation is

that following the mitochondrial depolarization induced by cyanide, there is some loss of dequenched TMRE from the mitochondria and cytoplasm (via diffusion into the whole-cell pipette or to the extracellular environment). Alternatively, there may be a slow partial recovery of mitochondrial potential due to the presence of ATP (5 mM from the whole-cell pipette) to fuel the reversal of ATP synthase. Nevertheless, in 5 cells examined, cyanide increased TMRE fluorescence by $64 \pm 11\%$, much larger than that induced by 23 mM extracellular HCO_3^- ($19 \pm 2\%$; Fig. 4-11B). Although the change in mitochondrial potential could not be precisely quantified with TMRE fluorescence, my results show that physiological $[HCO_3^-]_{ext}$ caused an obviously smaller mitochondrial depolarization when compared with cyanide. Yet, the slowing of cytosolic Ca^{2+} decay by physiological $[HCO_3^-]_{ext}$ (~2.8 fold; Fig. 4-2C) was comparable to that evoked by cyanide (~2 fold; Fig. 3-5). Therefore, it is unlikely that the mitochondrial depolarization can fully account for the inhibitory action of HCO_3^- on mitochondrial Ca^{2+} uptake.

4.2.8 The inhibitory action of HCO_3^- on mitochondrial Ca^{2+} uptake could not be detected in adrenal chromaffin cells

The inhibitory action of HCO_3^- on mitochondrial Ca^{2+} uptake in glomus cells raises the issue whether a similar mechanism may also occur in other cell types. To test this possibility, I employed rat adrenal chromaffin cells which were reported to utilize mitochondrial Ca^{2+} uptake as a major cytosolic Ca^{2+} clearance mechanism (Babcock *et al.*, 1997). In this experiment, single chromaffin cells

were loaded with rhod-2 AM as described above for glomus cells. Each chromaffin cell was whole-cell voltage clamped at -70 mV and a depolarizing voltage step was first delivered to activate VGCCs in a HCO_3^--free bath solution. As shown in the example in Fig. 4-12A, such a depolarization evoked a robust increase in the rhod-2 fluorescence in a HCO_3^--free bath solution, reflecting an increase in mitochondrial $[Ca^{2+}]$. When the bath solution was switched to one containing physiological $[HCO_3^-]_{ext}$, another depolarization could still evoke a robust increase in the rhod-2 fluorescence in chromaffin cells (Fig. 4-12A). In 4 chromaffin cells examined, the depolarization-evoked increase in the rhod-2 fluorescence in the presence of physiological $[HCO_3^-]_{ext}$ was only ~17% smaller than that evoked by the 1st depolarization in HCO_3^--free bath solution (c.f. ~70% inhibition in glomus cells; Fig. 4-12B). Thus, the robust inhibitory effect of HCO_3^- on mitochondrial Ca^{2+} uptake is not universal even among cells in which the mitochondria play a dominant role in the clearance of a cytosolic Ca^{2+} load.

4.3 Discussion

In this study, I investigated whether the presence of physiological $[HCO_3^-]_{ext}$ could affect the Ca^{2+} dynamics in glomus cells. My results show that in the presence of physiological $[HCO_3^-]_{ext}$ (23 mM) with or without CO_2 bubbling slowed the time course of cytosolic Ca^{2+} clearance following VGCC-mediated extracellular Ca^{2+} entry by ~2.8-fold (Figs. 4-2C and 4-3B). The slowing of cytosolic Ca^{2+} clearance by physiological $[HCO_3^-]_{ext}$ was not affected by the inhibition of carbonic anhydrase with acetazolamide but was dependent on the

concentration of extracellular HCO_3^-. A slowing in the decay of the depolarization-triggered Ca^{2+} signal could be detected in the presence of 10 mM $[HCO_3^-]_{ext}$ but not in 2 mM $[HCO_3^-]_{ext}$ (Fig. 4-3), suggesting that transmembrane HCO_3^- transport affects Ca^{2+} homeostasis in glomus cells.

Previous studies have shown that the transport of extracellular HCO_3^- into glomus cells is in part mediated via the Na^+/HCO_3^- cotransporter (Buckler *et al.*, 1991) and Na^+-dependent HCO_3^-/Cl^- exchanger (Rocher *et al.*, 1991). My results show that the omission of extracellular Na^+ from the HCO_3^--buffered bath solution did not prevent the HCO_3^--mediated slowing in the decay of the depolarization-triggered Ca^{2+} transient. Thus, the involvement of the reverse mode of NCX can be ruled out. Note that in the absence of extracellular Na^+, the HCO_3^--mediated slowing of $[Ca^{2+}]_i$ decay was more dramatic than that in the presence of extracellular Na^+ (~5.2-fold vs. ~2.8-fold; Fig. 4-5B and Fig. 4-2C). One possible explanation is that the inhibition of NCX (due to the absence of extracellular Na^+) caused further slowing of cytosolic Ca^{2+} clearance. Consistent with this, in Chapter 3 I have shown that the inhibition of NCX slows cytosolic Ca^{2+} clearance by 1.7-fold. My experimental results in this chapter also rule out the involvement of cytosolic acidification in the effect of HCO_3^- on cytosolic Ca^{2+} clearance; the lowering of pH_i in glomus cells from 7.4 to 7.0 did not cause any slowing in the decay of the Ca^{2+} signal in HCO_3^--free bath solution and did not occlude the effect of physiological $[HCO_3^-]_{ext}$ (Fig. 4-6).

My findings in Chapter 3 indicate that mitochondria have a dominant role in cytosolic Ca^{2+} clearance. Consistent with this, my measurement of mitochondrial

Ca^{2+} signal (with rhod-2) shows a rise in mitochondrial $[Ca^{2+}]$ following a short depolarization (to activate VGCCs; Fig. 4-7A). The rapid rise in mitochondrial $[Ca^{2+}]$ was followed by a much slower decline, reflecting a slow extrusion of Ca^{2+} from the mitochondria, possibly via the mitochondrial NCX. A problem frequently associated with the use of rhod-2 in monitoring mitochondrial $[Ca^{2+}]$ is that some rhod-2 is present in the cytosol. Under this condition, an increase in rhod-2 fluorescence may in part reflect a rise in cytosolic $[Ca^{2+}]$. If the rhod-2 signal primarily reflects cytosolic $[Ca^{2+}]$, depolarization is anticipated to evoke a more robust increase in rhod-2 fluorescence in the presence of CCCP. In contrast, my results show that CCCP reduces the depolarization-evoked increase in the rhod-2 fluorescence by ~84%, indicating that the rhod-2 signal arose primarily from the mitochondria. In glomus cells voltage clamped in the whole-cell mode, physiological $[HCO_3^-]_{ext}$ reduced the depolarization-evoked increase in mitochondrial $[Ca^{2+}]$ by ~68% (Fig. 4-7D). A similar reduction was also found in glomus cells recorded with the perforated-patch mode (~60%; Fig. 4-9D). This finding indicates that the slowing of cytosolic Ca^{2+} clearance in glomus cells in the presence of physiological $[HCO_3^-]_{ext}$ is due to a reduction in mitochondrial Ca^{2+} uptake. I have shown in Chapter 3 that mitochondrial inhibitors (CCCP and cyanide) elevated basal $[Ca^{2+}]_i$ in glomus cells by ~140 nM and the basal $[Ca^{2+}]_i$ elevation was dependent on the presence of extracellular Ca^{2+}. As described in Appendix 1, the basal $[Ca^{2+}]_i$ elevation in the presence of mitochondrial inhibitors was not associated with a large increase in Ca^{2+}-permeable leak at the plasma membrane (Fig. A-1A and Table A-1a in Appendices). We speculate that

mitochondrial Ca^{2+} uptake contributes to balance a basal Ca^{2+} influx into glomus cells (described in section 3.3 of Chapter 3). Consistent with the notion that mitochondrial Ca^{2+} uptake was reduced in physiological $[HCO_3^-]_{ext}$, the basal $[Ca^{2+}]_i$ of glomus cells was elevated by 98 ± 18 nM in physiological $[HCO_3^-]_{ext}$ (Fig. 4-2D) and this elevation was abolished by the removal of extracellular Ca^{2+}.

Mitochondrial Ca^{2+} uptake can be mediated via the uniporter, Ca^{2+}/H^+ antiporter or RaM (Santo-Domingo & Demaurex, 2010). I have shown in Chapter 3 that mitochondrial Ca^{2+} uptake in glomus cells was reduced by ruthenium red (Fig. 3-9). Since the uniporter, Ca^{2+}/H^+ antiporter as well as RaM can be affected by ruthenium red (Santo-Domingo & Demaurex, 2010), it is unclear whether the action of HCO_3^- is selective on any of these mitochondrial Ca^{2+} uptake mechanisms. In my experiments, the lowering of pH_i from 7.4 to 7.0 did not cause a slowing in the decay of the depolarization-evoked Ca^{2+} signal (Fig. 4-6) and the raising of pH_i to 8.0 did not reduce the inhibitory effect of physiological $[HCO_3^-]_{ext}$ on mitochondrial Ca^{2+} uptake (Fig. 4-8). Thus, it is unlikely that the mitochondrial Ca^{2+}/H^+ antiporters play an important role in the action of HCO_3^- on glomus cells. Note that RaM was reported to only activate for ~30 ms at the beginning of each repetitive Ca^{2+} transient (Gunter & Gunter, 2001; Bazil & Dash, 2011). In my study, the rising phase of the depolarization-evoked Ca^{2+} transient lasted for slightly longer than 500 ms. Even if RaM is present in the glomus cells, the activation of RaM may limit the amplitude of the cytosolic Ca^{2+} transient; but it is unlikely that RaM influenced the decay phase of the Ca^{2+} signal under my experimental condition. My overall findings are consistent with the possibility

that the effect of HCO_3^- on glomus cells is primarily mediated via a reduction in the activity of the mitochondrial Ca^{2+} uniporter.

Although the effects of physiological $[HCO_3^-]_{ext}$ on the Ca^{2+} signal resemble the effects of mitochondrial inhibitors or uncouplers which are known to cause mitochondrial depolarization (Duchen & Biscoe, 1992b; Buckler & Vaughan-Jones, 1998), I found that the extracellular HCO_3^- caused only a small mitochondrial depolarization (Fig. 4-11), indicating that the HCO_3^--mediated suppression of mitochondrial Ca^{2+} uptake was not due to a dissipation of mitochondrial potential. In addition, although sAC has been identified in rat carotid body (Nunes *et al.*, 2009), my result suggests that the activation of the sAC-cAMP-PKA signaling pathway is not involved in the inhibitory action of extracellular HCO_3^- as the membrane permeable cAMP analog, 8-CPT-cAMP did not affect mitochondrial Ca^{2+} uptake (Fig. 4-10).

Most importantly, I found that the ROS scavengers, GSH or NAC, abolished the inhibitory effect of extracellular HCO_3^- on mitochondrial Ca^{2+} uptake (Fig. 4-9). This finding indicates that the HCO_3^--mediated reduction in mitochondrial Ca^{2+} uptake is related to the cellular level of ROS and raises the possibility that the activity of the mitochondrial uniporter can be suppressed by ROS. At present, it remains unclear whether the production of ROS in glomus cells is enhanced in the presence of extracellular HCO_3^-. Alternatively, HCO_3^- may interact with the hydroxyl radical (the most common ROS) to form the carbonate radical which is a very strong oxidant (Goss *et al.*, 1999; Ezraty *et al.*, 2011) and an increase in the cellular level of carbonate radical in turn suppresses mitochondrial Ca^{2+} uptake.

124

Interestingly, HCO_3^- did not cause any reduction of mitochondrial Ca^{2+} uptake in chromaffin cells (Fig. 4-12), suggesting that the inhibitory action of HCO_3^- may be specific for glomus cells. Carotid body is known to have a high rate of respiration; even under normoxic conditions, the rate of O_2 consumption in the carotid body is near maximum (Duchen & Biscoe, 1992a). Thus, it is possible that ROS production in glomus cells is much higher than in chromaffin cells. Since the inhibitory action of HCO_3^- on mitochondrial Ca^{2+} uptake is dependent on an elevated cellular level of ROS, the ROS level in chromaffin cells may be too low to support the action of HCO_3^-.

Overall, my result shows that, in the presence of physiological $[HCO_3^-]_{ext}$, mitochondrial Ca^{2+} uptake in glomus cells is reduced, resulting in a slowing in cytosolic Ca^{2+} clearance. As shown in Chapter 3, a slowing in the rate of cytosolic Ca^{2+} clearance resulted in an enhancement of exocytotic response in glomus cells (Fig. 3-11). Therefore, it is likely that a slowing in the rate of cytosolic Ca^{2+} clearance in glomus cells in the presence of physiological $[HCO_3^-]_{ext}$ contributes to the potentiation of hypoxic chemotransduction of the carotid body (Shirahata & Fitzgerald, 1991; Panisello & Donnelly, 1998).
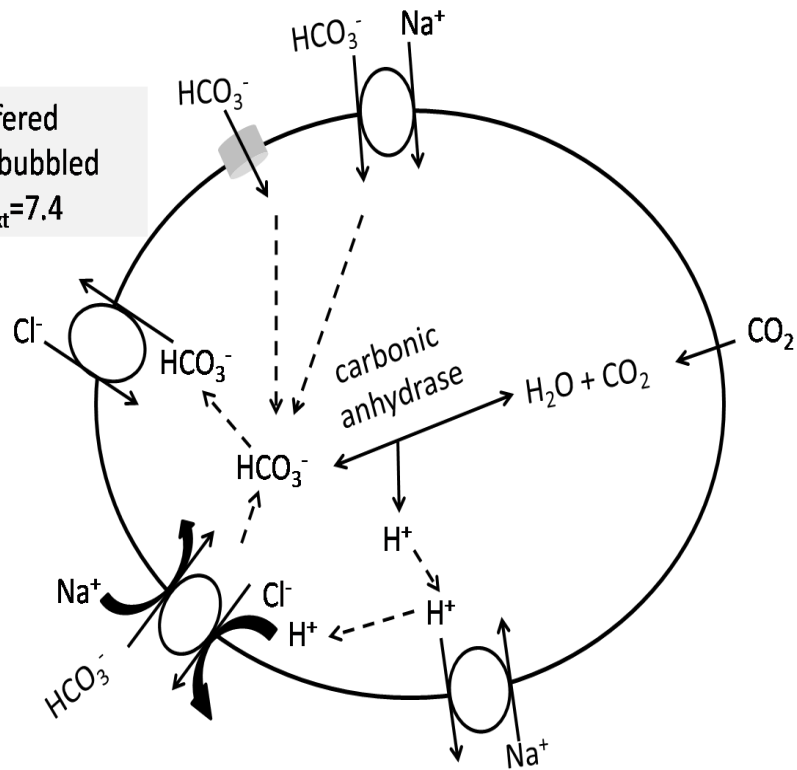
Figure 4-1 Role of HCO_3^- in the regulation of intracellular pH. Although physiological $[HCO_3^-]_i$ is unknown, the extracellular $[HCO_3^-]$ (23 mM) is likely to result in the transport of HCO_3^- into glomus cell via the Na^+/HCO_3^- cotransporter or Na^+-dependent HCO_3^-/Cl^- exchanger. Some HCO_3^- may enter the cell via the anion channel. CO_2 in the bath diffuses into the cell and is converted by the intracellular enzyme carbonic anhydrase into HCO_3^- and H^+. With the rise in $[HCO_3^-]_i$, some HCO_3^- is expected to be extruded from the cell via the HCO_3^-/Cl^- exchanger. Some intracellular H^+ can be extruded via the Na^+/H^+ exchanger.
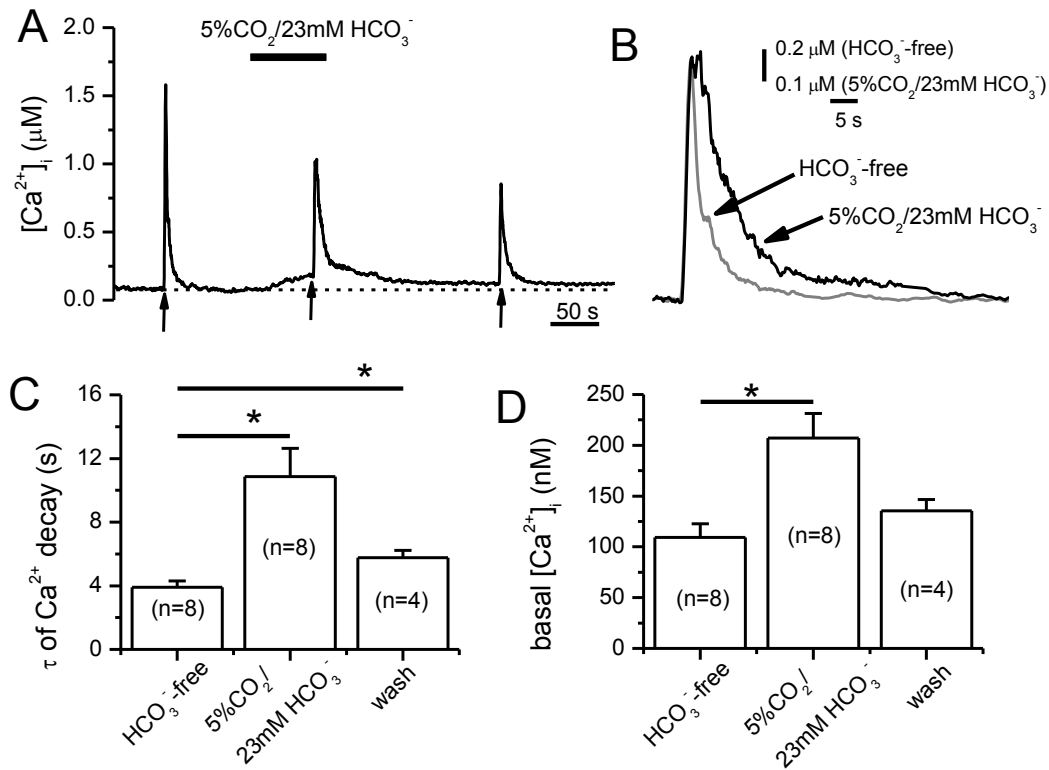
126

Figure 4-2 Influence of extracellular HCO_3^- on the Ca^{2+} dynamics of glomus cells. (A) A voltage clamped glomus cell was depolarized once while it was bathed in a HCO_3^--free solution. The basal $[Ca^{2+}]_i$ increased in this cell when the bath was switched from a HCO_3^--free solution to one containing 23 mM $NaHCO_3$ (bubbled with 5% CO_2). When the HCO_3^--evoked rise in basal $[Ca^{2+}]_i$ reached a plateau, a depolarizing step was delivered to trigger a Ca^{2+} transient. Note that the decay of the Ca^{2+} transient was slower in the presence of extracellular HCO_3^-. The delivery of each voltage step was indicated by an arrow. The dashed line denotes the initial basal $[Ca^{2+}]_i$. (B) Superimposed traces of Ca^{2+} transients in the absence or presence of extracellular HCO_3^- (same cell as in A). For comparison, the amplitude of the Ca^{2+} transient recorded in the presence of HCO_3^- was scaled up to match that recorded in the absence of HCO_3^-. (C) and (D) Comparison of mean values of the time constant (τ) of the single exponential fitted to the decay phase of the Ca^{2+} transient and mean values of basal $[Ca^{2+}]_i$ for cells bathed first in a HCO_3^--free solution, in 23 mM $[HCO_3^-]_{ext}$ and following the removal of extracellular HCO_3^-.
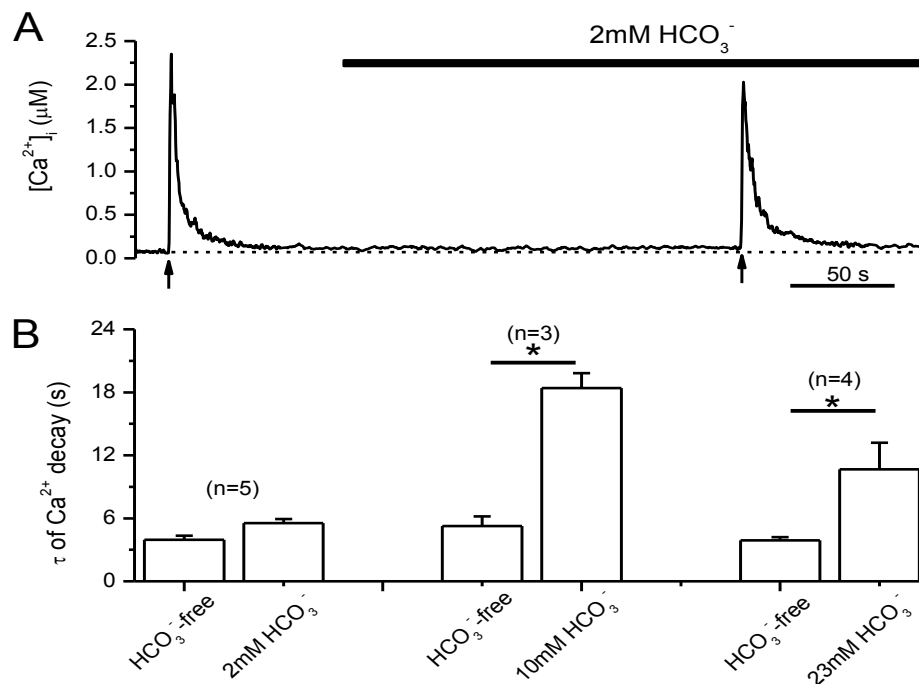
127

Figure 4-3 The slowing of cytosolic Ca^{2+} clearance is dependent on the concentration of extracellular HCO_3^-. (A) Exposure of glomus cell to a bath solution containing 2 mM HCO_3^- did not affect basal $[Ca^{2+}]_i$ or the decay of the depolarization-triggered Ca^{2+} signal. The delivery of each voltage step was indicated by an arrow. (B) Comparison of the mean decay τ values of the depolarization-triggered Ca^{2+} signal when the bath solution was switched from a HCO_3^--free solution to one containing 2, 10 or 23 mM $[HCO_3^-]_{ext}$ (buffered with 10 mM HEPES and with the omission of CO_2 bubbling) for >3 min (with bath perfusion). Note that there was no slowing in cytosolic Ca^{2+} clearance with 2 mM $[HCO_3^-]_{ext}$ but 10 or 23 mM $[HCO_3^-]_{ext}$ resulted in a significant slowing.

23mM HCO_3^--buffered external solution bubbled with 5% CO_2; pH_{ext}=7.4

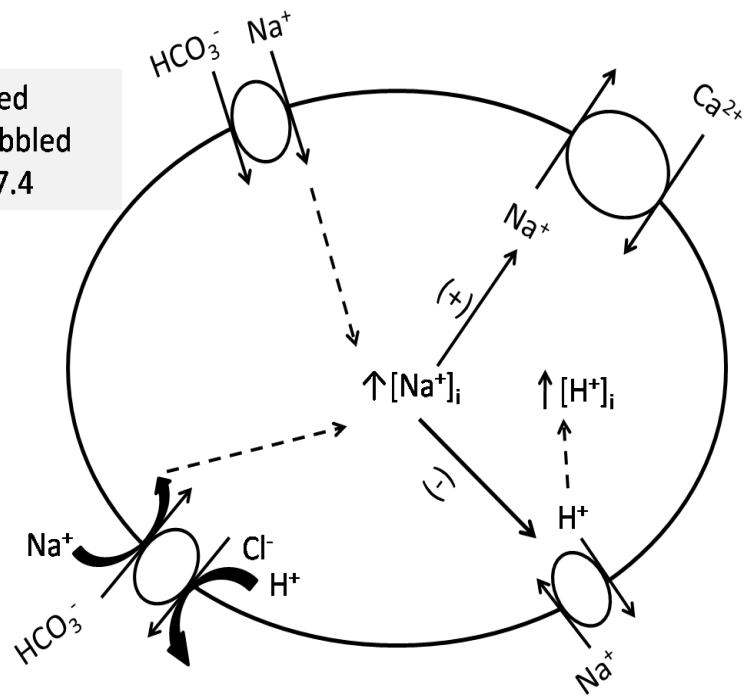**Figure 4-4** Influence of HCO_3^- transport on NCX and cytosolic pH. The transport of HCO_3^- into glomus cell via the Na^+/HCO_3^- cotransporter or Na^+-dependent HCO_3^-/Cl^- exchanger increases $[Na^+]_i$ which may in turn stimulates the reverse mode of NCX. The increase $[Na^+]_i$ may also reduce the extrusion of H^+ via the Na^+/H^+ exchanger, resulting in cytosolic acidification.
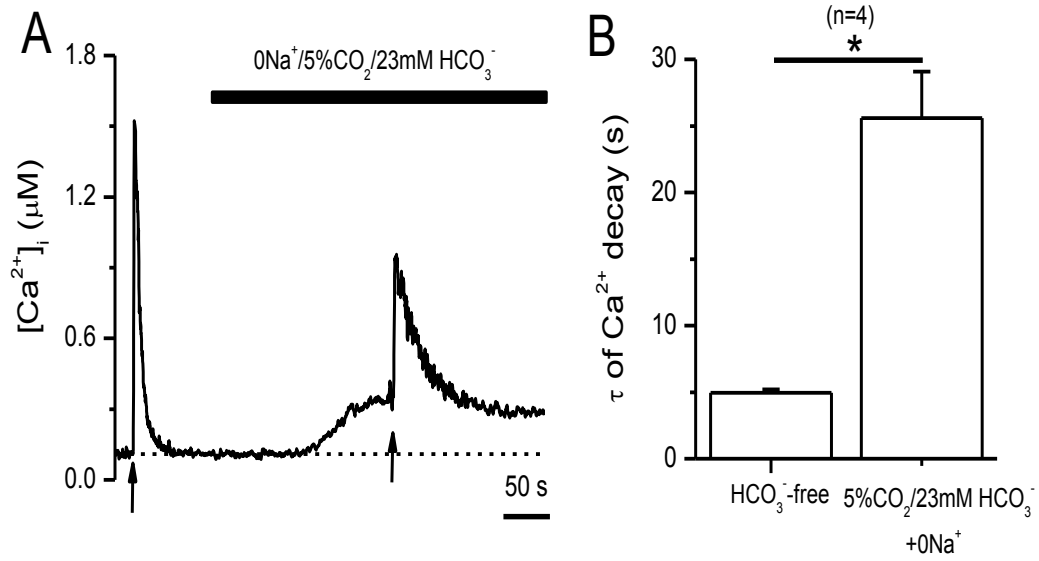
Figure 4-5 The slowing of $[Ca^{2+}]_i$ decay by extracellular HCO_3^- did not require extracellular Na^+. (A) The omission of Na^+ from the HCO_3^--buffered bath solution (bubbled with 5% CO_2) did not prevent the elevation of basal $[Ca^{2+}]_i$ and slowing of $[Ca^{2+}]_i$ decay induced by extracellular HCO_3^-. (B) Comparison of the mean τ values of $[Ca^{2+}]_i$ decay before and after exposure to the Na^+-free HCO_3^--buffered bath solution.

130
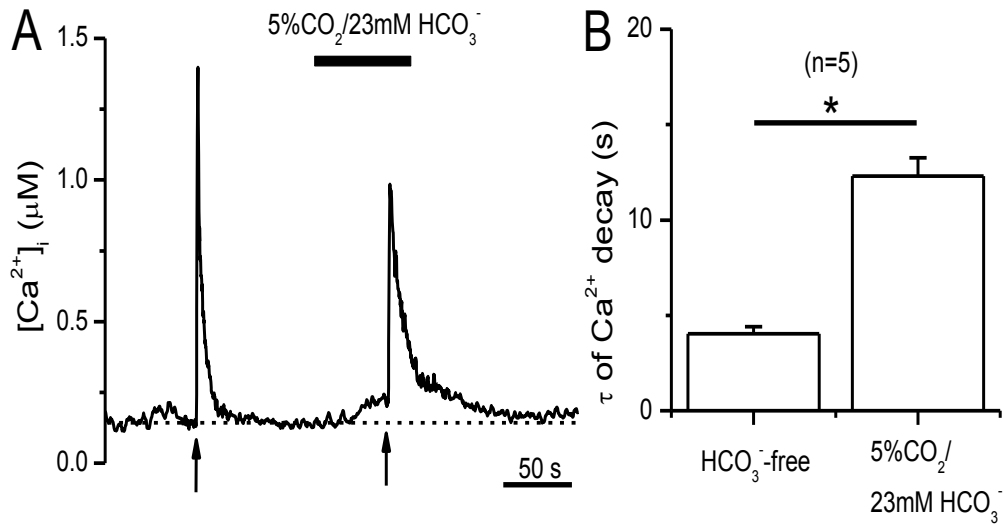
Figure 4-6 Lowering cytosolic pH to 7.0 did not mimic or prevent the effects of extracellular HCO_3^- on the $[Ca^{2+}]_i$ decay of glomus cell. (A) Example of a cell recorded with a whole-cell pipette solution of pH 7.0. When the bath solution was switched from a HCO_3^--free bath solution to a 23 mM HCO_3^--buffered bath solution (bubbled with 5% CO_2), there was a rise in basal $[Ca^{2+}]_i$ and a slowing in the decay of the depolarization-triggered Ca^{2+} signal. The delivery of each voltage step was indicated by an arrow. (B) Comparison of the mean decay τ values of the depolarization-triggered Ca^{2+} signal from cells recorded with a whole-cell pipette solution of pH 7.0 before and after exposure to 23 mM $[HCO_3^-]_{ext}$.

131

Figure 4-7 Mitochondrial Ca^{2+} uptake in glomus cells is reduced in the presence of physiological $[HCO_3^-]_{ext}$. (A) An example of mitochondrial $Ca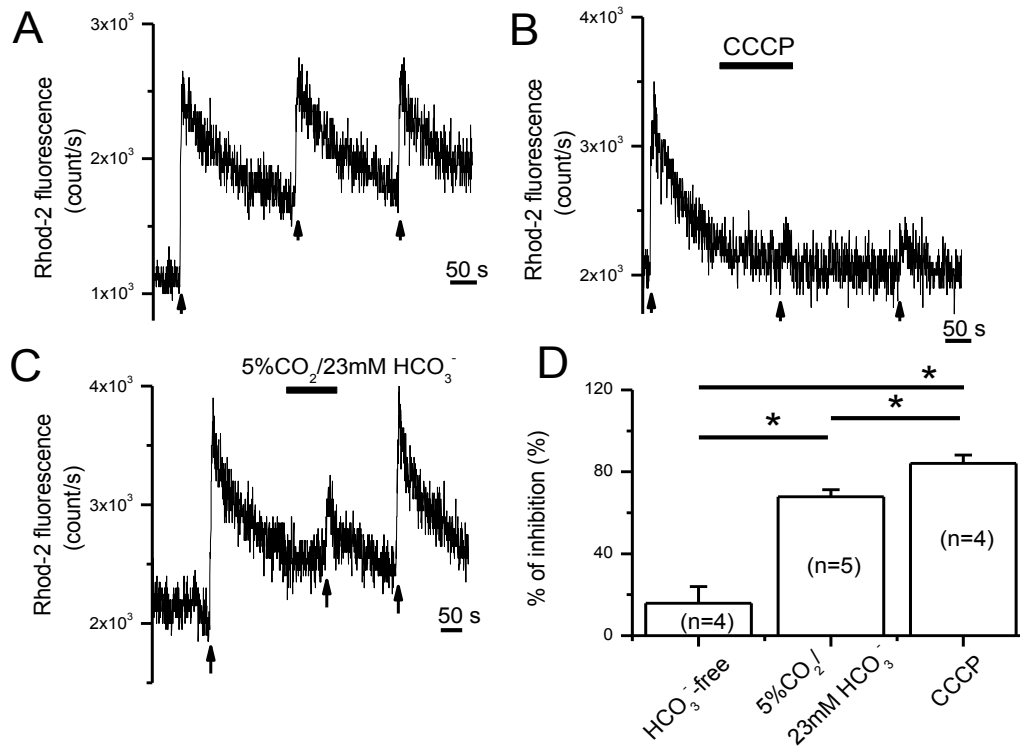^{2+}$ signal measurement from a glomus cell bathed in a HCO_3^--free solution. Mitochondrial Ca^{2+} signal was recorded with rhod-2 AM. The cell was voltage clamped at -70 mV. At the time indicated by each arrow, a voltage step (500 ms) to 0 mV was delivered to evoke voltage-gated Ca^{2+} entry. Following each depolarization, rhod-2 fluorescence increased rapidly and then slowly decayed. (B) In the presence of CCCP (2 μM), mitochondrial Ca^{2+} uptake following depolarization was almost abolished. (C) In a HCO_3^--buffered bath solution (23 mM HCO_3^- and with 5% CO_2 bubbling), depolarization evoked a much smaller increase in mitochondrial $[Ca^{2+}]$. Upon removal of extracellular HCO_3^-, the same depolarization evoked a larger increase in mitochondrial $[Ca^{2+}]$. (D) Comparison of the mean reduction in mitochondrial Ca^{2+} uptake in cells exposed to 23 mM $[HCO_3^-]_{ext}$, or CCCP (2 μM) when compared with time-matched controls (in a HCO_3^--free solution). The percentage of inhibition was calculated by the decrease in the amplitude of the 2nd depolarization-evoked rhod-2 fluorescence increase when compared with that evoked by the 1st depolarization (in a HCO_3^--free solution) for the same cell.
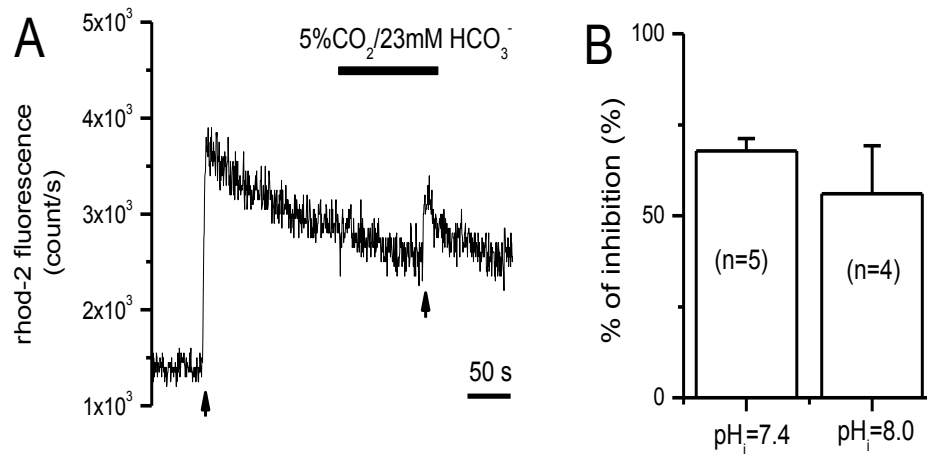
Figure 4-8 Raising intracellular pH to 8.0 did not reduce the inhibition of mitochondrial Ca^{2+} uptake induced by HCO_3^-. (A) An example of a cell recorded with a whole-cell pipette solution buffered to pH 8.0. The depolarization-evoked mitochondrial Ca^{2+} uptake was smaller in the presence of a HCO_3^--buffered bath solution. (B) Plots of the mean reduction in mitochondrial Ca^{2+} uptake in cells recorded with whole-cell pipette solution of pH 8.0 or pH 7.4 when exposed to 23 mM $[HCO_3^-]_{ext}$.
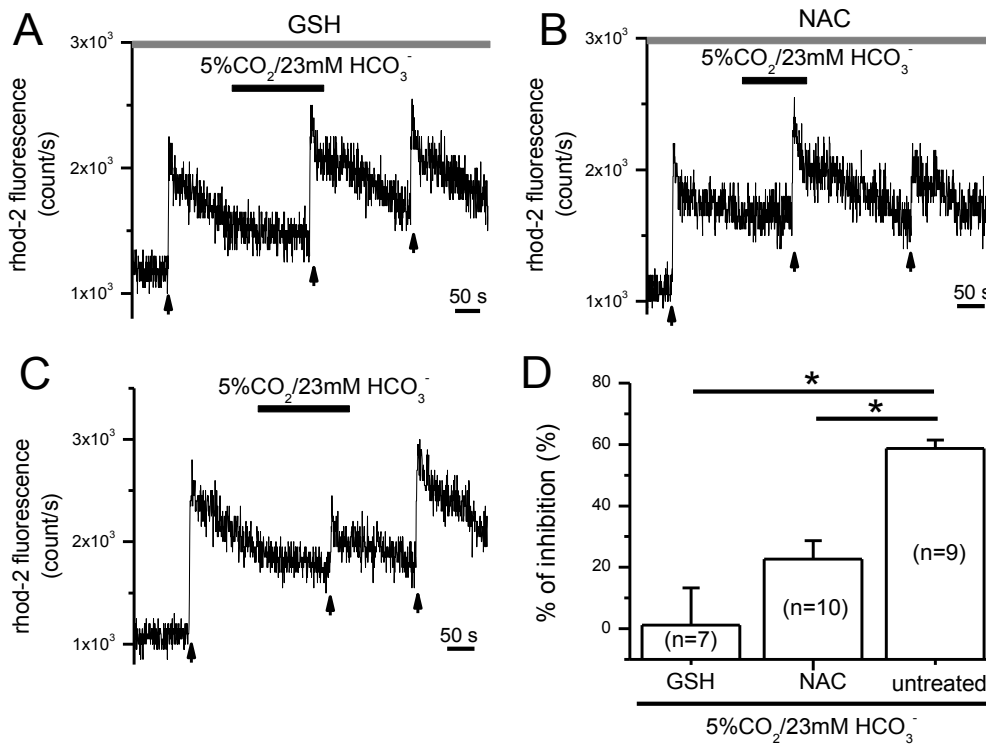
Figure 4-9 ROS scavengers reduced the inhibitory effect of HCO_3^- on mitochondrial Ca^{2+} uptake. (A) In a cell that was pretreated with GSH (2 mM) and then bathed continuously in a solution containing GSH, depolarization could evoke a robust increase in mitochondrial $[Ca^{2+}]$ in extracellular HCO_3^-. The cell was voltage clamped with perforated-patch clamp technique. (B) The effect of GSH could be mimicked by another ROS scavenger, NAC (2 mM). (C) In an untreated cell recorded with perforated-patch clamp technique, extracellular HCO_3^- reduced the increase in mitochondrial $[Ca^{2+}]$ following a depolarization. (D) Comparison of the mean reduction in mitochondrial Ca^{2+} uptake by physiological $[HCO_3^-]_{ext}$ in cells recorded with perforated-patch clamp and treated with a ROS scavenger or untreated.

134
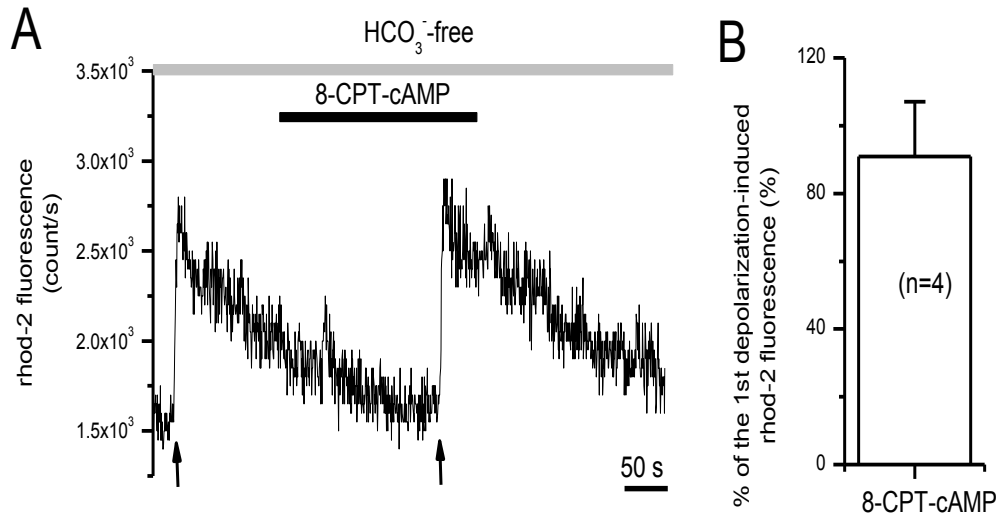
Figure 4-10 Elevation of cellular cAMP did not affect mitochondrial Ca^{2+} uptake. (A) Application of the membrane permeable 8-CPT-cAMP (0.5 mM) did not cause any reduction in the depolarization-evoked increase in mitochondrial $[Ca^{2+}]$. The cell was voltage clamped with perforated-patch clamp technique. (B) The mean amplitude of the 2nd depolarization-evoked mitochondrial Ca^{2+} signal when normalized to the 1st one in the same cell.
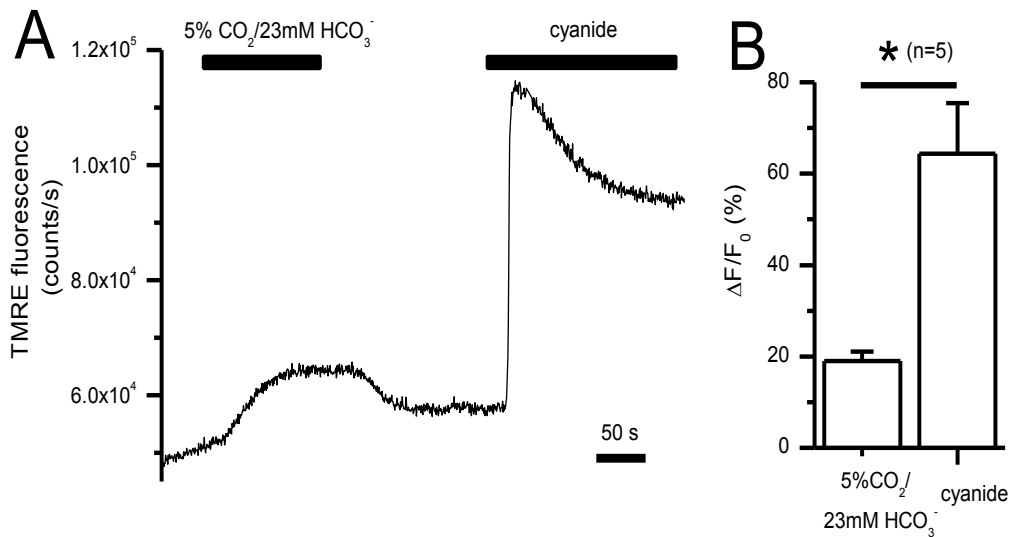
Figure 4-11 Relative to cyanide, physiological $[HCO_3^-]_{ext}$ caused a weaker mitochondrial depolarization in glomus cells. (A) An example of mitochondrial depolarization (reflected by an increase in TMRE fluorescence) in a glomus cell when the bath solution was switched from a HCO_3^--free solution to one containing 23 mM HCO_3^- (bubbled with 5% CO_2). Subsequent challenge of the cell with 5 mM cyanide resulted in a more robust mitochondrial depolarization. (B) Comparison of the mean percentage increase in the amplitude of TMRE fluorescence (ΔF) relative to the basal TMRE fluorescence (F_0) in cells exposed to 23 mM $[HCO_3^-]_{ext}$, or 5 mM cyanide.
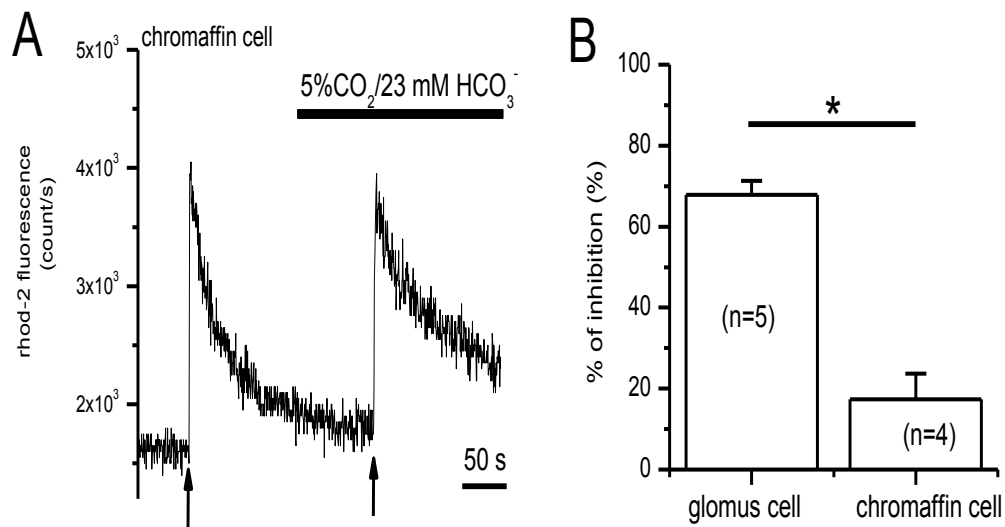
Figure 4-12 Mitochondrial Ca^{2+} uptake in rat chromaffin cells is not affected by extracellular HCO_3^-. (A) In a rat chromaffin cell, depolarization evoked a robust increase in rhod-2 fluorescence in the presence of physiological $[HCO_3^-]_{ext}$. The cell was whole-cell voltage clamped with the same protocol as described in Fig. 4-7. (B) Comparison of the mean reduction in mitochondrial Ca^{2+} uptake by physiological $[HCO_3^-]_{ext}$ in chromaffin cells and glomus cells.

137

Reference List

Acin-Perez R, Salazar E, Kamenetsky M, Buck J, Levin LR, & Manfredi G (2009). Cyclic AMP produced inside mitochondria regulates oxidative phosphorylation. *Cell Metab* **9**, 265-276.

Babcock DF, Herrington J, Goodwin PC, Park YB, & Hille B (1997). Mitochondrial participation in the intracellular Ca^{2+} network. *J Cell Biol* **136**, 833-844.

Bazil JN & Dash RK (2011). A minimal model for the mitochondrial rapid mode of Ca(2)+ uptake mechanism. *PLoS One* **6**, e21324.

Buckler KJ & Vaughan-Jones RD (1998). Effects of mitochondrial uncouplers on intracellular calcium, pH and membrane potential in rat carotid body type I cells. *J Physiol* **513 (Pt 3)**, 819-833.

Buckler KJ, Vaughan-Jones RD, Peers C, & Nye PC (1991). Intracellular pH and its regulation in isolated type I carotid body cells of the neonatal rat. *J Physiol* **436**, 107-129.

Chalmers S & McCarron JG (2008). The mitochondrial membrane potential and Ca^{2+} oscillations in smooth muscle. *J Cell Sci* **121**, 75-85.

Duchen MR & Biscoe TJ (1992a). Mitochondrial function in type I cells isolated from rabbit arterial chemoreceptors. *J Physiol* **450**, 13-31.

Duchen MR & Biscoe TJ (1992b). Relative mitochondrial membrane potential and $[Ca^{2+}]_i$ in type I cells isolated from the rabbit carotid body. *J Physiol* **450**, 33-61.

Duchen MR, Leyssens A, & Crompton M (1998). Transient mitochondrial depolarizations reflect focal sarcoplasmic reticular calcium release in single rat cardiomyocytes. *J Cell Biol* **142**, 975-988.

Ezraty B, Chabalier M, Ducret A, Maisonneuve E, & Dukan S (2011). CO_2 exacerbates oxygen toxicity. *EMBO Rep* **12**, 321-326.

Goss SP, Singh RJ, & Kalyanaraman B (1999). Bicarbonate enhances the peroxidase activity of Cu,Zn-superoxide dismutase. Role of carbonate anion radical. *J Biol Chem* **274**, 28233-28239.

Gunter TE & Gunter KK (2001). Uptake of calcium by mitochondria: transport and possible function. *IUBMB Life* **52**, 197-204.

Iturriaga R & Lahiri S (1991). Carotid body chemoreception in the absence and presence of CO_2-HCO_3^-. *Brain Res* **568**, 253-260.

Jiang D, Zhao L, & Clapham DE (2009). Genome-wide RNAi screen identifies Letm1 as a mitochondrial Ca^{2+}/H^+ antiporter. *Science* **326**, 144-147.

Kumar S, Kostin S, Flacke JP, Reusch HP, & Ladilov Y (2009). Soluble adenylyl cyclase controls mitochondria-dependent apoptosis in coronary endothelial cells. *J Biol Chem* **284**, 14760-14768.

Litvin TN, Kamenetsky M, Zarifyan A, Buck J, & Levin LR (2003). Kinetic properties of "soluble" adenylyl cyclase. Synergism between calcium and bicarbonate. *J Biol Chem* **278**, 15922-15926.

Mari M, Morales A, Colell A, Garcia-Ruiz C, Kaplowitz N, & Fernandez-Checa JC (2012). Mitochondrial glutathione: Features, regulation and role in disease. *Biochim Biophys Acta*.

Nagasaka S, Katoh H, Niu CF, Matsui S, Urushida T, Satoh H, Watanabe Y, & Hayashi H (2007). Protein kinase A catalytic subunit alters cardiac mitochondrial redox state and membrane potential via the formation of reactive oxygen species. *Circ J* **71**, 429-436.

Nunes AR, Monteiro EC, Johnson SM, & Gauda EB (2009). Bicarbonate-regulated soluble adenylyl cyclase (sAC) mRNA expression and activity in peripheral chemoreceptors. *Adv Exp Med Biol* **648**, 235-241.

Nurse CA (1990). Carbonic anhydrase and neuronal enzymes in cultured glomus cells of the carotid body of the rat. *Cell Tissue Res* **261**, 65-71.

Panisello JM & Donnelly DF (1998). Chemotransduction by carotid body chemoreceptors is dependent on bicarbonate currents. *Respir Physiol* **112**, 265-281.

Rocher A, Obeso A, Gonzalez C, & Herreros B (1991). Ionic mechanisms for the transduction of acidic stimuli in rabbit carotid body glomus cells. *J Physiol* **433**, 533-548.

Santo-Domingo J & Demaurex N (2010). Calcium uptake mechanisms of mitochondria. *Biochim Biophys Acta* **1797**, 907-912.

Shirahata M & Fitzgerald RS (1991). The presence of CO_2/HCO_3^- is essential for hypoxic chemotransduction in the in vivo perfused carotid body. *Brain Res* **545**, 297-300.

Stea A & Nurse CA (1989). Chloride channels in cultured glomus cells of the rat carotid body. *Am J Physiol* **257**, C174-C181.

Stea A & Nurse CA (1991). Contrasting effects of HEPES vs HCO3(-)-buffered media on whole-cell currents in cultured chemoreceptors of the rat carotid body. *Neurosci Lett* **132**, 239-242.

Summers BA, Overholt JL, & Prabhakar NR (2000). Augmentation of L-type calcium current by hypoxia in rabbit carotid body glomus cells: evidence for a PKC-sensitive pathway. *J Neurophysiol* **84**, 1636-1644.

Wuttke MS, Buck J, & Levin LR (2001). Bicarbonate-regulated soluble adenylyl cyclase. *JOP* **2**, 154-158.

Wyatt CN & Buckler KJ (2004). The effect of mitochondrial inhibitors on membrane currents in isolated neonatal rat carotid body type I cells. *J Physiol* **556**, 175-191.

Yamamoto Y, Fujimura M, Nishita T, Nishijima K, Atoji Y, & Suzuki Y (2003). Immunohistochemical localization of carbonic anhydrase isozymes in the rat carotid body. *J Anat* **202**, 573-577.

Zippin JH, Chen Y, Nahirney P, Kamenetsky M, Wuttke MS, Fischman DA, Levin LR, & Buck J (2003). Compartmentalization of bicarbonate-sensitive adenylyl cyclase in distinct signaling microdomains. *FASEB J* **17**, 82-84.

Chapter 5

General Discussion

All the experiments described in this thesis were performed on enzymatically dissociated single glomus cells of rat carotid bodies. Since the Ca^{2+} signal in glomus cells plays a key role in the hypoxic chemotransduction of the carotid body, I employed a combination of $[Ca^{2+}]_i$ measurement and electrophysiological techniques to examine two aspects, mitochondria and extracellular HCO_3^-, that shape the Ca^{2+} signal in rat glomus cells. In this chapter, I shall summarize the findings presented in Chapters 3, 4 and the Appendices, and discuss the limitations and future directions of my findings.

5.1 Project 1: role of mitochondria in the regulation of the Ca^{2+} signal in rat glomus cells

5.1.1 Ca^{2+} uptake into mitochondria plays a dominant role in cytosolic Ca^{2+} clearance in rat glomus cells

As described in Chapter 1, hypoxia evokes membrane depolarization and an increase in $[Ca^{2+}]_i$ in glomus cells, resulting in the release of transmitters and the stimulation of the CSN. The effects of hypoxia can be mimicked by mitochondrial inhibitors (Mulligan *et al.*, 1981; Duchen & Biscoe, 1992b; Ortega-Saenz *et al.*, 2003; Wyatt & Buckler, 2004). The relationship between mitochondria and glomus cell excitation is not completely understood, but recent studies suggested that ATP production may be an important link (Gonzalez *et al.*, 2010; Peers *et al.*, 2010). The current model (Fig. 5-1) depicts that a decrease in mitochondrial ATP

production during hypoxia results in an elevation in the cytosolic ADP/ATP ratio. The conversion of ADP to AMP by adenylate kinase activates AMPK which in turn suppresses the opening of BK and TASK-like K^+ channels (Evans *et al.*, 2005; Wyatt *et al.*, 2007). The decrease in cellular ATP level may also cause a direct suppression of TASK-like K^+ channels (Wyatt & Buckler, 2004). The inhibition of TASK-like K^+ and the BK channels leads to membrane depolarization and activation of VGCCs.

When extracellular Ca^{2+} ions enter the cytosol via the opening of VGCCs, they are rapidly bound by endogenous Ca^{2+} buffers and only a fraction of the Ca^{2+} appears as free Ca^{2+}. As described in Appendix 2, I estimated the intracellular Ca^{2+} buffering capacity in rat glomus cells by measuring the amount of Ca^{2+} entering the cytosol during VGCC activation (i.e. the time integral of the Ca^{2+} current) and the corresponding elevations in $[Ca^{2+}]_i$ (monitored with 25 μM indo-1 that was introduced into the cytosol via a whole-cell pipette). My finding suggests that only one out of every 85 Ca^{2+} ions that entered a rat glomus cell was free and the other 84 Ca^{2+} ions were bound by intracellular buffers or rapidly taken up into the intracellular organelles (Fig. A-2 in the Appendices). Since my experiments were conducted at ~3 min after the establishment of whole-cell configuration (to allow diffusion of indo-1 into the cytosol), the Ca^{2+} buffering capacity estimated here arose from buffers that did not wash out of the cytosol via diffusion into the whole-cell pipette. The estimated intracellular Ca^{2+} buffering capacity in glomus cells is comparable to that reported in rat gonadotropes in which one out of every 130 Ca^{2+} entering was free when recorded under similar

experimental conditions (i.e. with 25 μM indo-1 in the whole-cell pipette) (Tse *et al.*, 1994). While the amplitude of the Ca^{2+} signal is influenced by the intracellular Ca^{2+} buffers, the time course of the decay of the Ca^{2+} signal is regulated by the various cytosolic Ca^{2+} clearance mechanisms as long as the Ca^{2+} buffering remains unchanged. My findings in Chapter 3 show that under whole-cell voltage clamp conditions (in the HCO_3^--free bath solution), acute application of the mitochondrial inhibitor CCCP to glomus cells caused a dramatic slowing (~3-6-fold) in the decay of the depolarization-triggered Ca^{2+} signal (Fig. 3-4). Intracellular introduction of ruthenium red (which is an inhibitor of the uniporter, Ca^{2+}/H^+ antiporter and RaM in the mitochondria) also slowed the decay of the depolarization-triggered Ca^{2+} signal (Fig. 3-9). In contrast, inhibition of NCX, PMCA pump or SERCA pump had smaller effects (~20-30%; Fig. 3-8B). Fig. 5-2 summarizes the role of the various cytosolic Ca^{2+} clearance mechanisms in rat glomus cells. Following a rise in $[Ca^{2+}]_i$, a large fraction of the Ca^{2+} in the cytosol is taken up into the mitochondria. The remaining Ca^{2+} is pumped into the ER store via the SERCA pump or moved to the extracellular space by the PMCA pump and NCX on the plasma membrane (Fig. 5-2).

5.1.2   Reduction in mitochondrial Ca^{2+} uptake during hypoxia enhances exocytosis in rat glomus cells

Hypoxia has been shown to cause mitochondrial depolarization in intact glomus cells (Duchen & Biscoe, 1992b). In my experiments, when glomus cells were recorded under the voltage clamp condition with the perforated-patch

configuration, hypoxia caused a slowing in cytosolic Ca^{2+} clearance (~2-fold; Fig. 3-10). This finding suggests that during hypoxia, mitochondrial depolarization reduces the driving force across the inner membrane of mitochondria and thus decreases Ca^{2+} uptake into the mitochondria (Fig. 5-2). By monitoring $[Ca^{2+}]_i$ simultaneously with exocytosis (membrane capacitance measurement), we found that the increase in the duration of the depolarization-triggered Ca^{2+} signal in the cytosol after mitochondrial inhibition was associated with an enhancement of the exocytotic response (~3-fold; Fig. 3-11). These findings indicate that other than its effect on cellular excitability, mitochondrial inhibition can also regulate transmitter release via changes in Ca^{2+} dynamics (Fig. 5-2).

In summary, the intertwined roles of mitochondria in cellular excitability, Ca^{2+} homeostasis and transmitter release in rat glomus cells highlight the importance of mitochondria in the hypoxic chemotransduction.

5.1.3 Limitations and future directions of Project 1

5.1.3.1 Influence of temperature

Since all my experiments in Project 1 involve the use of whole-cell voltage clamp techniques and the stability of the seal between the patch-type pipette and the cell surface tends to be unstable at 37 ^{o}C (probably due to an increase in cell membrane fluidity), I have conducted all my experiments at room temperature (20-23°C). However, many cellular functions are sensitive to temperature.

145

Therefore, it is important to consider the influence of temperature on several aspects of my experimental results in Project 1. Firstly, in my experiments, Ca^{2+} signal in glomus cells was evoked by the activation of VGCCs. It has been reported that L-type VGCCs are enhanced at high temperatures (McAllister-Williams & Kelly, 1995; Peloquin *et al.*, 2008) and reduced by temperature lowering (Allen, 1996). Since most of the VGCCs in rat glomus cells are L-type (Fieber & McCleskey, 1993; Silva & Lewis, 1995), it is likely that the amplitudes of the Ca^{2+} current and $[Ca^{2+}]_i$ transient observed in my experiments at room temperature are smaller than those at physiological temperature. Secondly, the process of exocytosis accelerates with temperature (Ohta *et al.*, 1990; Renstrom *et al.*, 1996; Gil *et al.*, 2001). Thus, it is likely that the amount of exocytosis evoked by depolarization (Fig. 3-11) in glomus cells is underestimated in my experiments at room temperature. Thirdly, the time course of cytosolic Ca^{2+} clearance is temperature-sensitive (David & Barrett, 2000; Hughes *et al.*, 2006; Kang *et al.*, 2008). In adult rat dorsal root ganglion (DRG) neurons, the rate of cytosolic Ca^{2+} clearance was increased by ~1.4 fold when the temperature was raised from 20 to 30 ^{o}C (Kang *et al.*, 2008). The higher temperature also caused an increase in the Ca^{2+} buffering ability of DRG neurons via an enhancement of mitochondrial Ca^{2+} uptake (Kang *et al.*, 2008). An increase in mitochondrial Ca^{2+} uptake with temperature was also reported in mouse motor nerve terminals (David & Barrett, 2000). However, a higher temperature did not alter the relative contribution of the cytosolic Ca^{2+} clearance mechanisms in some cell types. A previous study from our laboratory (Hughes *et al.*, 2006) has shown that while increasing the

146

temperature from 22 to 35 $^{\circ}$C accelerated the rate of cytosolic Ca^{2+} clearance in rat pancreatic β cells by ~2.5 fold, the relative contribution of the SERCA pump, mitochondria, NCX and PMCA pump to cytosolic Ca^{2+} clearance was not affected. In rat carotid glomus cells, I have found that mitochondria are the dominant cytosolic Ca^{2+} clearance mechanisms at room temperature (Chapter 3). Therefore, it is likely that at physiological temperature, mitochondrial Ca^{2+} uptake is enhanced in glomus cells, resulting in a faster rate of cytosolic Ca^{2+} clearance than that reported in my study.

5.1.3.2 *Influence of mitochondria on the amplitude of the Ca^{2+} signal*

Since mitochondrial Ca^{2+} uptake is the dominant mechanism of cytosolic Ca^{2+} clearance in rat glomus cells, it is possible that a rapid uptake of cytosolic Ca^{2+} following VGCC activation also limits the amplitude of the depolarization-triggered Ca^{2+} transient. Such a scenario has been shown in rat pancreatic β cells in which the amplitude of the depolarization-triggered Ca^{2+} transient was increased following the inhibition of the SERCA pump (which is the major mechanism of cytosolic Ca^{2+} clearance in β cells) (Hughes *et al.*, 2006). However, this possibility could not be addressed in my study because VGCC tended to rundown during the time course of the experiment (e.g. Fig. 3-2C). One way to circumvent the problem of VGCC rundown is to normalize the amplitude of the Ca^{2+} transient to the amount of Ca^{2+} entry (calculated from the time integral of the Ca^{2+} current). Unfortunately, even with the presence of Cs^{+} and TEA in the pipette solution (to block outward K^{+} currents), the inward Ca^{2+} current recorded

beyond ~3 min in the whole-cell mode was progressively more contaminated by an outward current that was activated during the depolarizing step and the magnitude of the net inward current became obviously smaller at the 2nd depolarization in all of my protocols (e.g. Fig. 3-2B). Therefore, I was unable to estimate the amount of Ca^{2+} entry during the 2nd depolarizing voltage step (i.e. following the application of mitochondrial inhibitor). The identification of this gradually developing outward current was not explored in my study. In addition to an unblocked voltage-activated K^+ current, another possible candidate of an outward current during a depolarizing voltage step to 0 mV is a Cl^- current: the whole-cell pipette solution in my experiments contained 25 mM Cl^- and the HEPES-buffered bath solution contained 161.5 mM Cl^- (therefore the reversal potential of a Cl^- current is about -47 mV). Three types of Cl^- channels have been reported in glomus cells (Stea & Nurse, 1989; Stea & Nurse, 1991; Carpenter & Peers, 1997; Petheo *et al.*, 2001). Future experiments to examine whether the development of the outward current during prolonged whole-cell recordings can be prevented by Cl^- channel blockers (e.g. 9-AC and niflumic acid) would help to resolve the problem in estimating the amount of Ca^{2+} entry during the depolarization step. However, such pharmacological blockers are also expected to perturb some transport of HCO_3^- in glomus cells. Nevertheless, an increase in the amplitude of the depolarization-triggered Ca^{2+} transient in the presence of CCCP could be observed in some cells (e.g. Fig. 3-4A & D). Thus, it is likely that in glomus cells, mitochondrial Ca^{2+} uptake also limits the amplitude of the $[Ca^{2+}]_i$ rise during VGCC activation. An increase in the amplitude of the depolarization-

triggered Ca^{2+} transient following mitochondrial inhibition is expected to trigger more exocytosis. Therefore, in addition to the prolongation of the Ca^{2+} signal during mitochondrial inhibition, mitochondrial inhibition may also increase the amplitude of the Ca^{2+} signal and both of these mechanisms will contribute to an enhancement of transmitter release from glomus cells.

5.1.3.3 Impact of hypoxia on mitochondrial function

An important question in Project 1 is whether the mitochondrial depolarization evoked by hypoxia in glomus cells is sufficient to cause a slowing in cytosolic Ca^{2+} clearance. In previous studies, hypoxia was typically induced by perfusing intact glomus cells (in a closed chamber) with the bath solution bubbled with N_2. However, in my experiments, glomus cells must be voltage clamped at - 70 mV to prevent hypoxia-induced depolarization and thus an open chamber was employed. Since the recording chamber was exposed to atmospheric O_2 and the bath solution was continuously perfused at a relatively slow rate (~3 ml/min) to minimize disturbance to the seal between the cell and the patch-type electrode, it is challenging to induce hypoxia under my experimental conditions. The inclusion of dithionite, an O_2 scavenger, in the bath solution (without N_2 bubbling) lowered pO_2 to 10 mm Hg (Jiang & Eyzaguirre, 2004), but it has been reported that dithionite alone induced only a transient hypoxic condition, possibly due to the continuous replenishment of O_2 from the atmosphere (Archer *et al.*, 1995). In the literature, dithionite was frequently used in conjunction with 100% N_2 bubbling to intensify the hypoxic stimulus to glomus cells (Biscoe & Duchen, 1990; Buckler

& Vaughan-Jones, 1994). Therefore, I employed the same procedure to induce hypoxia. It has been postulated that dithionite may activate a VGCC-independent Ca^{2+} influx in glomus cells and this action is not related to hypoxia (Carpenter *et al.*, 2000). In my experiments, a small elevation (~30 nM) of basal $[Ca^{2+}]_i$ could be detected in some glomus cells when exposed to hypoxia (e.g. Fig. 3-10A). Since mitochondrial inhibition also elevates basal $[Ca^{2+}]_i$ (Fig. 3-4), it is unclear whether the small rise in basal $[Ca^{2+}]_i$ in the hypoxic condition is due to the hypoxia-induced mitochondrial inhibition or the hypoxia-independent effect of dithionite. Nevertheless, as described in Fig. 3-3A, the rate of cytosolic Ca^{2+} clearance was not affected when the basal $[Ca^{2+}]_i$ was in the range of 25-250 nM. Thus, the slowing in the cytosolic Ca^{2+} clearance in hypoxia is likely due to a reduction in mitochondrial function under the hypoxic condition. Note that the addition of dithionite to the perfusate of isolated rat lungs with normoxic or hypoxic ventilation was reported to increase the production of superoxide radicals (Archer *et al.*, 1995). Since I found in my second project (Chapter 4) that the HCO_3^--induced inhibition of mitochondrial Ca^{2+} uptake was dependent on an elevated cellular level of ROS (section 4.2.6), it is possible that under my experimental condition (hypoxia induced by dithionite in conjunction with N_2 bubbling), the applied dithionite may increase cellular ROS and thus enhance the suppression of mitochondrial function induced by hypoxia.

In my experiments, the pO_2 level in the bath solution was not measured, so the degree of hypoxia is not known. Since the effect of hypoxia on cytosolic Ca^{2+} clearance is modest in comparison to that of CCCP (~1.6-fold slowing versus ~6-

fold), it is likely that the hypoxic condition in my experiments was not severe. Since hypoxia has been shown to cause mitochondrial depolarization (Duchen & Biscoe, 1992b), I postulated that the slowing in cytosolic Ca^{2+} clearance during hypoxia was related to mitochondrial depolarization which in turn results in an impairment of mitochondrial Ca^{2+} uptake. Future experiments involving measurement of mitochondrial potential when glomus cells are exposed to different pO_2 levels will help to clarify the sensitivity of the mitochondrial membrane function to hypoxia.

5.2 Project 2: Influence of HCO_3^- on mitochondrial Ca^{2+} transport in rat carotid glomus cells

5.2.1 Extracellular HCO_3^- slows cytosolic Ca^{2+} clearance in glomus cells via a reduction in mitochondrial Ca^{2+} uptake

Other than its role of pH regulation, a physiological concentration of extracellular HCO_3^- ($[HCO_3^-]_{ext}$ = 23 mM; 5% CO_2 bubbling) was reported to enhance the hypoxia-triggered CSN discharge and catecholamine release from carotid bodies in different species (Iturriaga & Lahiri, 1991; Shirahata & Fitzgerald, 1991; Panisello & Donnelly, 1998), but the underlying mechanism is not clear. My findings in Chapter 4 have shown that extracellular HCO_3^- affects the dynamics of the Ca^{2+} signal in rat glomus cells. When the bath was switched from a HCO_3^--free solution to one containing 2 mM HCO_3^- or one containing

151

physiological [HCO_3^-] (23 mM), the rate of cytosolic Ca^{2+} clearance was unchanged in 2 mM [HCO_3^-]$_{ext}$ but slowed by ~2.8-fold in 23 mM [HCO_3^-]$_{ext}$ (Fig. 4-3). Thus, the rate of cytosolic Ca^{2+} clearance in glomus cells is influenced by [HCO_3^-]$_{ext}$ in the physiological range. The effect of extracellular HCO_3^- on cytosolic Ca^{2+} clearance did not require extracellular Na^+ entry, indicating that neither the reverse mode of NCX nor cytosolic acidification (via a decrease in the activity of the Na^+/H^+ exchanger) was involved. Consistent with my finding in Project 1 that Ca^{2+} uptake into the mitochondria is the major mechanism for cytosolic Ca^{2+} clearance in glomus cells, measurement of mitochondrial Ca^{2+} signal (monitored with rhod-2) shows that the voltage clamped activation of VGCCs triggered a rise in mitochondrial [Ca^{2+}] (Fig. 4-7A). In the presence of physiological [HCO_3^-]$_{ext}$, the amplitude of the depolarization-evoked rise in mitochondrial [Ca^{2+}] was reduced by ~68% (Fig. 4-7). Thus, the slowing of cytosolic Ca^{2+} clearance in physiological [HCO_3^-]$_{ext}$ is due to a reduction in mitochondrial Ca^{2+} uptake.

Ca^{2+} uptake into the mitochondria may be mediated via the uniporter, Ca^{2+}/H^+ antiporter and RaM. Under my experimental conditions (single Ca^{2+} transient evoked by a 500 ms depolarization), RaM probably has no contribution to the decay phase of the Ca^{2+} transient as the activation of RaM is only transient (~30 ms) (Gunter & Gunter, 2001; Bazil & Dash, 2011). The involvement of the mitochondrial Ca^{2+}/H^+ antiporter is minor because cytosolic alkalinisation or acidification (which enhances or suppresses the activities of the mitochondrial Ca^{2+}/H^+ antiporter respectively) did not affect the action of HCO_3^-. Therefore, it is

likely that the effect of HCO_3^- on glomus cells is primarily mediated via a reduction in the activities of the mitochondrial uniporter. The inhibitory action of HCO_3^- on mitochondrial Ca^{2+} uptake was abolished when glomus cells were pretreated with the ROS scavenger, GSH or NAC (Fig. 4-9), suggesting that the activity of the mitochondrial uniporter can be suppressed by an elevated level of ROS.

The link between HCO_3^- and ROS was not studied in my experiments. One possibility is that in the presence of physiological $[HCO_3^-]_{ext}$, there is an enhancement of ROS production in glomus cells and the elevation in ROS suppresses mitochondrial Ca^{2+} uptake. Fig. 5-3 depicts a possible mechanism by which extracellular HCO_3^- can lead to an increase in mitochondrial ROS production. During respiration, CO_2 is produced from the tricarboxylic acid (TCA) or Krebs cycle. CO_2 rapidly diffuses out of the mitochondria into the cytosol (down the CO_2 gradient) and a fraction of the CO_2 may be converted into HCO_3^- by mitochondrial carbonic anhydrase. In the presence of physiological $[HCO_3^-]_{ext}$, HCO_3^- is transported into the cytosol of glomus cells via the Na^+/HCO_3^- cotransporter, Na^+-dependent HCO_3^-/Cl^- exchanger or anion channels (Fig. 4-1). In the cytosol, carbonic anhydrase catalyzes the conversion of HCO_3^- into CO_2, resulting in an elevation of cytosolic levels of CO_2 (Fig. 5-3). Therefore, switching the extracellular solution from a HCO_3^--free one to one containing physiological $[HCO_3^-]_{ext}$ will reduce the CO_2 gradient between the mitochondria and the cytosol. As a result, less CO_2 diffuses from the mitochondria into the cytosol and there is a higher level of mitochondrial CO_2. An elevated level of

153

atmospheric CO_2 was reported to suppress respiration in isolated plant (e.g. soybean) as well as bovine heart mitochondria via a reduction in the activities of succinate dehydrogenase (complex II) and cytochrome c oxidase (complex IV) of the electron transport chain (ETC) (Gonzalez-Meler *et al.*, 1996). Therefore, it is conceivable that an elevated level of CO_2 in the mitochondria may lead to a decrease in the efficiency of electron transport along the ETC, resulting in an increase in mitochondrial ROS production (Poyton *et al.*, 2009).

Another possibility is that the suppression of mitochondrial Ca^{2+} uptake is due to the interaction of HCO_3^- with ROS. With the high rate of respiration in glomus cells (Duchen & Biscoe, 1992a), ROS production may already be high in these cells. As described above, mitochondrial CO_2 levels increase in the presence of physiological $[HCO_3^-]_{ext}$. In the mitochondria, CO_2 can be converted into HCO_3^- via mitochondrial carbonic anhydrase, resulting in an elevation of mitochondrial $[HCO_3^-]$. It is also possible that some cytosolic HCO_3^- is transported into the mitochondria. Mitochondrial inner membrane anion channels (IMAC) were found to be permeable to Cl^- (Powers *et al.*, 1994; Liu *et al.*, 1996), but anion channels are typically not particularly selective among small anions (Hille, 2001). Therefore, cytosolic HCO_3^- may also diffuse into the mitochondria via IMAC (Fig. 5-3). An elevated $[HCO_3^-]$ in the mitochondria increases the interaction of HCO_3^- with the hydroxyl radical (the most common ROS) which results in the formation of the carbonate radical (Fig. 5-3). Since the carbonate radical is a very strong oxidant (Goss *et al.*, 1999; Ezraty *et al.*, 2011), it may

modulate the function of the mitochondrial uniporter, resulting in a reduction of mitochondrial Ca^{2+} uptake (Fig. 5-3).

5.2.2 Extracellular HCO_3^- enhanced the hypoxia-mediated Ca^{2+} signal in glomus cells

In addition to the slowing in cytosolic Ca^{2+} clearance described above (section 5.2.1), I found that the ability of hypoxia to evoke a rise in $[Ca^{2+}]_i$ in glomus cells (not voltage clamped) was enhanced in the presence of physiological $[HCO_3^-]_{ext}$ (details described in Appendix 3). When intact glomus cells were challenged with moderate hypoxia in a HCO_3^--free bath solution or in the presence of physiological $[HCO_3^-]_{ext}$, the majority of glomus cells (~85%) exhibited a Ca^{2+} response in a bath solution with physiological $[HCO_3^-]_{ext}$ but not in a HCO_3^--free bath solution (Fig. A-3C in Appendices). For cells that exhibited a Ca^{2+} signal during hypoxia in the HCO_3^--free bath solution, their mean time integral of the hypoxia-mediated Ca^{2+} signal was smaller than that evoked in the presence of extracellular HCO_3^- (Fig. A-3D in Appendices). The more sustained hypoxia-evoked Ca^{2+} signal in physiological $[HCO_3^-]_{ext}$ is consistent with the finding in Chapter 4 that extracellular HCO_3^- caused a slowing in cytosolic Ca^{2+} clearance.

Using perforated-patch clamp recording, I investigated whether the resting membrane potential or the hypoxia-evoked depolarization was affected by physiological $[HCO_3^-]_{ext}$ (details described in Appendix 3). I found that

155

extracellular HCO_3^- did not affect the resting membrane potential (~-50 mV) of glomus cells (Fig. A-4B in Appendices). However, in the presence of physiological $[HCO_3^-]_{ext}$, hypoxia triggered a larger depolarization (~17 mV versus ~8 mV in HCO_3^--free; Fig. A-4C in Appendices). Consequently, in the presence of physiological $[HCO_3^-]_{ext}$, the hypoxia-evoked depolarization was sufficient to trigger bursts of action potentials that probably involved robust activation of VGCCs (Fig. A-4B in Appendices). In contrast, the smaller depolarization evoked by hypoxia in the absence of HCO_3^- was below the threshold for triggering any action potentials (or even for any significant activation of VGCCs). These results indicate that in the presence of physiological $[HCO_3^-]_{ext}$, hypoxia evokes a larger depolarization in glomus cells and thus increases the fraction of glomus cells that exhibit a Ca^{2+} signal in response to a moderate hypoxic challenge.

Overall, my results in Project 2 show that physiological $[HCO_3^-]_{ext}$ enhances the hypoxia-mediated Ca^{2+} signal in glomus cells via not only an increase in the hypoxia-evoked depolarization but also a suppression of mitochondrial Ca^{2+} uptake (which leads to a slowing in cytosolic Ca^{2+} clearance). Consequently, a larger fraction of glomus cells exhibit $[Ca^{2+}]_i$ elevation when challenged with a moderate hypoxia and the duration of their hypoxia-mediated Ca^{2+} signal is prolonged. As shown in Chapter 3, an increase in the duration of the Ca^{2+} signal resulted in an enhancement of the exocytotic response in glomus cells (Fig. 3-11). The above mechanisms in glomus cells are expected to contribute significantly to the previously reported phenomenon that a physiological $[HCO_3^-]_{ext}$ enhanced

CSN discharge and catecholamine release from carotid bodies in more intact perparations (Iturriaga & Lahiri, 1991; Shirahata & Fitzgerald, 1991; Panisello & Donnelly, 1998).

5.2.3 Limitations and future directions of Project 2

5.2.3.1 Influence of extracellular HCO_3^- on mitochondrial ROS production

My findings in Chapter 4 raise the possibility that HCO_3^- suppresses mitochondrial uniporter Ca^{2+} uptake via a mechanism that is dependent on an elevation of cellular ROS. However, I found that in rat chromaffin cells extracellular HCO_3^- did not affect mitochondrial Ca^{2+} uptake (Fig. 4-12). A possible reason for the difference between the two cell types is that HCO_3^- significantly increases the production of ROS in glomus cells but not in chromaffin cells. Alternatively, the cellular level of ROS in glomus cells may be much higher than that in chromaffin cells such that more carbonate radicals (due to the interaction between HCO_3^- and the hydroxyl radical) are formed in glomus cells. Future experiments to compare the cellular level of ROS between chromaffin cells and glomus cells (with or without extracellular HCO_3^-), for example with a fluorescent ROS indicator, such as membrane permeable 2',7'-dichlorodihydrofluorescein diacetate (H_2-DCFDA), may be able to resolve this. Following the uptake of H_2-DCFDA into cells, it is cleaved by the intracellular esterases. When oxidized by ROS, the non-fluorescent H_2-DCFDA is converted to

the fluorescent DCF. Therefore a rise in the fluorescence of DCF trapped in the cell (at 485 nm excitation and 535 nm emission wavelengths) reflects an increase in the cellular level of ROS (Acin-Perez *et al.*, 2009). Note that H_2-DCFDA may not reflect changes in the level of carbonate radicals. At present, there is no experimental tool for measuring the cellular level of carbonate radicals. Thus, it will remain unclear whether HCO_3^- interacts with hydroxyl radical to form a carbonate radical.

5.2.3.2 *Mechanism underlying the potentiation of hypoxia-evoked depolarization by extracellular HCO_3^-*

It is not clear why hypoxia is able to evoke a larger depolarization in the presence of extracellular HCO_3^- (Fig. A-4 in Appendices). Since the resting membrane potential was not affected by extracellular HCO_3^-, it is unlikely that extracellular HCO_3^- affected the activities of background TASK-like K^+ and BK channels. One possibility is that the sensitivity of the TASK-like K^+ and/or BK channels to hypoxia is enhanced in the presence of extracellular HCO_3^-. In view of the key role of ROS in the suppression of mitochondrial Ca^{2+} uptake by extracellular HCO_3^-, it is possible that an elevated cellular ROS level enhances the AMPK-mediated suppression of TASK-like K^+ and BK channels during hypoxia. This possibility can be addressed by examining whether treatment of glomus cells with ROS scavengers (e.g. with GSH or NAC as shown in Fig. 4-9) can attenuate the hypoxia-evoked depolarization in the presence of extracellular HCO_3^-.

5.2.3.3 Molecular mechanisms underlying the suppression of the mitochondrial uniporter by extracellular HCO_3^-

The important role of ROS in the HCO_3^--mediated suppression of mitochondrial Ca^{2+} uptake raises the possibility that specific proteins involved in the regulation of the mitochondrial uniporters may be the target of ROS. Recent studies have shown that Ca^{2+} uptake via the mitochondrial uniporter is regulated by two proteins: "mitochondrial calcium uniporter regulator 1" (MCUR1) (Mallilankaraman *et al.*, 2012a) and "mitochondrial calcium uptake 1" (MICU1) (Perocchi *et al.*, 2010; Mallilankaraman *et al.*, 2012b). Knockdown of MCUR1 was found to reduce mitochondrial Ca^{2+} uptake both at basal and stimulated conditions (e.g. triggering of intracellular Ca^{2+} release) while overexpression of MCUR1 enhanced mitochondrial Ca^{2+} uptake and reduced the amplitude of the Ca^{2+} transient in the cytosol (Mallilankaraman *et al.*, 2012a). Similarly, knockdown of MICU1 was found to reduce mitochondrial Ca^{2+} uptake both at basal and stimulated conditions (Perocchi *et al.*, 2010). However, a subsequent study found that knockdown of MICU1 enhanced basal mitochondrial Ca^{2+} concentration and mitochondrial Ca^{2+} uptake when $[Ca^{2+}]_i$ was lower than ~3 μM, but failed to affect mitochondrial Ca^{2+} uptake at higher cytosolic $[Ca^{2+}]_i$ (Mallilankaraman *et al.*, 2012b). In addition, knockdown of MICU1 did not affect the kinetic properties (e.g. K_d and Hill coefficient) of the mitochondrial Ca^{2+} uniporter (Mallilankaraman *et al.*, 2012b). An immunoprecipitation study has shown that the mitochondrial Ca^{2+} uniporter interacts either with MRCU1 or with MICU1 (there is no interaction between MRCU1 and MICU1), raising the

possibility that mitochondrial Ca^{2+} uniporter forms a complex with either MRCU1 or MICU1 (Mallilankaraman *et al.*, 2012a). It has been postulated that MICU1 functions as a "gatekeeper" to inhibit mitochondrial Ca^{2+} uptake at low $[Ca^{2+}]_i$ while MRCU1 stimulates mitochondrial Ca^{2+} uptake at high $[Ca^{2+}]_i$ (Mallilankaraman *et al.*, 2012b). In view of this, it is possible that a modulation on the function of MICU1 or MRCU1 by ROS may underlie the suppression of mitochondrial uniporter Ca^{2+} uptake in glomus cells. Experiments to address this issue await the availability of molecular tools in the future.
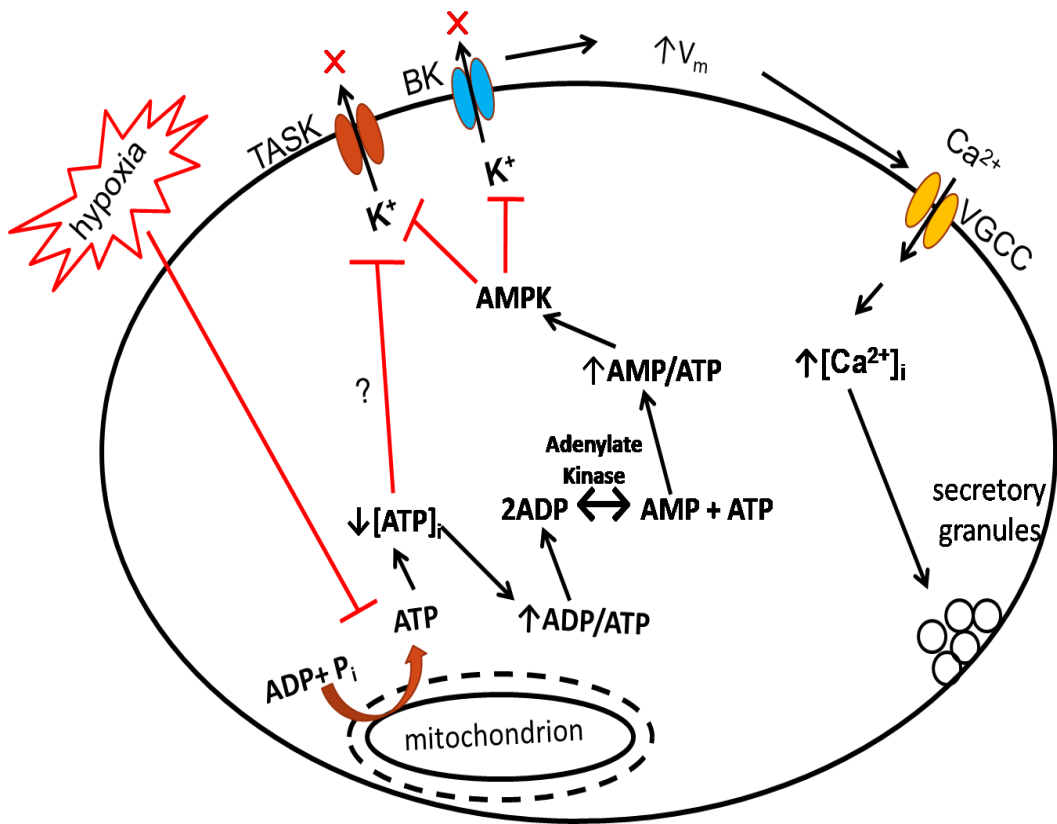
Figure 5-1 A model that depicts the role of mitochondria in the regulation of glomus cell excitability during a hypoxic challenge. Hypoxia reduces mitochondrial ATP production. The resultant reduction in cytosolic ATP concentration ($[ATP]_i$) may directly suppress TASK-like K^+ channels. $[ATP]_i$ reduction leads to an increase in cytosolic ADP/ATP ratio. The conversion of ADP to AMP by adenylate kinase causes AMPK activation which in turn inhibits BK and TASK-like K^+ channels, resulting in membrane depolarization and activation of VGCCs. The resultant rise in $[Ca^{2+}]_i$ triggers the release of transmitters.
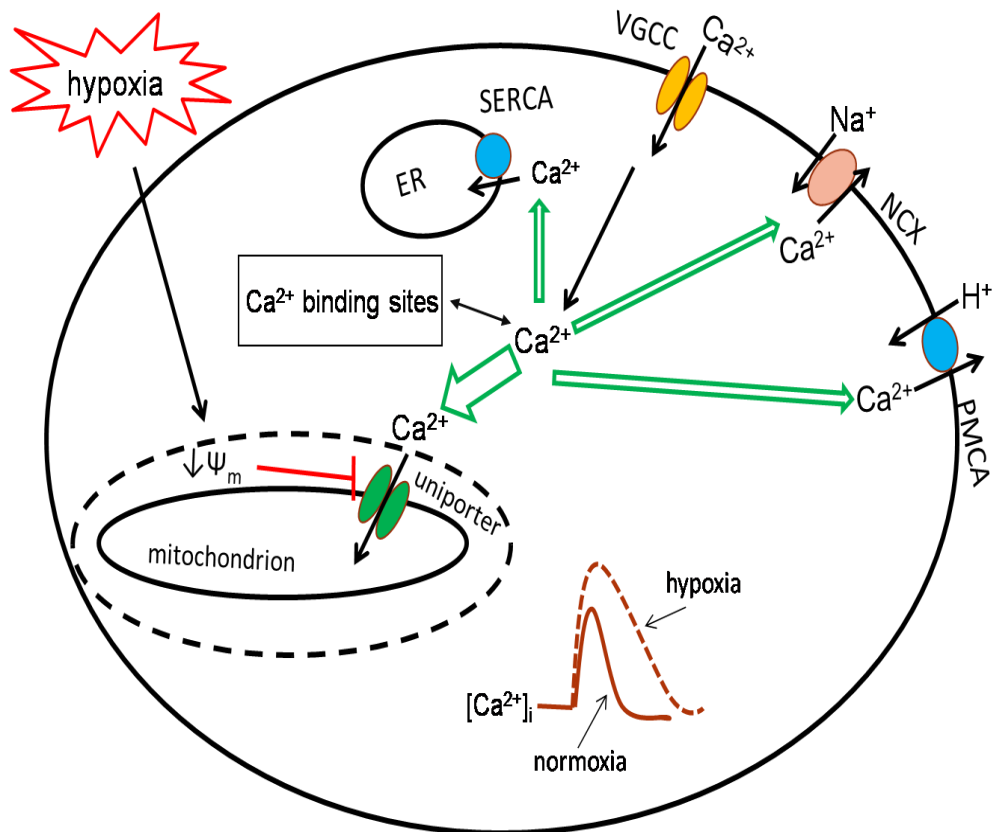
Figure 5-2 The shaping of the Ca^{2+} signal in glomus cells by mitochondria. Following VGCC-mediated Ca^{2+} entry, most cytosolic Ca^{2+} is taken up into the mitochondria via the uniporter. The SERCA pump on the ER and PMCA pump and NCX on the plasma membrane have minor roles in cytosolic Ca^{2+} clearance. Hypoxia causes mitochondrial depolarization and thus a reduction in Ca^{2+} uptake via the uniporter. As a result, both the amplitude and the duration of the Ca^{2+} signal are increased.

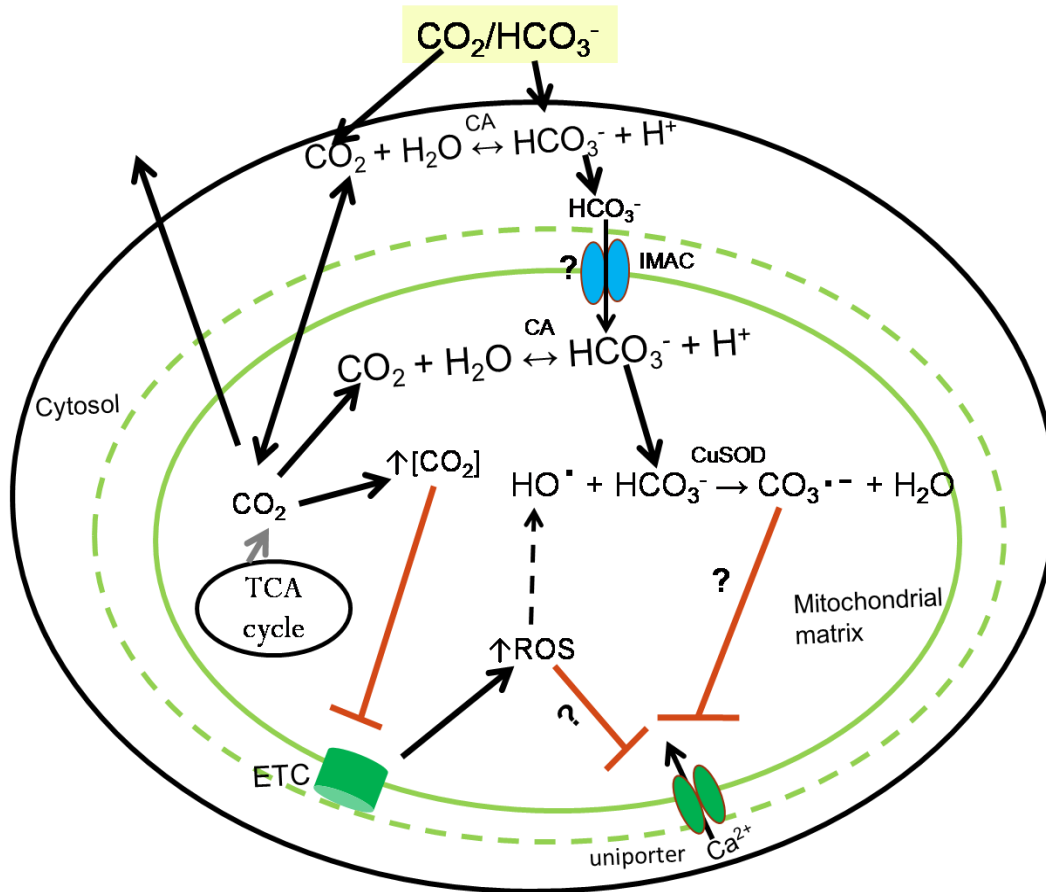**Figure 5-3** Influence of HCO_3^- on mitochondrial Ca^{2+} uptake in glomus cells. Following the entry of HCO_3^- into the cytosol, HCO_3^- can be converted into CO_2 by carbonic anhydrase (CA). The elevation in cytosolic CO_2 reduces the diffusion of CO_2 (generated from TCA cycle) from the mitochondria to the cytosol. Cytosolic HCO_3^- may enter the mitochondria via the mitochondrial inner membrane anion channel (IMAC). Elevation in mitochondrial CO_2 may reduce the efficiency of electron transport chain (ETC), resulting in an increase in mitochondrial ROS production. The function of mitochondrial uniporter may be modulated by ROS or by carbonate radical which is formed by hydroxyl radical interacting with HCO_3^-.

Reference List

Acin-Perez R, Salazar E, Kamenetsky M, Buck J, Levin LR, & Manfredi G (2009). Cyclic AMP produced inside mitochondria regulates oxidative phosphorylation. *Cell Metab* **9**, 265-276.

Allen TJ (1996). Temperature dependence of macroscopic L-type calcium channel currents in single guinea pig ventricular myocytes. *J Cardiovasc Electrophysiol* **7**, 307-321.

Archer SL, Hampl V, Nelson DP, Sidney E, Peterson DA, & Weir EK (1995). Dithionite increases radical formation and decreases vasoconstriction in the lung. Evidence that dithionite does not mimic alveolar hypoxia. *Circ Res* **77**, 174-181.

Bazil JN & Dash RK (2011). A minimal model for the mitochondrial rapid mode of Ca(2)+ uptake mechanism. *PLoS One* **6**, e21324.

Biscoe TJ & Duchen MR (1990). Responses of type I cells dissociated from the rabbit carotid body to hypoxia. *J Physiol* **428**, 39-59.

Buckler KJ & Vaughan-Jones RD (1994). Effects of hypoxia on membrane potential and intracellular calcium in rat neonatal carotid body type I cells. *J Physiol* **476**, 423-428.

Carpenter E, Hatton CJ, & Peers C (2000). Effects of hypoxia and dithionite on catecholamine release from isolated type I cells of the rat carotid body. *J Physiol* **523 Pt 3**, 719-729.

Carpenter E & Peers C (1997). Swelling- and cAMP-activated Cl^- currents in isolated rat carotid body type I cells. *J Physiol* **503 (Pt 3)**, 497-511.

David G & Barrett EF (2000). Stimulation-evoked increases in cytosolic [Ca(2+)] in mouse motor nerve terminals are limited by mitochondrial uptake and are temperature-dependent. *J Neurosci* **20**, 7290-7296.

Duchen MR & Biscoe TJ (1992a). Mitochondrial function in type I cells isolated from rabbit arterial chemoreceptors. *J Physiol* **450**, 13-31.

Duchen MR & Biscoe TJ (1992b). Relative mitochondrial membrane potential and $[Ca^{2+}]_i$ in type I cells isolated from the rabbit carotid body. *J Physiol* **450**, 33-61.

Evans AM, Mustard KJ, Wyatt CN, Peers C, Dipp M, Kumar P, Kinnear NP, & Hardie DG (2005). Does AMP-activated protein kinase couple inhibition of mitochondrial oxidative phosphorylation by hypoxia to calcium signaling in O_2-sensing cells? *J Biol Chem* **280**, 41504-41511.

Ezraty B, Chabalier M, Ducret A, Maisonneuve E, & Dukan S (2011). CO_2 exacerbates oxygen toxicity. *EMBO Rep* **12**, 321-326.

Fieber LA & McCleskey EW (1993). L-type calcium channels in type I cells of the rat carotid body. *J Neurophysiol* **70**, 1378-1384.

Gil A, Viniegra S, & Gutierrez LM (2001). Temperature and PMA affect different phases of exocytosis in bovine chromaffin cells. *Eur J Neurosci* **13**, 1380-1386.

Gonzalez C, Agapito MT, Rocher A, Gomez-Nino A, Rigual R, Castaneda J, Conde SV, & Obeso A (2010). A revisit to O_2 sensing and transduction in the carotid body chemoreceptors in the context of reactive oxygen species biology. *Respir Physiol Neurobiol* **174**, 317-330.

Gonzalez-Meler MA, Ribas-Carbo M, Siedow JN, & Drake BG (1996). Direct inhibition of plant mitochondrial respiration by elevated CO_2. *Plant Physiol* **112**, 1349-1355.

Goss SP, Singh RJ, & Kalyanaraman B (1999). Bicarbonate enhances the peroxidase activity of Cu,Zn-superoxide dismutase. Role of carbonate anion radical. *J Biol Chem* **274**, 28233-28239.

Gunter TE & Gunter KK (2001). Uptake of calcium by mitochondria: transport and possible function. *IUBMB Life* **52**, 197-204.

Hille B (2001). selective permeability:independence. In *Ion channels of excitable membranes* pp. 460-462. SINAUER ASSOCIATES, INC., Sunderland, Massachusetts U.S.A.

Hughes E, Lee AK, & Tse A (2006). Dominant role of sarcoendoplasmic reticulum Ca^{2+}-ATPase pump in Ca^{2+} homeostasis and exocytosis in rat pancreatic beta-cells. *Endocrinology* **147**, 1396-1407.

Iturriaga R & Lahiri S (1991). Carotid body chemoreception in the absence and presence of CO_2-HCO_3^-. *Brain Res* **568**, 253-260.

Jiang RG & Eyzaguirre C (2004). Effects of hypoxia and putative transmitters on $[Ca^{2+}]_i$ of rat glomus cells. *Brain Res* **995**, 285-296.

Kang SH, Carl A, McHugh JM, Goff HR, & Kenyon JL (2008). Roles of mitochondria and temperature in the control of intracellular calcium in adult rat sensory neurons. *Cell Calcium* **43**, 388-404.

Liu G, Hinch B, Davatol-Hag H, Lu Y, Powers M, & Beavis AD (1996). Temperature dependence of the mitochondrial inner membrane anion channel. The relationship between temperature and inhibition by protons. *J Biol Chem* **271**, 19717-19723.

Mallilankaraman K, Cardenas C, Doonan PJ, Chandramoorthy HC, Irrinki KM, Golenar T, Csordas G, Madireddi P, Yang J, Muller M, Miller R, Kolesar JE, Molgo J, Kaufman B, Hajnoczky G, Foskett JK, & Madesh M (2012a). MCUR1 is an essential component of mitochondrial Ca^{2+} uptake that regulates cellular metabolism. *Nat Cell Biol* **14**, 1336-1343.

Mallilankaraman K, Doonan P, Cardenas C, Chandramoorthy HC, Muller M, Miller R, Hoffman NE, Gandhirajan RK, Molgo J, Birnbaum MJ, Rothberg BS, Mak DO, Foskett JK, & Madesh M (2012b). MICU1 is an essential gatekeeper for MCU-mediated mitochondrial Ca(2+) uptake that regulates cell survival. *Cell* **151**, 630-644.

McAllister-Williams RH & Kelly JS (1995). The temperature dependence of high-threshold calcium channel currents recorded from adult rat dorsal raphe neurones. *Neuropharmacology* **34**, 1479-1490.

Mulligan E, Lahiri S, & Storey BT (1981). Carotid body O_2 chemoreception and mitochondrial oxidative phosphorylation. *J Appl Physiol* **51**, 438-446.

Ohta M, Nelson D, Nelson J, Meglasson MD, & Erecinska M (1990). Oxygen and temperature dependence of stimulated insulin secretion in isolated rat islets of Langerhans. *J Biol Chem* **265**, 17525-17532.

Ortega-Saenz P, Pardal R, Garcia-Fernandez M, & Lopez-Barneo J (2003). Rotenone selectively occludes sensitivity to hypoxia in rat carotid body glomus cells. *J Physiol* **548**, 789-800.

Panisello JM & Donnelly DF (1998). Chemotransduction by carotid body chemoreceptors is dependent on bicarbonate currents. *Respir Physiol* **112**, 265-281.

Peers C, Wyatt CN, & Evans AM (2010). Mechanisms for acute oxygen sensing in the carotid body. *Respir Physiol Neurobiol* **174**, 292-298.

Peloquin JB, Doering CJ, Rehak R, & McRory JE (2008). Temperature dependence of Cav1.4 calcium channel gating. *Neuroscience* **151**, 1066-1083.

Perocchi F, Gohil VM, Girgis HS, Bao XR, McCombs JE, Palmer AE, & Mootha VK (2010). MICU1 encodes a mitochondrial EF hand protein required for Ca(2+) uptake. *Nature* **467**, 291-296.

Petheo GL, Molnar Z, Roka A, Makara JK, & Spat A (2001). A pH-sensitive chloride current in the chemoreceptor cell of rat carotid body. *J Physiol* **535**, 95-106.

Powers MF, Smith LL, & Beavis AD (1994). On the relationship between the mitochondrial inner membrane anion channel and the adenine nucleotide translocase. *J Biol Chem* **269**, 10614-10620.

Poyton RO, Ball KA, & Castello PR (2009). Mitochondrial generation of free radicals and hypoxic signaling. *Trends Endocrinol Metab* **20**, 332-340.

Renstrom E, Eliasson L, Bokvist K, & Rorsman P (1996). Cooling inhibits exocytosis in single mouse pancreatic B-cells by suppression of granule mobilization. *J Physiol* **494 (Pt 1)**, 41-52.

Shirahata M & Fitzgerald RS (1991). The presence of CO_2/HCO_3^- is essential for hypoxic chemotransduction in the in vivo perfused carotid body. *Brain Res* **545**, 297-300.

Silva MJ & Lewis DL (1995). L- and N-type Ca^{2+} channels in adult rat carotid body chemoreceptor type I cells. *J Physiol* **489 (Pt 3)**, 689-699.

Stea A & Nurse CA (1989). Chloride channels in cultured glomus cells of the rat carotid body. *Am J Physiol* **257**, C174-C181.

Stea A & Nurse CA (1991). Contrasting effects of HEPES vs HCO3(-)-buffered media on whole-cell currents in cultured chemoreceptors of the rat carotid body. *Neurosci Lett* **132**, 239-242.

Tse A, Tse FW, & Hille B (1994). Calcium homeostasis in identified rat gonadotrophs. *J Physiol* **477 (Pt 3)**, 511-525.

Wyatt CN & Buckler KJ (2004). The effect of mitochondrial inhibitors on membrane currents in isolated neonatal rat carotid body type I cells. *J Physiol* **556**, 175-191.

Wyatt CN, Mustard KJ, Pearson SA, Dallas ML, Atkinson L, Kumar P, Peers C, Hardie DG, & Evans AM (2007). AMP-activated protein kinase mediates carotid body excitation by hypoxia. *J Biol Chem* **282**, 8092-8098.

Appendices

This chapter describes additional experimental data and analysis that are supplementary to Chapters 3 and 4. All the experiments shown here were performed by me.

Appendix 1 *The basal $[Ca^{2+}]_i$ rise evoked by mitochondrial inhibitors, SERCA pump inhibitors or extracellular HCO_3^- was not due to a large increase in Ca^{2+}-permeable leak at the plasma membrane*

As described in Chapter 3, there was a small rise in basal $[Ca^{2+}]_i$ of glomus cells (whole-cell voltage clamped at -70 mV) upon application of mitochondrial inhibitors (CCCP, cyanide; Fig. 3-4 & 3-5) or SERCA pump inhibitor (Fig. 3-6). Similarly, my experiments in Chapter 4 showed that switching the bath solution from a HCO_3^--free bath solution to one containing HCO_3^- (10 or 23 mM) resulted in an elevation of basal $[Ca^{2+}]_i$ (Fig. 4-2). One possible cause for the increase in basal $[Ca^{2+}]_i$ is the activation of an inward current that is permeable to Ca^{2+}. Therefore, I examined whether the rise in basal $[Ca^{2+}]_i$ following the inhibition of specific cytosolic Ca^{2+} clearance mechanisms was associated with an increase in the amplitude of the holding current.

Table A-1a shows the mean value of the amplitude of holding current (at -70 mV) immediately before the 1st (control) and the 2nd depolarization (in control cells and in cells following the inhibition of a specific cytosolic Ca^{2+} clearance mechanism). Cells were bathed in a HCO_3^--free (HEPES-buffered) bath solution throughout the experiment. Before the 1st depolarization, the amplitude of the holding current in glomus cells ranged from -7 to -32 pA (Table A-1a). Note that

for the three groups of cells that were exposed to mitochondrial inhibitors (2 or 10 μM CCCP, 5 mM cyanide) after the 1st depolarization, their holding current before the 1st depolarization (-19 to -32 pA) was similar to the control cells (-28 pA; Table A-1a) and the basal $[Ca^{2+}]_i$ before the 1st depolarization (data not shown) was similar among all 8 groups of cells. The amplitude of the holding current tended to increase with the duration of whole-cell recording with or without the manipulation to inhibit one of the cytosolic Ca^{2+} clearance mechanisms (an exception is the application of cyanide; Table A-1a). Fig. A-1A plots the difference in holding current immediately before the 1st and 2nd depolarization and the change in basal $[Ca^{2+}]_i$ for the same cells. The mitochondrial inhibitor CCCP (2 or 10 μM) caused the largest elevation in basal $[Ca^{2+}]_i$ but the increase in holding current by CCCP was ~8 pA, much smaller than the ~40 pA in the control cells (Fig. A-1A). For cells exposed to cyanide, the elevation in basal $[Ca^{2+}]_i$ was similar to that of CCCP but the holding current was reduced (Fig. A-1A). Inhibition of the SERCA pump (with BHQ or CPA) also caused an elevation in basal $[Ca^{2+}]_i$ but the increase in holding current with SERCA pump inhibitors was less than the control cells (Fig. A-1A). The largest increase in the amplitude of holding current was observed in the control cells (~40 pA; Fig. A-1Ai and Table A-1a) but there was little change in basal $[Ca^{2+}]_i$ (~22 nM; Fig. A-1Aii). Thus, the elevation in basal $[Ca^{2+}]_i$ upon inhibition of mitochondria or SERCA pump was not associated with a large increase in Ca^{2+}-permeable leak at the plasma membrane. These findings support the notion that

170

basal Ca^{2+} influx into glomus cells is balanced by Ca^{2+} uptake via mitochondria and SERCA pump (as described in Chapter 3).

I also examined whether the increase in basal $[Ca^{2+}]_i$ upon switching the bath solution from a HCO_3^--free bath solution to one containing HCO_3^- was associated with an increase in holding current. Table A-1b shows the amplitude of the holding current of glomus cells (whole-cell voltage clamped at -70 mV) upon switching from a HCO_3^--free bath solution to one containing various concentrations of HCO_3^-. Plots of the change in holding current and the change in basal $[Ca^{2+}]_i$ from the same cells were shown in Fig. A-1B. Note that upon switching from a HCO_3^--free bath solution to one containing 10 or 23 mM HCO_3^-, the increase in holding current tended to be smaller than the control cells (Fig. A-1Bi) but elevation in basal $[Ca^{2+}]_i$ that ranged from 98-201 nM was detected (Fig. A-1Bii). Thus, the rise in basal $[Ca^{2+}]_i$ induced by extracellular HCO_3^- was not due to a large increase in Ca^{2+}-permeable leak at the plasma membrane. As described in Chapter 4, the presence of 10 or 23 mM extracellular HCO_3^- suppresses mitochondrial Ca^{2+} uptake in glomus cells. Therefore, it is likely that the elevation in basal $[Ca^{2+}]_i$ evoked by extracellular HCO_3^- is due to the suppression of mitochondrial uniporter.

Appendix 2 *Estimation of intracellular Ca^{2+} buffering capacity*

As described in Fig. 3-1, most of the Ca^{2+} entering the cytosol is bound by endogenous Ca^{2+} binding sites (buffers) and only a small fraction appears as free Ca^{2+}. The intracellular Ca^{2+} buffering capacity can be estimated by comparing the

amount of Ca^{2+} entry during depolarization to the amplitude of the corresponding elevation in $[Ca^{2+}]_i$ (Tse *et al.*, 1994). In my experiments, $[Ca^{2+}]_i$ was monitored with 25 μM indo-1 in the whole-cell pipette solution. The pipette solution also contained Cs^+ and TEA to block K^+ currents. At ~3 min after the establishment of whole-cell configuration, the indo-1 in the whole-cell pipette solution was equilibrated with the cytosol. A single depolarizing voltage step (500 ms to 0 mV from a holding potential of -70 mV) was delivered to activate VGCC. Under this condition, an inward Ca^{2+} current was evoked (e.g. the 1st depolarization in Fig. 3-2B). The amount of Ca^{2+} entry was estimated from the time integral of the inward current and normalized to cell volume (Tse *et al.*, 1994). Cell volume was calculated from the cell membrane capacitance (estimated with an EPC-9 amplifier) and was based on the assumptions that 1 pF of membrane capacitance corresponded to 100 μm^2 of membrane surface area and that glomus cell was spherical. For the 18 rat glomus cells examined here, the average cell membrane capacitance was 3.9 ± 0.1 pF (range 2.8-5.2 pF) with a mean cell diameter of 11.1 μm and a volume of 722.5 μm^3. The Ca^{2+} entry and the corresponding elevation in $[Ca^{2+}]_i$ from each of the 18 glomus cells (open circles) was plotted in Fig. A-2. The solid line was the linear regression of all the data points and with the origin set at 0. The slope of the line is 1/85 (the 95% confidence interval is 1/75 to 1/96) with r^2 value of 0.8. This result suggests that under my experimental conditions, the buffering capacity of glomus cells is ~85, that is only one out of every 85 Ca^{2+} that entered the glomus cell was free and the other 84 Ca^{2+} were rapidly bound by

intracellular Ca^{2+} buffers (endogenous + indo-1) or taken up into the intracellular organelles (e.g. mitochondria).

Note that the Ca^{2+} buffering capacity measured with the method just described may be underestimated in several ways. Firstly, as described in Fig. 3-2, with increasing duration of whole-cell recording, the direction of the current during the depolarization step to 0 mV changed from inward to outward (probably because of the gradual development of a current with a reversal potential somewhere between -70 mV and 0 mV). Although I have limited my analysis to the inward current evoked by the 1st depolarization (~3 min after establishment of whole-cell configuration), it remains possible that some of the Ca^{2+} current is already partially masked by such an outward current and thus the amount of Ca^{2+} entry may be underestimated. Secondly, the cell volume may be overestimated. My analysis was based on the assumption that glomus cells are spherical in shape and Ca^{2+} equilibrates throughout the entire cell. However, a cell that flattens on the coverslip tends to have less volume than a cell with the same diameter but has a spherical shape. Moreover, the Ca^{2+} that entered a cell via VGCCs is initially distributed only throughout the cytosol instead of the entire cell volume. Thirdly, the peak $[Ca^{2+}]_i$ during VGCC entry may be higher than the measured value. Since $[Ca^{2+}]_i$ was measured every 200 ms, it is possible that the peak $[Ca^{2+}]_i$ rise might not be detected in my experiment. In addition, measurement of $[Ca^{2+}]_i$ with indo-1 (K_d = 0.23 μM) is only accurate when $[Ca^{2+}]_i$ is within the range of 0.023 to 2.3 μM. At $[Ca^{2+}]_i$ in the range of a few μM, a small noise in the ratio of the indo-1 fluorescence at the two wavelengths (Chapter 2) would result in a large

uncertainty for the estimated $[Ca^{2+}]_i$. Note that some of data points in Fig. A-2 have $[Ca^{2+}]_i$ values in the range of 3-4 μM. The uncertainty of the indo-1 measurements at high $[Ca^{2+}]_i$ values probably biased the linear regression fit and resulted in an underestimation of the intracellular Ca^{2+} buffering capacity. Lastly, some mobile endogenous Ca^{2+} buffers may be lost during whole-cell recording. However, a previous study in chromaffin cells has shown that the loss of endogenous Ca^{2+} buffers via the whole-cell pipette is small (buffering capacity of ~9) (Zhou & Neher, 1993). To address this issue in glomus cells, I compared the time course of the decay of the depolarization-triggered Ca^{2+} signal in cells recorded with the whole-cell patch clamp mode (25 μM indo-1 loaded via the whole-cell pipette) to those recorded with the perforated-patch clamp mode. For cells recorded with the perforated-patch mode, they were loaded with indo-1 AM (2.5 μM) in HEPES-buffered standard bath solution at 37 ^{o}C for ~15 min and then washed with standard bath solution at 20-23 ^{o}C for 15 min before recording. The indo-1 fluorescence was similar in both groups of cells, suggesting that they had similar concentration of cytosolic indo-1. I found that there was no significant difference in the time course of the decay between the two groups (decay τ of 5.1 $\pm$ 0.3 s (n = 22) in the whole-cell group versus 4.6 $\pm$ 0.3 s (n = 16) in the perforated-patch group). These results suggest that the loss of mobile endogenous Ca^{2+} buffers from glomus cells during whole-cell recording is probably small and does not contribute significantly to the time course of cytosolic Ca^{2+} clearance.

Appendix 3 Enhancement of hypoxia-triggered Ca^{2+} response in intact glomus cells by extracellular HCO$_3^-$

Since the presence of physiological [HCO$_3^-$]$_{ext}$ was reported to enhance hypoxia-triggered CSN discharge and hypoxia-mediated catecholamine release from glomus cells (Panisello & Donnelly, 1998) and my findings in Chapter 4 have shown that physiological [HCO$_3^-$]$_{ext}$ slowed cytosolic [Ca^{2+}] decay in glomus cells via a suppression of mitochondrial Ca^{2+} uptake, I examined whether the hypoxia-triggered Ca^{2+} signal in glomus cells (not voltage clamped) was affected by physiological [HCO$_3^-$]$_{ext}$. In this experiment, intact glomus cells were loaded with fura-2 AM (2.5 µM) in HEPES-buffered standard bath solution at 37 ^{o}C for 10 min and then washed with standard bath solution at 20-23 ^{o}C for 15 min before recording. [Ca^{2+}]$_i$ was monitored with digital imaging using a Tillvision imaging system equipped with Polychrome II high speed monochromator (Applied Scientific Instrument, OR, USA). Details of these procedures were as described previously (Xu *et al.*, 2003; Xu *et al.*, 2005). Fura-2 was excited sequentially by 340 and 380 nm lights delivered from a Xenon lamp via a 40×, 1.3 NA UV fluor oil objective (Olympus, Carsen Group, Markham, ON, Canada). Fluorescent images were collected at 510 nm every 5 s by a Peltier-cooled CCD camera. Since the cells were loaded with AM dyes, there was no correction for cell autofluorescence. The ratio of fluorescence, R (340 nm /380 nm) from individual cells was analyzed with Tillvision Software 3.02 (Till Photonics, Applied Scientific Instrument) on an IBM-compatible computer, according to the equation (Grynkiewicz *et al.*, 1985): [Ca^{2+}] = K* × (R − R$_{min}$)/(R$_{max}$ − R). R$_{min}$ is the

fluorescence ratio of Ca^{2+}-free indicator and R_{max} is the ratio of Ca^{2+}-bound indicator. K^* is a constant that was determined empirically. Calibrations for fura-2 were determined from single cells introduced with one of the three pipette solutions in whole-cell recording mode as described for indo-1 in Chapter 2. The values for R_{min}, R_{max} and K^* were 0.13, 3.4, and 2.72 µM, respectively.

In this experiment, hypoxia was induced by bubbling 100% N_2 in the HCO_3^--free bath solution or by bubbling 95% N_2 and 5% CO_2 in the bath solution that contained 23 mM extracellular HCO_3^-. Note that the recording chamber was exposed to atmospheric O_2 and thus the hypoxia induced under my experimental conditions was only moderate (pO_2 of the bath solution was ~40 mmHg (Xu et al., 2005)). In the majority of glomus cells examined, hypoxia failed to evoke any $[Ca^{2+}]_i$ elevation in the absence of extracellular HCO_3^- (e.g. Fig. A-3A). However, when the same cells were exposed to hypoxia in the presence of physiological $[HCO_3^-]_{ext}$, a robust $[Ca^{2+}]_i$ rise was triggered (e.g. Fig. A-3A). In a small fraction of glomus cells, the hypoxia-evoked Ca^{2+} signal could be detected with or without extracellular HCO_3^- but the hypoxia-mediated Ca^{2+} signal appeared to be more sustained in the presence of extracellular HCO_3^- (e.g. Fig. A-3B). Among the glomus cells that exhibited a hypoxia-mediated Ca^{2+} signal in physiological $[HCO_3^-]_{ext}$, only ~15% (8 out of 54 cells) responded to hypoxia when bathed in a HCO_3^--free bath solution (Fig. A-3C). As shown in Fig. A-3D, the mean time integral of the hypoxia-mediated Ca^{2+} signal in cells that responded to hypoxia in HCO_3^--free bath solution was smaller than that evoked in the presence of extracellular HCO_3^- (6.9 $\pm$ 1.6 µM s versus 12.2 $\pm$ 1.0 µM s).

While the slowing in cytosolic Ca^{2+} clearance by extracellular HCO_3^- probably contributes to the more sustained hypoxia-mediated Ca^{2+} signal, it is not clear why the ability of hypoxia to trigger a rise in $[Ca^{2+}]_i$ was enhanced by extracellular HCO_3^-. Previous studies from our laboratory have shown that the activation of cAMP-PKA (via the stimulation of adenosine or PACAP receptors) in rat glomus cells resulted in a suppression of the background TASK-like K^+ current, leading to membrane depolarization and VGCC activation (Xu *et al.*, 2006; Xu *et al.*, 2007). This raises the possibility that the activation of sAC by HCO_3^- (which leads to an elevation in the cellular level of cAMP) may enhance the electrical excitability of glomus cells via a suppression of TASK-like K^+ current. To address this possibility, I examined whether the resting membrane potential and/or the hypoxia-triggered membrane depolarization in glomus cells was affected by physiological $[HCO_3^-]_{ext}$. In this experiment, the membrane potential of individual glomus cells was recorded with the perforated-patch clamp technique. As shown in the example in Fig. A-4A, hypoxia evoked a small plateau depolarization when the cell was bathed in a HCO_3^--free solution. When the same cell was bathed in a solution containing 23 mM extracellular HCO_3^-, hypoxia evoked a larger plateau depolarization that was superimposed with action potential firings which are expected to activate VGCCs robustly (Fig. A-4A). Fig. A-4B plots the resting membrane potential and the hypoxia-mediated depolarization (amplitude of the plateau depolarization as shown in Fig. A-4A) averaged from 4 cells. Extracellular HCO_3^- by itself did not affect the resting membrane potential (-52.1 ± 1.2 mV and -53.0 ± 0.4 mV respectively in the

absence or presence of extracellular HCO_3^-; Fig. A-4B). However, hypoxia caused a larger plateau depolarization in the presence of extracellular HCO_3^- (16.7 ± 2.0 mV in HCO_3^- versus 8.2 ± 1.2 mV in HCO_3^--free; Fig. A-4C). Previous study in our laboratory has shown that in rat glomus cells, VGCC activation was detectable only at potentials more positive than -40 mV (Xu *et al.*, 2003). As shown in Fig. A-4B, in the presence of extracellular HCO_3^-, before the triggering of action potentials hypoxia depolarized the membrane potential to -36.3 ± 2.3 mV, which is above the threshold for detectable VGCC activation. In contrast, without extracellular HCO_3^-, hypoxia only depolarized the membrane potential to -43.9 ± 1.1 mV (Fig. A-4B), which is below this threshold. The above analysis suggests that in the absence of extracellular HCO_3^-, the hypoxia-evoked depolarization is typically too small to cause significant VGCC activation and thus explains why hypoxia failed to evoke $[Ca^{2+}]_i$ rise in the majority of glomus cells (Fig. A-3C). The enhancing effect of extracellular HCO_3^- on the hypoxia-mediated Ca^{2+} signal may contribute to the increase in hypoxia-mediated CSN discharge reported previously (Panisello & Donnelly, 1998).

Table A-1a Changes in the amplitude of the holding current (pA) of glomus cell (whole-cell voltage clamped at -70 mV) upon inhibition of the specific cytosolic Ca^{2+} clearance mechanism (in a HCO_3^--free bath solution)

Experimental manipulation before the 2nd depolarization	n	Before the 1st depolarization	Before the 2nd depolarization
Time-matched control	5	-28 ± 7.5	-68.6 ± 15.7
CCCP-2 µM	6	-26 ± 6.7	-34.2 ± 5.3
CCCP-10 µM	10	-19 ± 3.6	-26.5 ± 6.4
Cyanide-5 mM	5	-31.8 ± 7.7	-20.4 ± 6.9
BHQ-20 µM	6	-6.8 ± 1.30	-12.7 ± 2.2
CPA-50 µM	4	-13 ± 2.7	-29.7 ± 7.4
$pH_{ext} = 8.8$	7	-17 ± 2.3	-24.3 ± 4.5
$[Na^+]_{ext} = 0$	5	-7.2 ± 1.4	-10 ± 3.2

Table A-1b Changes in the amplitude of the holding current (pA) of glomus cell (whole-cell voltage clamped at -70 mV) when exposed to different $[HCO_3^-]_{ext}$

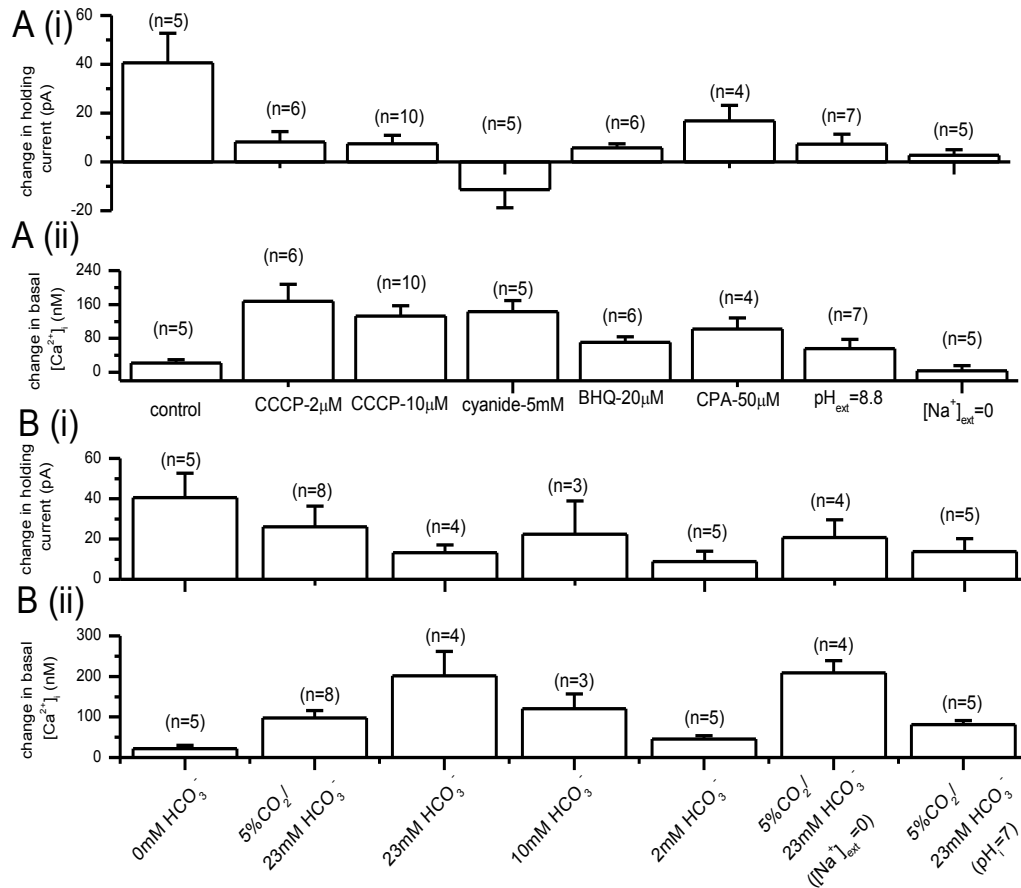| Manipulation before the 2nd depolarization	n	Before the 1st depolarization (HCO_3^--free solution)	Before the 2nd depolarization (HCO_3^--buffered solution)
0 mM HCO_3^-	5	-28 ± 7.5	-68.6 ± 15.7
5%CO_2/23mM HCO_3^-	8	-16.5 ± 3.7	-42.5 ± 10.0
23mM HCO_3^-	4	-8.5 ± 2.2	-21.7 ± 5.5
10mM HCO_3^-	3	-7.3 ± 0.7	-29.7 ± 16.9
2mM HCO_3^-	5	-8.4 ± 2.1	-17.2 ± 6.4
5%CO_2/23 mM HCO_3^- ($[Na^+]_{ext} = 0$)	4	-16.5 ± 7.9	-37.2 ± 5.2
5%CO_2/23mM HCO_3^- ($pH_i = 7$)	5	-13.4 ± 2.2	-27.2 ± 7.2

Figure A-1 Summary of the changes in holding current amplitude (at -70 mV) and basal $[Ca^{2+}]_i$ between the 1st and 2nd depolarization under different experimental conditions. (A) The elevation in basal $[Ca^{2+}]_i$ upon inhibition of mitochondria or the SERCA pump was not associated with a large increase in Ca^{2+}-permeable leak at the plasma membrane. Plots of the change in the holding current amplitude (Ai) and basal $[Ca^{2+}]_i$ (Aii) upon inhibition of various cytosolic Ca^{2+} clearance mechanisms. Cells were bathed in a HEPES-buffered (HCO_3^--free) bath solution throughout the experiment. CCCP or cyanide was used to inhibit mitochondrial functions. BHQ or CPA was used to inhibit the SERCA pump. NCX was inhibited by a Na^+-free bath solution and the PMCA pump was suppressed by a pH 8.8 bath solution. (B) The elevation in basal $[Ca^{2+}]_i$ upon switching from a HCO_3^--free bath solution to one containing 10 or 23 mM HCO_3^- was not associated with a large increase in Ca^{2+}-permeable leak at the plasma membrane. Plots of the change in the holding current amplitude (Bi) and basal $[Ca^{2+}]_i$ (Bii) upon switching from a HCO_3^--free bath solution to one containing various $[HCO_3^-]$. The change in holding current amplitude shown in (Ai) and (Bi) was the difference in holding current at -70 mV immediately before the 1st and 2nd depolarization. In both (A) and (B), cells were recorded in the whole-cell mode.
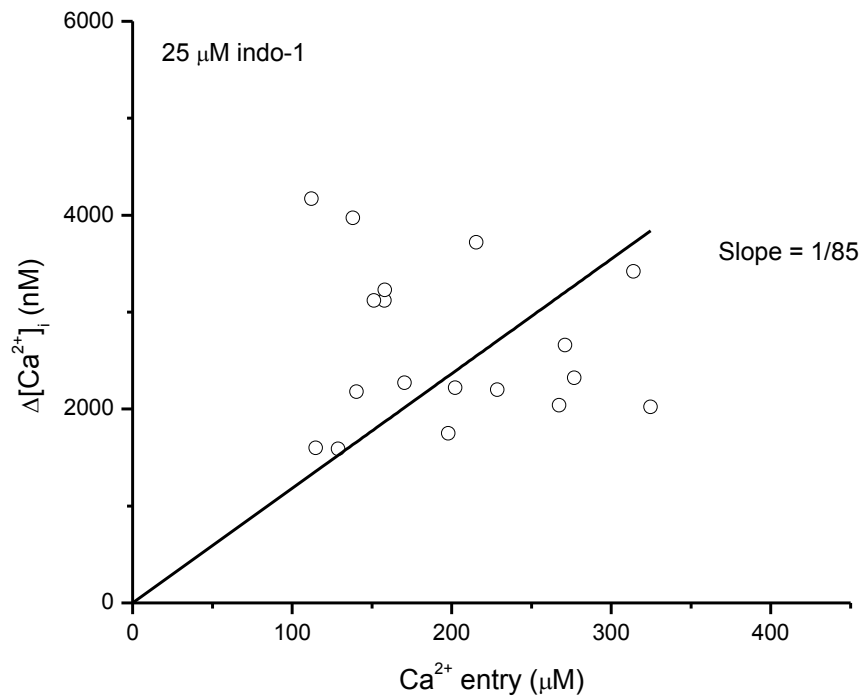
Figure A-2 Estimate of intracellular Ca^{2+}-buffering capacity of glomus cells. Each data point depicts the Ca^{2+} entry (integral of the Ca^{2+} current) during the 500 ms voltage step (from -70 to 0 mV) and the corresponding elevation in $[Ca^{2+}]_i$ from a single glomus cell. The solid line was the linear regression of all the data points and with the origin set at 0. The slope of the line is 1/85 with r^2 value of 0.8. Cells were recorded with 25 μM indo-1 in the whole-cell pipette solution.
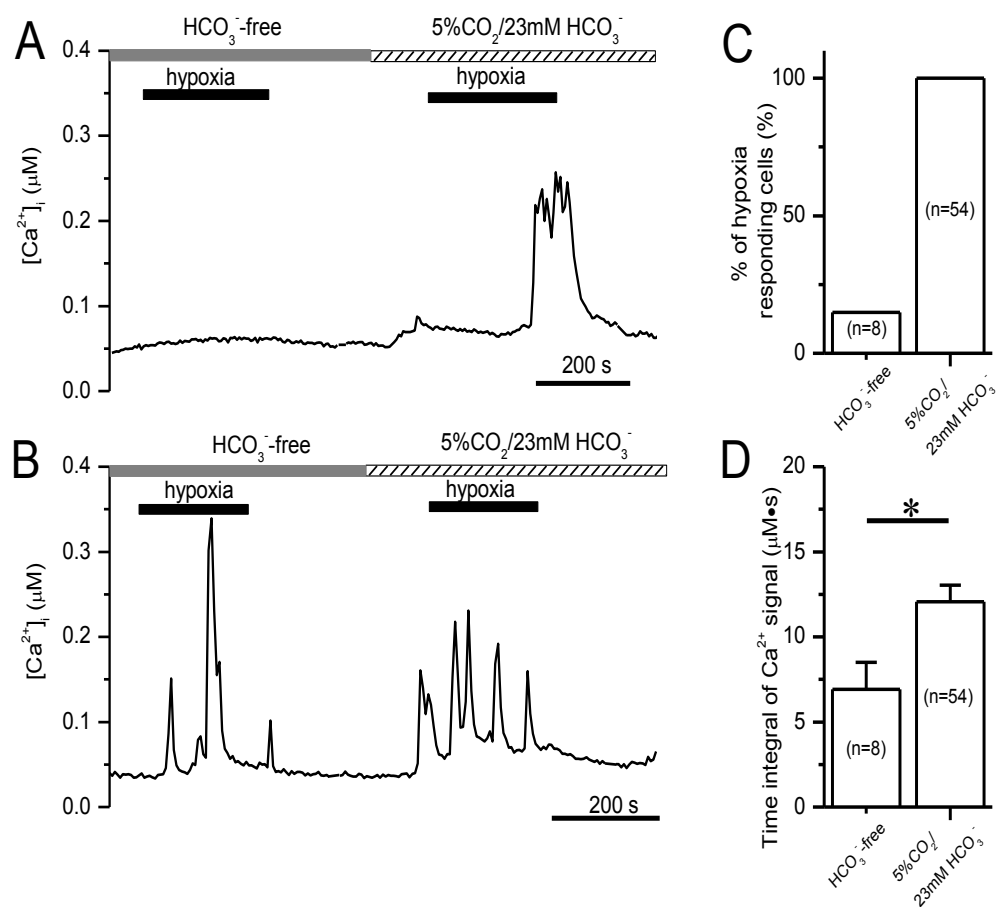
Figure A-3 Enhancement of hypoxia-mediated Ca^{2+} response by physiological $[HCO_3^-]_{ext}$. (A) An example of a glomus cell that did not exhibit any detectable $[Ca^{2+}]_i$ rise to hypoxia when bathed in a HCO_3^--free solution. Note that when the same cell was bathed in 23 mM HCO_3^-, hypoxia evoked a robust $[Ca^{2+}]_i$ rise. (B) An example of a glomus cell that exhibited a $[Ca^{2+}]_i$ rise when challenged with hypoxia in a HCO_3^--free solution. A subsequent hypoxic challenge to the same cell when bathed in 23 mM HCO_3^- could still trigger a robust $[Ca^{2+}]_i$ rise. (C) Among the glomus cells that exhibited a hypoxia-mediated Ca^{2+} signal in the presence of 23 mM HCO_3^-, only ~15% exhibited a hypoxia-mediated Ca^{2+} signal when bathed in a HCO_3^--free solution. (D) Hypoxia triggered a larger Ca^{2+} response in the presence of 23 mM $[HCO_3^-]_{ext}$. Plots of the mean time integral of hypoxia-triggered Ca^{2+} signal in the absence and presence of extracellular HCO_3^-.

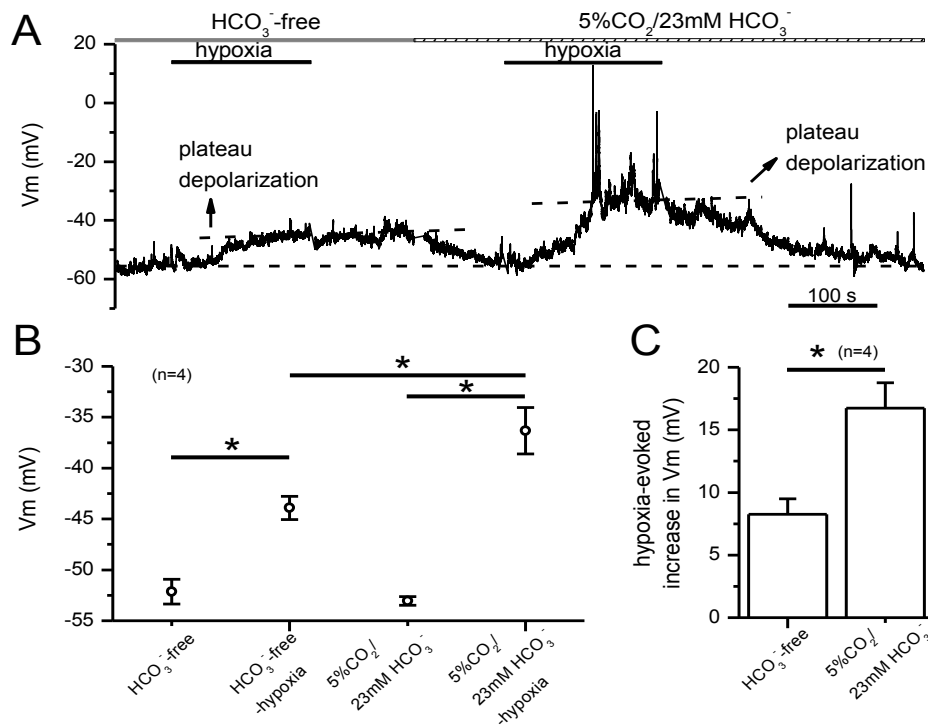**Figure A-4** Physiological [HCO_3^-]$_{ext}$ enhanced the hypoxia-evoked membrane depolarization without affecting the resting membrane potential. (A) Hypoxia evoked a small plateau depolarization (indicated by the dashed line) when the cell was bathed in a HCO_3^--free solution. Upon switching the bath to one containing 23 mM HCO_3^-, hypoxia evoked a larger plateau depolarization and firing of action potentials. Membrane potential was recorded with the perforated-patch clamp technique. (B) Summary of the resting membrane potential and the membrane potential in the presence of hypoxia (plateau depolarization) in the absence and presence of extracellular HCO_3^-. (C) Summary of hypoxia-evoked membrane depolarization (difference between the resting membrane potential and the plateau depolarization in hypoxia) in the absence or presence of extracellular HCO_3^-.

183

Reference List

Grynkiewicz G, Poenie M, & Tsien RY (1985). A new generation of Ca^{2+} indicators with greatly improved fluorescence properties. *J Biol Chem* **260**, 3440-3450.

Panisello JM & Donnelly DF (1998). Chemotransduction by carotid body chemoreceptors is dependent on bicarbonate currents. *Respir Physiol* **112**, 265-281.

Tse A, Tse FW, & Hille B (1994). Calcium homeostasis in identified rat gonadotrophs. *J Physiol* **477 (Pt 3)**, 511-525.

Xu F, Tse FW, & Tse A (2007). Pituitary adenylate cyclase-activating polypeptide (PACAP) stimulates the oxygen sensing type I (glomus) cells of rat carotid bodies via reduction of a background TASK-like K^+ current. *J Neurochem* **101**, 1284-1293.

Xu F, Xu J, Tse FW, & Tse A (2006). Adenosine stimulates depolarization and rise in cytoplasmic $[Ca^{2+}]$ in type I cells of rat carotid bodies. *Am J Physiol Cell Physiol* **290**, C1592-C1598.

Xu J, Tse FW, & Tse A (2003). ATP triggers intracellular Ca^{2+} release in type II cells of the rat carotid body. *J Physiol* **549**, 739-747.

Xu J, Xu F, Tse FW, & Tse A (2005). ATP inhibits the hypoxia response in type I cells of rat carotid bodies. *J Neurochem* **92**, 1419-1430.

Zhou Z & Neher E (1993). Mobile and immobile calcium buffers in bovine adrenal chromaffin cells. *J Physiol* **469**, 245-273.